Journal of the Electrochemical Society of India

Indian Institute of Science Campus, Bengaluru - 560 012, India

Guest Editor

Dr. T. M. Sridhar

Vol. No. 72 (3 & 4), July-December 2023

CODEN - JESIA 72 [3&4] 2023 ISSN:0013-466X

INSTRUCTIONS TO AUTHORS

GENERAL

Address all manuscripts to the Managing Editor, Electrochemical Society of India,(JECSI) Bengaluru-560012 and send it by email to arunaecsi@gmail.com / ecsiiisc@gmail.com. Submission of an article will be taken to imply that it has not been previously published and is not under consideration for publication elsewhere. And further that if accepted, it will not be published elsewhere. Submit an electronic version of the paper in WORD format along with a pdf version in order not to miss any portion due to transmission faults. Identify the address, affiliation, email address of the author (corresponding author in case of multiple authors). Also, identify the category in which the paper qualifies for publication.

Journal of the Electrochemical Society of India (JECSI) is a multidisciplinary journal in the general area of Electrochemical Science and Technology. Research and review papers of general significance that are written clearly and well organized will be given preference. All submitted papers will be reviewed by three experts to determine suitability. Paper found unsuitable in terms of the overall requirements of the Journal and those not accepted by the reviewers will be returned to the authors. Both solicited and unsolicited papers will be reviewed. Authors will be notified of acceptance, rejection or any need for revision before acceptance for publication. Any illustrations or other material reproduced from other publications must be properly credited. It is the author's responsibility to obtain the necessary permission in such cases.

CATEGORIES OF MANUSCRIPTS

General Articles, not exceeding 5000 words in length, should discuss current trends in research in a field that will be of interest to readers outside the field; interdisciplinary topics; Science policy and administration; Impact of Science and Technology on Society, etc. The paper should include a summary not exceeding 200 words, introductory paragraph(s), brief subheads at appropriate places to point to what follows, Illustrations that will help a general reader and references.

Review Articles, not exceeding 5000 words, are expected to survey and discuss recent developments in a relevant field. They should be well focused and organized. General text book style is not acceptable. Research Articles should report and discuss results of work of a fairly major significance. They should include an Abstract, introductory paragraph(s) and brief subheads indicating materials and methods used, major results and discussion of results, relevant illustrations and references.

Research Communications, not exceeding 2000 words, should contain important findings that are novel and are of fairly broad interest. They should not be broken up under subheads. Correspondences include letters, not exceeding 500 words that are of general interest to Scientist, Engineers and Technologists. Only selected letters will be published. Scientific Correspondence contains technical comments, including those on articles or communications published in JECSI. Appropriate letters will be published.

Book Reviews are reviews of books published in the major areas of Electrochemical Science, Technology and Engineering. Unsolicited reviews will also be considered. Reviews that simply 'list' the contents will not be acceptable for publication. Reviews should have 'context' and convey information about the subject of the book. Historical Comments and Notes inform readers about interesting aspects of personalities or institutions of Science or about watershed events in the history/ development of science. Most are expected to relate to India. Illustrations are welcome with due credit if already published elsewhere.

MANUSCRIPT PREPARATION

The manuscript should be in double line spacing in an area corresponding to A-4 size paper with 25 mm margin all around. Page numbers, including

that for the first page should be given at the bottom centre of the page. The title should be brief, specific and amenable to indexing. Give a maximum of 5 keywords which are carefully chosen and not phrases of several words. Summary and abstract should not have more than 200 words and should convey the main point of the paper, outline the results and conclusions and explain the significance of the work and results.

Text

Papers should begin with an introduction. The text should be intelligible to readers in different disciplines and technical terms should be defined. Tables and figures should be arranged in numerical order and referred to in that order. All symbols and abbreviations must be defined and used only when absolutely necessary. Superscripts and subscripts and ambiguous characters should be clearly indicated. Units of measure should be metric and preferably SI. Methods should, as far as possible, be described briefly in appropriate table and figure legends.

Figures are to be drawn in sizes that are clearly intelligible. Location and orientation of figures is the entire responsibility of the author(s). The actual location of figures and tables may be clearly indicated in the pdf format that accompanies the main word format submission. The same data should not be given in both tables and figures. Photomicrographs and other photographs that require a scale bar or a micron marker should be defined clearly in the caption. Magnifications are not acceptable in place of micron markers. Primary data should be submitted as far as possible as for example actual photograph of an electrophoretic gel rather than an idealized diagram.

References should be numbered in the order in which they appear first through the text and then through table and figure legends. Following examples indicate the different ways of writing the references:

Reference to a journal publication:

[1] J. Name, J.A.J. Name, R.A. Name, Title of article, J. Sci. Commun. Vol.no (year) page number xx–xy. https://doi.org/10.1016/ j.Sc.2010.00372.

Reference to a book:

[3] W. Name, E.B. Name, Title of the book, Edition, Publisher, Place name, year.

Reference to a chapter in an edited book:

[4] G.R. Name, L.B. Name, Chapter title, in: B.S. Name, R.Z. Name (Eds.), Title of book, Publisher, Place name, Year, pp. xxx–yyy.

Acknowledgments should be brief and clear.

Funding: This work was supported by Granting Agency Name [grant numbers xxxx, yyyy];

Cover Photographs. Good photographs (colour or black and white) that pertain to a submitted paper will be considered for use on the cover of an issue.

Proofs and Publication: A final pdf version of the paper may be sent to the author before publication if there are any inaccuracies or doubts of any nature. Such a procedure is redundant in case no major editorial changes are made in the paper.

Publication Ethics and Publication Malpractice Statement

The Journal of Electrochemical Society of India (JECSI) follows the Committee on Publication Ethics (COPE) *Code of Conduct and Best Practice Guidelines for Journal Editors and the Code of Conduct for Journal Publishers*. It is expected that authors, reviewers and editors follow the best-practice guidelines on ethical behaviour.

Responsibilities of Editorial board

Editors evaluate submitted manuscripts only on the basis of their merit such as novelty, originality, importance, and its relevance to the journal's scope. The information or ideas imparted to the editors due to handling the manuscript will be kept confidential and will not be used for their own benefit. The editors will refrain from reviewing a manuscript in which they have conflict of interest and will be handled by other editorial board members. Editors and editorial staff will maintain confidentiality about the submitted manuscripts.

All the manuscripts submitted to the journal will undergo peer-review by at least two reviewers who are experts in that area. Based on the evaluation reports received from the reviewers, copyright permissions and plagiarism will be checked and then the Chief Editor decides on the publication of the manuscript.

The Chief Editor will take actions when ethical concerns are raised with regard to a submitted manuscript or published paper followed by a correction, retraction, expression of concern or relevant other notes will be published in JECSI.

Responsibilities of Authors

The Authors should present detailed and correct account of the work to enable others to reproduce the work. Fraudulent or inaccurate statements are not accepted. If required the authors will be asked to provide the raw data of their study if some suspicious figures are provided in the manuscript. Authors should check their manuscript for originality check using the standard software. Only manuscripts with similarity report <20% will be considered for peer review. The authors should not simultaneously submit the same manuscript to multiple journals and is treated as unethical and such papers will be sent back to the authors and authors will be black listed.

Authors who have made significant contributions to the paper should only be included as authors in the manuscript and the role of each author has to be listed. The other peoples name should be included in the acknowledgement section.

The authors should disclose the conflict of interest that would have influenced the results or their interpretation. Authors should also properly acknowledge the work of others and ensure proper citation of such works in the manuscript. The authors should clearly state in the manuscript if the work involved the use of hazardous chemicals, procedures or equipment.

The authors should co-operate in submitting the revised manuscripts before the deadline and providing befitting replies to the reviewer comments. The authors should inform the Chief Editor when they discover significant errors or inaccuracies in their own published work and publish a corrigendum or retract the paper.

Journal of the Electrochemical Society of India

Vol. No. 72 (3&4), July/December 2023

CODEN - JESIA 72 [3&4] 2023 ISSN:0013-466X

Email : ecsiiisc@gmail.com

E-mail : ecsiiisc@gmail.com

Publication Ethics and Publication Malpractice Statement

The Journal of Electrochemical Society of India (JECSI) follows the Committee on Publication Ethics (COPE) *Code of Conduct and Best Practice Guidelines for Journal Editors* and the *Code of Conduct for Journal Publishers*. It is expected that authors, reviewers and editors follow the best-practice guidelines on ethical behaviour.

Responsibilities of Editorial Board

Editors evaluate submitted manuscripts only on the basis of their merit such as novelty, originality, importance, and its relevance to the journal's scope. The information or ideas imparted to the editors due to handling the manuscript will be kept confidential and will not be used for their own benefit. The editors will refrain from reviewing a manuscript in which they have conflict of interest and will be handled by other editorial board members. Editors and editorial staff will maintain confidentiality about the submitted manuscripts.

All the manuscripts submitted to the journal will undergo peer-review by at least two reviewers who are experts in that area. Based on the evaluation reports received from the reviewers, copyright permissions and plagiarism will be checked and then the Chief Editor decides on the publication of the manuscript.

The Chief Editor will take actions when ethical concerns are raised with regard to a submitted manuscript or published paper followed by a correction, retraction, expression of concern or relevant other notes will be published in JECSI.

Responsibilities of Authors

The Authors should present detailed and correct account of the work to enable others to reproduce the work. Fraudulent or inaccurate statements are not accepted. If required the authors will be asked to provide the raw data of their study if some suspicious figures are provided in the manuscript. Authors should check their manuscript for originality check using the standard software. Only manuscripts with similarity report <20% will be considered for peer review. The authors should not simultaneously submit the same manuscript to multiple journals and is treated as unethical and such papers will be sent back to the authors and authors will be black listed.

Authors who have made significant contributions to the paper should only be included as authors in the manuscript and the role of each author has to be listed. The other peoples' name should be included in the acknowledgement section.

The authors should disclose the conflict of interest that would have influenced the results or their interpretation. Authors should also properly acknowledge the work of others and ensure proper citation of such works in the manuscript. The authors should clearly state in the manuscript if the work involved the use of hazardous chemicals, procedures or equipment. The authors should co-operate in submitting the revised manuscripts before the deadline and providing befitting replies to the reviewer comments.

The authors should inform the Chief Editor when they discover significant errors or inaccuracies in their own published work and publish a corrigendum or retract the paper.

Journal of The Electrochemical Society of India

CODEN JESIA, No. 72 (3&4), July / December 2023. ISSN 0013-466X

Patrons of the Society

M/S Ronuk Industries
M/S Titanium Equipment and anode Mfg. Co.,
M/s Reliance Engineers, Bengaluru
M/s Degussa Electroplating Company
M/s B. T. Solders Pvt. Ltd., Mysore
M/s Khoday India Ltd., Bengaluru
M/s Metrohm India Pvt Ltd.
Ms. Mridula Shaw
Dr. C. H. Krishnamurthy Rao
Sri. S. K. Jain
Dr. Franz Simon
Sri. Arvind Toshniwal
Dr. N. Rajalakshmi, Former Head, CFCT, ARCI
Sri. Srihari Khoday

Donor Members

M/s. Mascot Chemical Works, Bengaluru
M/s. Indian Telephone Industries Ltd., Bengaluru
M/s. Kangovi Electronics (P) Ltd., Bengaluru
M/s. Aquair Control Systems, Bengaluru
M/s. Stiver Equipment Pvt. Ltd., Bengaluru
M/s. Hindustan Aeronautics Ltd., Bengaluru
M/s. High Energy Batteries, Madurai
M/s. Electroplating Equipment Co., Bengaluru
M/s. Galvanosols Pvt. Ltd., Bengaluru
M/s. Pyro Technologies, Bengaluru
M/s. Shruthi Enterprises, Bengaluru
M/s. Grauer Weil (India) Ltd., Mumbai
M/s. Zaveri Brothers (P) Ltd., Mumbai
M/s. Standard Batteries, Mumbai
M/s. Geep Industries Syndicate Ltd.
M/s. Larsen and Toubro Ltd., Mysore
M/s. IR Technology Services Pvt. Ltd.
M/s. Brite Platers and Electrical Engineers, Bengaluru
M/s. Vijaya Metal Finishers, Bengaluru
M/s. Vinpla Plating Pvt. Ltd., Bengaluru
M/s. Surface Chem Finishers, Bengaluru

Permanent Sustaining Members

M/s. Tata Chemical
M/s Ashok Charitable Trust, Karaikudi
M/s. Mysore Paper Mills, Bhadravathi
M/s. Tata Iron and Steel Company Ltd., Jamshedpur
M/s. DCM Chemical Works
M/s. Indian Aluminum Company Ltd., Alwaye
M/s. Visveswaraya Iron and Steel Ltd., Bhadravathi

THE ELECTROCHEMICAL SOCIETY OF INDIA

Indian Institute of Science Campus, Bangalore - 560012
Email: ecsiiisc@gmail.com
Website: www.ecsi.in

Governing Council 2023-2024

President

Dr. S.T. Aruna

Chief Editor, JECSI

Dr. U. Kamachi Mudali

Immediate Past President

Dr. U. Kamachi Mudali

Vice Presidents

Prof. S. Sampath, Mr. Deepak Parab, Prof. V. S. Raja, Prof. Alka Sharma

General Secretary	***Joint Secretary***	***Treasurer***
Dr. Prathibha B S	Dr. Ashwini Ravi	Sri. C. Antonisamy

Former Presidents

Prof. E.S. Dwarakadasa, Dr. H. B. Rudresh, Dr. Balagangadhar, Prof. A.K Sharma, Mr. M. Ravindranath

Former Secretaries

Dr. H.P. Nagaswarupa, Mr. Rajeev Deekshith, Dr. J.N. Balaraju, Dr. J.R Mudakavi

Members

Dr. Chaitanya Lekshmi, Dr. Pooja Sharma, Dr. Chittaranjan Hegde, Dr. J.N. Balaraju, Dr. N. Rajendran, Dr. Jagadeeshvara Rao, Dr. M. S. Santhosh, Dr. ShaheenTaj, Mr. P. G. Chandramani, Dr. T. M. Sridhar

Conducting polymeric hybrid implant coating: A strategy to improve electrochemical and osteocompatible properties

V Sudhisha, N Rajendran*

Department of Chemistry, CEG Campus, Anna University,

Chennai - 600 025, Tamil Nadu, India.

**Corresponding author Email: nrajendran@annauniv.edu*

Abstract:

The replacement of entire joint extent is one of the actual effective and common surgical techniques to support both hip as well as knee reconstruction. To cover-up with the mechanical strength and biological effect of in-situ natural bone, titanium is the only material of superior choice. In recent years, conducting polymers provide a complimentary platform as coating material, exclusively for orthopaedic application. Polythiophene derivatives have particular attention and in context poly(3,4-ethylenedioxythiophene) (PEDOT) is considered as the most gainful polythiophene derivative with its outstanding properties. PEDOT is practically used in device production, biomedicine, and bio-implants owing to the peculiar electrochemical and environmental permanency with respect to its oxidation state. The trace salt of gallium element boosts the content of phosphorous and calcium in bone, that in contrast electively serve for hypercalcemias as well. Gallium in hydroxyapatite matrix acts as a shield to improve the skeletal structure and in turn the biomechanical properties. In the current research an effort is made to understand the application of innovative implant with gallium doped PEDOT on titanium for orthopaedic practice. Through primary studies like SEM, EDX and FTIR the presence of predictable layer of PEDOT with Ga was acknowledged. Contact angle, electrochemical corrosion studies and in vitro immersion studies were performed and the outstanding results meet the required physicochemical standards to enrich in loco osteosynthesis.

Keywords: *Titanium; Poly(3,4-ethylenedioxythiophene) (PEDOT); Gallium; Corrosion; Bioactivity; Orthopaedic*

1. Introduction

Bone is exposed to numerous loading situations, sometimes the exposed load could cause cracks or affect the patient majorly [1]. To support such aforementioned problems, a substitute is used that maintain the prime concern and stay compatible with the bone. Biomaterials are observed with an express growth in research field of bone implants. After implantation, the occupied states of implants due to jumping, loading and running for a long term performance could lack the compatibility with original bone. Henceforth, the development of an implant should necessarily focus on mechanical strength and other properties to serve without any knockback [2]. To decrease the second revised surgery, the upgraded techniques have been initiated. Still 26% of failure cases were recorded in the past decade among aged patients. Metals have ensured the dominance for load bearing role in implant field [3]. Among the different metals used in orthopaedic, titanium is the strongest and lightweight metal that plays a critical load bearing function than other medically used implant metals such as cobalt-chromium alloys and steel. This material exhibits excellent biocompatibility that is attributed to the naturally obtained TiO2 layer on the surface. This oxide layer develops an osteoconductive layer with the interface and therefore bone cells get attracted. The surface roughness of titanium influences the growth factors. Thus, remodelling the titanium surface to achieve the roughness in implants provides in site cellular responses for a long time

in implants [4]. The surface coating is an important method to improve the significant performance of titanium.

Different biocompatible polymers are used in biomedical applications, out of that the conducting polymers such as poly(3,4-ethylenedioxythiophene) (PEDOT) have similar features to that of melanin. PEDOT polymer is known for its conductivity and chemical and environmental stability. The PEDOT coated surfaces are soft, remain relatively bioactive and protect the material from electrochemical corrosion [5]. Since the coating material is a very important part that provides the improved performance in implants, gallium was doped with PEDOT. The bioactivities such as skeletal metabolism, stress relief and bone resorption are improved with gallium. Plenty of reported cases were published with gallium for treating cancer-based hypercalcemia's and osteoporosis. There are studies proving the antimicrobial activities of the gallium metal. In accordance, gallium ions are gaining significance in medical field with anti-inflammatory, antiresorptive, immune suppressive behaviour and antiosteoporotic behaviour. Gallium is a highly efficient element that works effectively for treating hypercalcemia's [6]. In orthopaedics, gallium hinders the rate of apatite growth by adsorbing into crystal surface therefore, used in various biotechnological performances [7].

Electropolymerization is ordinarily accomplished through three methods such as (i) galvanostatic: performed by maintaining the constant current, (ii) potentiostatic: executed by applying constant voltage and (iii) potentiodynamic: within a definite voltage window, the cyclic voltage gets swept out. Fine tuning of the parameters of electropolymerization method, concentration of the dopant used, solvents and the type of dopant used the morphology, conductivity and thickness of the layer can be precisely controlled [8]. The aim of this research is to electropolymerize a layer of gallium doped PEDOT on titanium metal surface for improving the biological and electrochemical properties of titanium implant for a long term and load bearing application. This is mainly to eliminate the second painful revised surgery to replace the implant.

2. Materials and Methods

Commercial pure Titanium (Cp-Ti) samples sized 15 mm × 20 mm × 2mm acquired from TI Anode Fabricators Pvt. Ltd. Chennai, India were used. The test samples were mechanically polished by silicon carbide (SiC) papers from 80 to 1000 grits. The polished samples were washed with acetone and then with the distilled water.

Cyclic voltametric method was used for the electro-polymerization of EDOT and gallium nitrate on the titanium surface since it is a suitable, cost-effective and an easy process. The electropolymerization was carried out using PGSTAT Autolab-302 N electrochemical workstation by using a three-electrode cell system. Polished titanium substrate was used as working electrode (WE), a saturated calomel electrode was taken as reference electrode (RE) and a platinum foil was taken as a counter electrode (CE) respectively. The electrolyte used for the electrochemical polymerization was prepared using different concentrations of gallium nitrate, 0.3 M lithium perchlorate and 0.1 M EDOT. Poly (3,4-ethylene dioxythiophene) and gallium nitrate were polymerized on titanium surface at a sweeping potential rate between -0.1 and + 2.0 V with a scan rate of 0.03 mVs-1 for 5 cycles. After electro polymerization, the polymer coated substrate was washed with distilled water to eradicate the monomer particles and dried.

2.1. Characterization Techniques

The surface characterization of electropolymerized samples were examined using SEM with EDS (Tescan Vega 3 XMU). The chemical composition of the sample was confirmed through ATR-FTIR (Perkin Elmer Spectrum two, USA). The Contact angle analyser: Phoenix 300 plus was applied to observe the wettability of the samples.

2.2. Electrochemical Corrosion Studies

The potentiodynamic polarization studies were carried out for the samples having an exposed area of 1 cm^2. A conventional three electrode glass cell was used for all the electrochemical measurements. The cell assembly consisted of the test specimen as

the working electrode, a platinum foil as the counter electrode and the saturated calomel electrode (SCE) as reference electrode. The tests were performed in 250 ml Hanks` solution. The electrochemical workstation (PGSTAT model 302N, Meterohm Autolab B.V, Netherlands) was controlled by Nova 2.0 software. Potentiodynamic polarization studies were carried out in the potential range from -1.0 to 1.0V at a scan rate of 0.001V/s. The potentials recorded are with respect to standard calomel electrode. The corrosion current density (Icorr) and corrosion potential (Ecorr) were obtained from the polarization curves. The obtained corrosion current and corrosion potential represents the rate of corrosion of the working electrode. The current density is obtained using Stern – Geary equation given below [9].

$$i_{corr} = \frac{\beta a \times \beta b}{2.3\, Rp(\beta a + \beta b)}$$

Where βa and βb are the Tafel slopes of the anodic and cathodic parts of the Tafel plot respectively and Rp is the polarization resistance.

2.3. *In Vitro* Studies

In vitro studies were accomplished to inspect the apatite progression. The sample was immersed in freshly synthesized Hanks' solution with 7.4 pH. After 7 days of protective immersion, the characterizations such as SEM, and EDX were used to confirm the growth of apatite.

3. Results And Discussion

3.1. Morphological Studies of Ga/PEDOT

The titanium surface was coated with gallium doped PEDOT with different concentrations of gallium nitrate (0.005 and 0.006 M). Higher magnification SEM images of the coatings obtained by means of cyclic voltammetry are shown in Fig. 1. A stable coating of Ga/PEDOT was seen on both the sample surfaces with porous structure that are connected and branched in such a way with gallium oxide on it. In Ga/PEDOT(1), the coating is satisfactorily layered with PEDOT and gallium oxide and in case of Ga/PEDOT(2) the coating was very least coated. The surface should be completely covered and the appearance of random irregular voids provides a beneficial adherence of coatings. The monomers of EDOT have experienced the initial nucleation and fine accumulation with complete polymerization and deposition in Ga/PEDOT(1) on contrast of that of Ga/PEDOT(2) [10]. From the FESEM image, it is evident that the titanium surface is completely wrapped with Ga/PEDOT(1) and therefore, this sample was progressively used in this research.

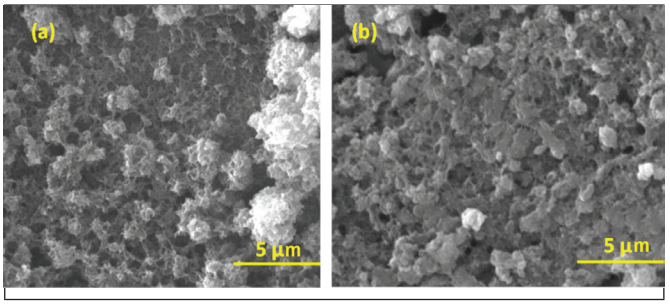

Fig. 1. SEM images of (a) Ga/PEDOT(1) and (b) Ga/PEDOT(2).

The quantitative chemical composition of Ga/PEDOT(1) was obtained through EDX microanalysis. Table 1 shows the relevant most variations of elements present in the implant material. In particular, titanium is the most abundant element with intense peak and Ga is the most minor element as shown in Fig.2. The presence of all essential elements such as Ti, O, C, S and Ga are ascribed to the trend of chemical composition and their presence on the surface of the fabricated implant material.

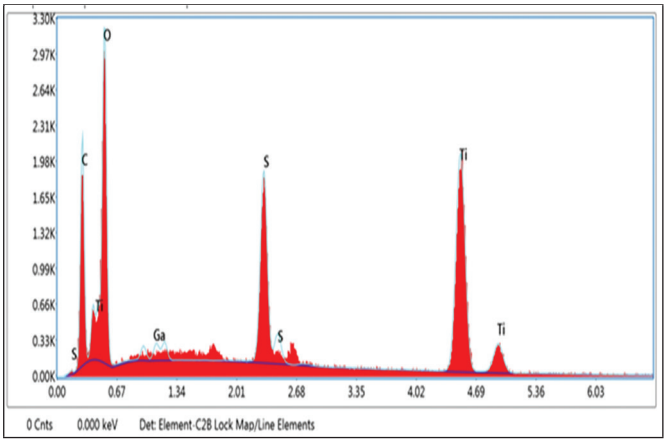

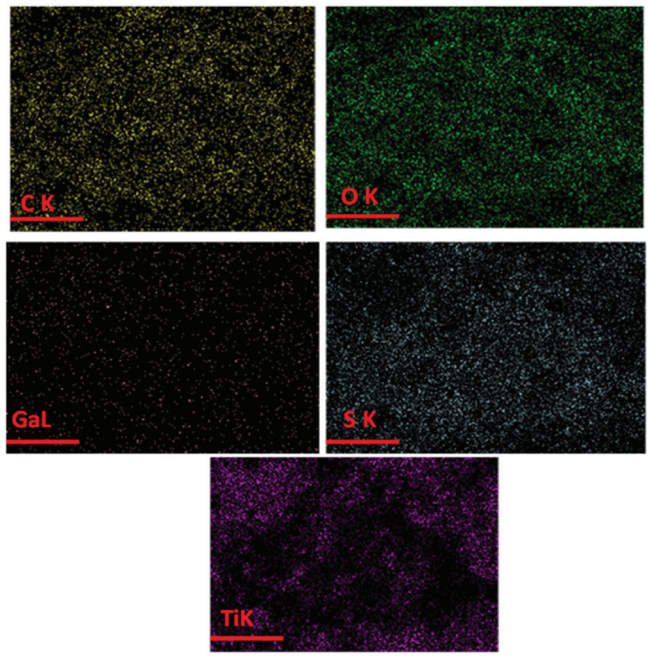

Fig. 2. EDX profile of Ga/PEDOT (1).

Table 1. Parameters obtained from EDX profile of Ga/PEDOT (1)

S.No.	Elements	Weight %	Atomic %	Error %
1.	C K	9.14	20.77	9.22
2.	O K	21.55	36.78	10.50
3.	Ga L	0.95	0.38	8.92
4.	S K	11.07	9.42	3.70
5.	Ti K	57.29	32.65	4.27

3.2. Electropolymerization using cyclic voltammetry method

In cyclic voltammetry of Ga doped PEDOT, both anodic and cathodic scans during the completion of electropolymerization are shown in Fig. 3. Through the anodic reaction, Ga and PEDOT are coated and the coating removal occurs during the cathodic scans. It is a reversible scanning process and both the scans require equal charges and develop a nucleation loop. The monomer EDOT and $Ga(NO_3)_3$ with the support of $LiClO_4$ get coated as Ga/PEDOT on titanium substrate. Technically in the graph, next to the switching potential one can observe that the current at oxidation scan is more than the current produced at the reduction scan that represents the effects of polymer nucleation process. This is the evident that there is a homogeneous connection that occurs within the starting monomer ions and the oligomer products respectively [11].

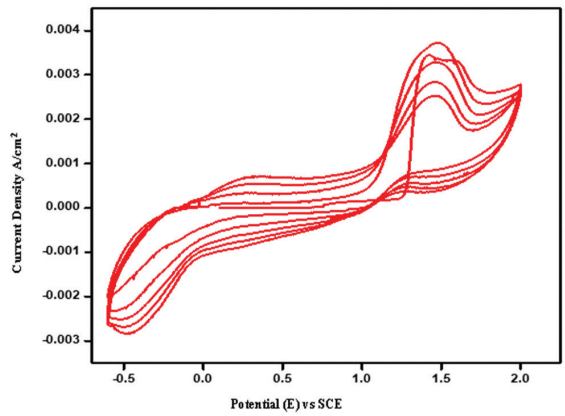

Fig. 3. Cyclic voltammogram curves of Ga/PEDOT (1).

As the coating is an electro active polymer layer, the thickness of the coating increases when the additional crosslinking deponent Ga is used. If the coated layer becomes thicker and bulky, this bulking effect will limit the adhesion towards the titanium substrate. Therefore, a uniform and flat layered coatings of the polymer without any bulking features aids the positive interactions necessary for orthopaedic applications and stay for a long period [12]. For this reason, only 5 scans were accomplished for the successful electropolymerization of Ga/PEDOT on titanium surface.

3.3. ATR-FTIR analysis

To identify the functional groups, ATR-FTIR spectra of bare and Ga/PEDOT(1) were recorded in the range of 450–4000 cm^{-1} (Fig. 4). The bare substrate spectrum shows a dominant peak of titanium at 489 cm^{-1}. The surface of titanium contains its oxide layer and therefore, the oxide formation of titanium is represented through this resultant peak. The spectrum of Ga/PEDOT (1) shows a peak at 495 cm^{-1} which indicates the presence of Ti-O stretching vibrations. The peak obtained at 628 cm^{-1} represents the appearance of stretching vibrations

in Ga-O [13]. A small bend at 811 cm^{-1} is obtained which is attributed to C-S of the thiophene ring. The peak at 1010 cm-1 describes the bending vibration of oxyethylene thiophene ring [14]. At 1329 cm^{-1}, the small peak shows the occurrence of C-C bond and at 1537 cm^{-1} shows the confirmation of alternative C=C bond in the ring structure [15]. The absorption peak at 1818 cm^{-1} is attributed to C-O bond of PEDOT. The peaks at 2050 cm^{-1}, 2240 cm^{-1} and 2647 cm^{-1} represents -CH_2 bond. The formation of –OH group was identified and matched with the peaks at 3199 cm^{-1} and 3799 cm^{-1}. The presence of gallium doped PEDOT was further confirmed through this characterization technique and the possible interactions and bonding were verified.

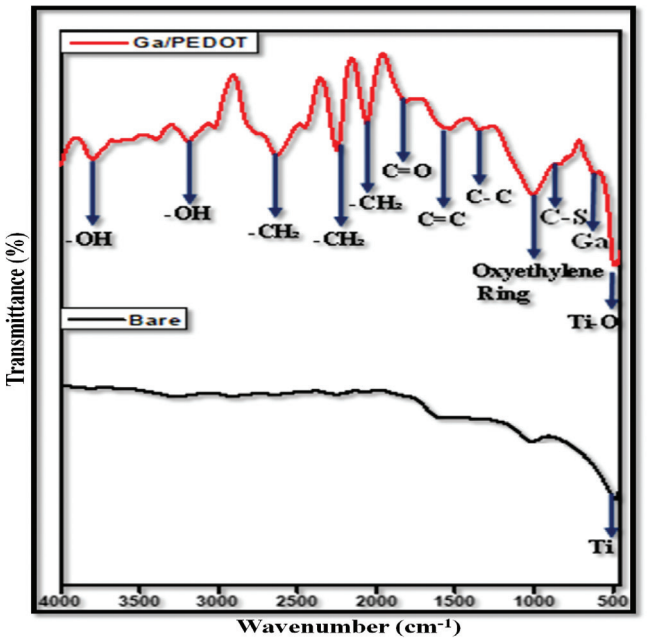

Fig. 4. ATR FTIR of bare and Ga/PEDOT (1).

3.4. Contact angle measurements

Any bio-implant should be studied for its surface wettability to understand the bioactivity including protein adsorption, proliferation and cell adhesion. The wettability of an implant surface are connected with the topography and chemistry of that particular surface [16]. The contact angle measurements were carried out on the Ti substrate and the substrates coated with Ga/PEDOT(1) and Ga/PEDOT(2) and the graphical representation with images are shown in Fig. 5. The roughness found at the metal surface affects the properties and significant structures that develop a live interaction with biological matter [17]. With respect to this, the material surface showing a water contact angle (WCA) greater than 90º is considered scientifically as a hydrophobic one [18]. Therefore, the bare substrate with TiO_2 on the surface exhibits WCA of 104.2º, which is hydrophobic and represents the obstacles in adhesion, migration and growth of cells. The particles gets aggregated into the body fluids and develop weaker cell bonding [19]. In coated samples, the initial oxidized layer has been covered with polymer PEDOT and gallium. Thus, Ga/PEDOT(1) and Ga/PEDOT(2) shows hydrophilicity with the average WCA values were 67.6º and 51.0º respectively. The cell walls in human tend to interconnect and attach with the hydrophilic surfaces for the betterment of growth [20]. More roughness develops the wettability and enhances the cell attachments by the adsorption of required proteins.

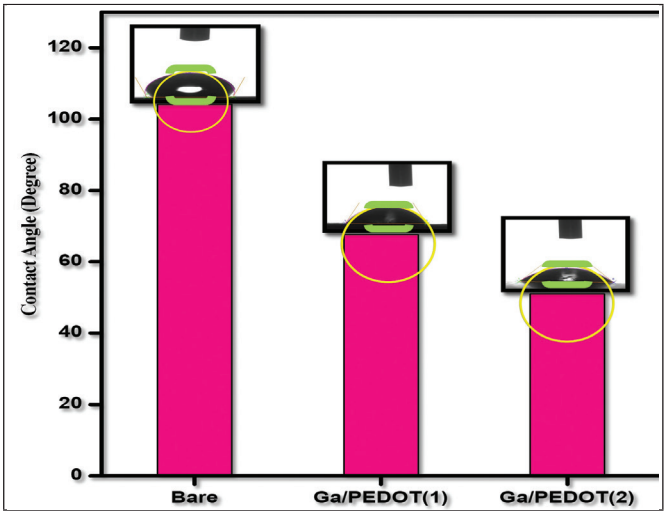

Fig. 5. Contact angle measurements on Ti and coated surfaces.

3.5. Electrochemical corrosion studies

3.5.1. Potentiodynamic polarization studies

The potentiodynamic polarization curves were recorded for bare titanium and Ga/PEDOT(1) coating in Hanks' solution as the electrolyte to assess the corresponding biological activity of the implant. The unique potentiodynamic polarization curves plotted for bare and Ga/PEDOT(1) are shown in Fig. 6 and the respective electrochemical values calculated are summarized in table 2. The corrosion

current density called Icorr value is established from cathodic curves of the graph. The Ecorr value obtained from the graph shows a positive shift in Ga/PEDOT(1) with respect to the bare substrate. This indicates improved corrosion resistance of the titanium surface containing gallium-PEDOT. In the literature it has been reported improved corrosion resistance of gallium and its alloys [21]. The uniform coating of conducting polymer, PEDOT as a passive layer increases the protective mechanism in the corrosive medium [22]. Overall, Ga/PEDOT(1) is a promising coating for orthopaedic applications with respect to corrosion performance.

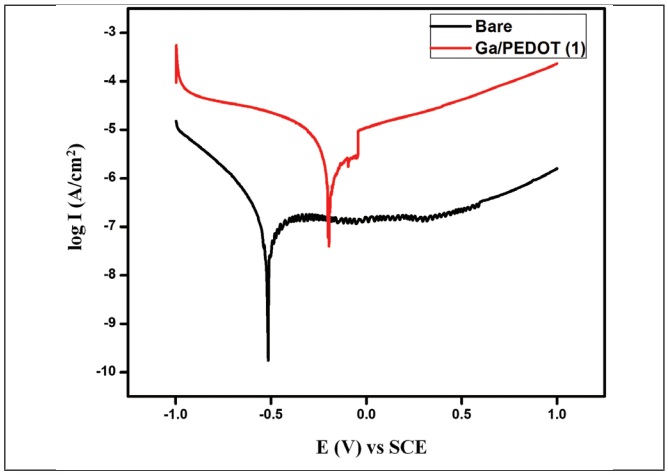

Fig. 6. Potentiodynamic polarization curves of bare and Ga/PEDOT (1).

Table 2: Parameters of potentiodynamic polarization studies

S. No.	Sample	E_{corr} (V)	Icorr (μA/cm²)
1	Bare	-0.515	0.54
2	Ga/PEDOT(1)	-0.194	1.49

3.5.2. Electrochemical impedance spectroscopic studies

An ideal orthopaedic implant material in human body should retain outstanding corrosion resistance against the physiological environment. Electrochemical impedance spectroscopy (EIS) is a very beneficial approach to observe the electrochemical in situ changes. This method helps in understanding the physical deviations happening at the interface of electrode and electrolyte [23]. The obtained results were plotted in the form of Nyquist, Bode phase angle and Bode impedance. The respective graphs of bare and Ga/PEDOT(1) are displayed in Fig. 7. The Nyquist graphs (Fig.7a) shows a higher diameter for Ga/PEDOT(1) than the bare sample. This explains that the more passivity of Ga/PEDOT(1) against corrosion. This is again verified with Bode studies which is a reliable method to gain extracted information about diffusion impedance, rate of charge transfer and its processes, solution resistance and double layer capacitance. The conducting polymer (PEDOT) coatings with low porosity, dense and adherent layer of gallium nitrate maintains a restricted access for the electrolytic oxidants and ions. Here the conducting polymer coating forms a protective layer on the surface of metals, this mechanism is called as anodic protection mechanism [24]. From Fig. 7 (b & c) also shows improved corrosion resistance of Ga/PEDOT(1) than bare material.

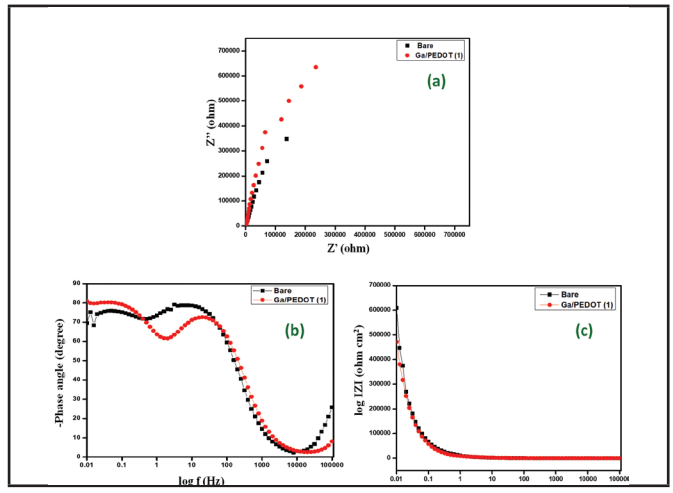

Fig. 7. Electrochemical impedance plots of bare Ti and Ga/PEDOT(1) surface on Ti.

3.6. *In vitro* studies

The biomineralization is a process that provides a bridging the bone-implant with the natural bone. The natural bone of human could get fused with the biomaterial implant and osseointegration takes place. As an initial prediction, the sample was taken for Hanks' immersion test. Ga/PEDOT(1) was soaked in Hanks' solution for 7 days to identify the early bioactivity of the material. After 7 days, the bioactivity of the material depends directly on the amount of apatite induced on the implant surface.

Based on this, the material will be considered as a bioactive one [25]. Fig. 8 shows the SEM image of Ga/PEDOT(1) after 7 days of immersion in Hanks' solution.

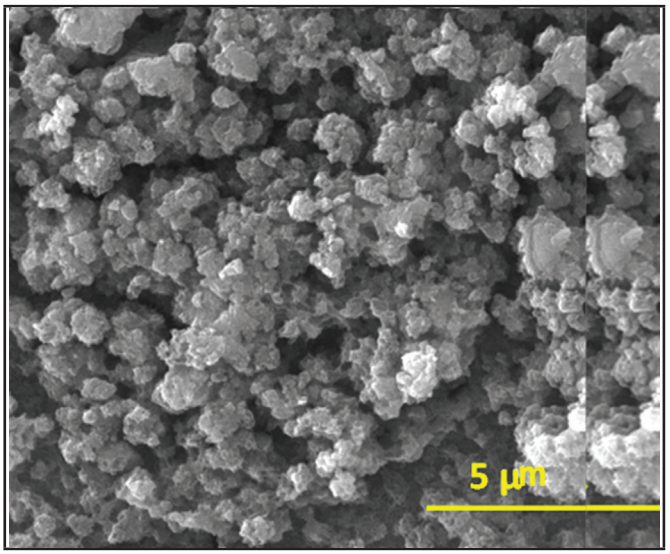

Fig. 8. SEM of Ga/PEDOT(1) after 7 days of Hanks' soaking.

There are few parameters to prominently modify the bone forming aptitude of the biomaterial including roughness, impurity content, crystal size, surface chemistry and morphology [26]. By taking all the above criteria we could match with the apatite growth on the surface through the top view SEM image after 7 days of immersion. The clear growth of hydroxyapatite is layered up as crystalline spherical structures with calcium and phosphate groups on it.

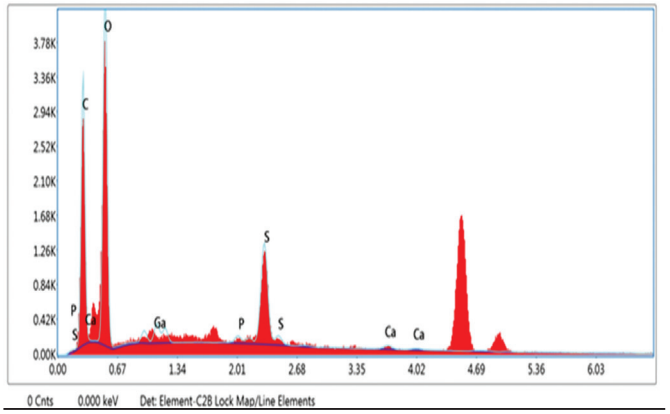

Fig. 9. EDX profile of Ga/PEDOT(1) after 7 days of Hanks' soaking.

The growth of apatite as calcium and phosphate along with the occurrence of carbon, oxygen, sulphur and gallium is verified through EDX (Fig. 9) of Ga/PEDOT(1) after 7 days of immersion respectively. The clear discrimination of the weight percentage in each element is represented through the data given in Table. 3. The total in vitro characterization represents that Ga/PEDOT(1) is biologically active by establishing a positive osseointegration accountable for orthopaedic application that meets up the expectations of the researchers.

Table 3 Elemental analysis of Ga/PEDOT(1) after immersion in Hanks' solution for 7 days

S. No.	Elements	Weight %	Atomic %	Error %
1.	C K	38.11	50.86	9.57
2.	O K	38.28	38.35	8.46
3.	Ga L	3.12	0.72	6.07
4.	P K	1.01	0.52	15.29
5.	S K	17.60	8.80	3.85
6.	Ca K	1.87	0.75	29.22

4. Conclusions

In conclusion, this work examined the improved electrochemical and biological performance of modified polymeric hybrid titanium implant. The surface modification of titanium by the electropolymerization of gallium doped PEDOT was strategically performed at different concentrations of gallium using cyclic voltammetry method. The confirmation of the overlaid coating was verified with SEM, EDX and FTIR. The gallium addition in PEDOT matrix in a very small amount has effectively enhanced the corrosion resistance. The thin degradable layer of Ga/PEDOT on titanium surface ensures the positive attitude towards the biological performance required for osseointegration, determined through immersion studies. This has been correlated with contact angle measurement showing good wettability on Ga/PEDOT(1) surface. In summary, the developed polymeric hybrid implant material containing appropriate amount of gallium improves the patient's expectancy in progressive bone healing (Hip & knee) with titanium base.

References

[1] RP Verma. Titanium based biomaterial for bone implants: A mini review. Materials Today: Proceedings 2020;26:3148-51.

[2] C Hu, D Ashok, DR Nisbet, V Gautam. Bioinspired surface modification of orthopedic implants for bone tissue engineering. Biomaterials 2019;219:119366.

[3] AI Greer, V Goriainov, J Kanczler, CR Black, L-A Turner, RM Meek, et al. Nanopatterned titanium implants accelerate bone formation in vivo. ACS applied materials & interfaces 2020;12:33541-9.

[4] K Suzuki, K Aoki, K Ohya. Effects of surface roughness of titanium implants on bone remodeling activity of femur in rabbits. Bone 1997;21:507-14.

[5] M Chozhanathmisra, D Govindaraj, P Karthikeyan, K Pandian, L Mitu, R Rajavel. Fabrication of Bilayer Coating of Poly (3, 4-ethylenedioxythiophene)-Halloysite/ Chitosan and Mg^{2+}/Sr^{2+}-Doped HAP on Titanium Alloy for Biomedical Implant Applications: Physicochemical and In Vitro Biological Performances Studies. Journal of Chemistry 2018; https://doi.org/10.1155/2018/9813827.

[6] P Melnikov, A Malzac, MdB Coelho. Gallium and bone pathology. Acta Ortopédica Brasileira 2008;16:54-7, https://doi.org/10.1590/S1413-78522008000100011.

[7] B Nayak, PK Misra. Exploration of the structural and dielectric characteristics of a potent hydroxyapatite coated gallium bioceramics for the forthcoming biomedical and orthopedic applications. Materials Chemistry and Physics 2020;239:121967, https://doi.org/10.1016/j.matchemphys.2019.121967.

[8] C Bodart, N Rossetti, JE Hagler, P Chevreau, D Chhin, F Soavi, et al. Electropolymerized poly (3, 4-ethylenedioxythiophene)(PEDOT) coatings for implantable deep-brain-stimulating microelectrodes. ACS applied materials & interfaces 2019;11:17226-33, https://doi.org/10.1021/acsami.9b03088.

[9] M Stern, AL Geary. Electrochemical polarization: I. A theoretical analysis of the shape of polarization curves. Journal of the electrochemical society 1957;104:56, 10.1149/1.2428496 .

[10] A Madhankumar, S Ramakrishna, P Sudhagar, H Kim, YS Kang, I Obot, et al. An electrochemical, in vitro bioactivity, and quantum chemical approach to nanostructured copolymer coatings for orthopedic applications. Journal of Materials Science 2014;49:4067-80, 10.1007/s10853-014-8094-6 .

[11] E Tamburri, S Orlanducci, F Toschi, ML Terranova, D Passeri. Growth mechanisms, morphology, and electroactivity of PEDOT layers produced by electrochemical routes in aqueous medium. Synthetic metals 2009;159:406-14, https://doi.org/10.1016/j.synthmet.2008.10.014.

[12] B Wei, J Liu, L Ouyang, C-C Kuo, DC Martin. Significant enhancement of PEDOT thin film adhesion to inorganic solid substrates with EDOT-acid. ACS applied materials & interfaces 2015;7:15388-94, https://doi.org/10.1021/acsami.5b03350.

[13] HA Aldossary, MM Khalaf, M Gouda, A Elmushyakhi, MF Abou Taleb, HM Abd El-Lateef. Wound dressing candidate materials based on casted films of cellulose acetate modified with zirconium oxide (ZrO^2), and gallium oxide (Ga^2O^3). Materials Today Communications 2023;34:105299, https://doi.org/10.1016/j.mtcomm.2022.105299.

[14] V Sudhisha, K Saranya, M Kalaiyarasan, N Rajendran. Silver nanoparticles doped poly (3, 4-ethylene dioxythiophene) on titania nanotubes for orthopaedic application. Applied Surface Science 2023;610:155416, https://doi.org/10.1016/j.apsusc.2022.155416.

[15] V Sudhisha, N Rajendran. ZnP-PEDOT: A potential hybrid coating on titania nanotubes For orthopaedic applications. Surfaces and Interfaces 2023;39:102898, https://doi.org/10.1016/j.surfin.2023.102898.

[16] Behera R, Das A, Hasan A, Pamu D, Pandey L, Sankar M. Deposition of biphasic calcium phosphate film on laser surface textured Ti–6Al–4V and its effect on different biological properties for orthopedic applications. Journal of Alloys and Compounds 2020;842:155683, https://doi.org/10.1016/j.jallcom.2020.155683.

[17] N Eliaz, S Shmueli, I Shur, D Benayahu, D Aronov, G Rosenman. The effect of surface treatment on the surface texture and contact angle of electrochemically deposited hydroxyapatite coating and on its interaction with bone-forming cells. Acta biomaterialia 2009;5:3178-91, https://doi.org/10.1016/j.actbio.2009.04.005.

[18] P Sawadkar, J Mohanakrishnan, P Rajasekar, B Rahmani, N Kohli, L Bozec, et al. A synergistic relationship between polycaprolactone and natural polymers enhances the physical properties and biological activity of scaffolds. ACS applied materials & interfaces 2020;12:13587-97, https://doi.org/10.1021/acsami.9b19715 .

[19] AC De Felice, V Di Lisio, I Francolini, A Mariano, A Piozzi, A Scotto d'Abusco, et al. One-Pot Preparation of Hydrophilic Polylactide Porous Scaffolds by Using Safe Solvent and Choline Taurinate Ionic Liquid. Pharmaceutics 2022;14:158, https://doi.org/10.3390/pharmaceutics14010158.

[20] S Bauer, J Park, K von der Mark, P Schmuki. Improved attachment of mesenchymal stem cells on super-hydrophobic TiO^2 nanotubes. Acta biomaterialia 2008;4:1576-82, https://doi.org/10.1016/j.actbio.2008.04.004.

[21] Z Wu, J Hu, L Yu, K Wang, W Zhang, H Fan, et al. Corrosion behavior investigation of gallium coating on magnesium alloy in simulated body fluid. Journal of Materials Research and Technology 2023, https://doi.org/10.1016/j.jmrt.2023.09.271.

[22] V Sudhisha, P Agilan, P Cheranmadevi, N Rajendran. Electropolymerized PEDOT/TNTA hybrid composite: A promising biomaterial for orthopaedic application. Applied Surface Science 2022;595:153534, https://doi.org/10.1016/j.apsusc.2022.153534.

[23] SHS Zein, MF Abdullah. Electrochemical Impedance Spectroscopy (EIS) study of modified type-316L Stainless Steel (SS) as an effective biomaterial for orthopedic implant applications. Journal of Nanomedicine and Nanotechnology 2012;3, https://doi.org/10.4172/2157-7439.1000e108.

[24] PP Deshpande, NG Jadhav, VJ Gelling, D Sazou. Conducting polymers for corrosion protection: a review. Journal of Coatings Technology and Research 2014;11:473-94, 10.1007/s11998-014-9586-7.

[25] X Wang, F Liu, Y Song. Enhanced corrosion resistance and in vitro bioactivity of NiTi alloys modified with hydroxyapatite-containing Al2O3 coatings. Surface and Coatings Technology 2018;344:288-94, https://doi.org/10.1016/j.surfcoat.2018.03.034.

[26] MS Safavi, J Khalil-Allafi, L Visai. Improved osteogenic activity of NiTi orthopedic implant by HAp-$N^{b2}O^5$ composite coatings: Materials and biological points of view. Biomaterials Advances 2023;150:213435, https://doi.org/10.1016/j.bioadv.2023.213435.

Corrosion performance of electroless Ni-B coatings reinforced with YSZ nanoparticle

C.Chenna Raidu[a,b], N. Arunachalam [b,*] and S. Boominatha sellarajan [b]

[a]*Combat Vehicles Research & Development Establishment (CVRDE), DRDO, Chennai–600054, India*

[b] *Department of Mechanical Engineering, Indian Institute of Technology Madras, Chennai–600036, India*

**Corresponding Author Email: chalam@iitm.ac.in*

Abstract :

This study investigates the corrosion performance of an electroless coating incorporating 3 mol% YSZ nanoparticle reinforcement in the matrix of Ni-B. The objective is to produce a nanoceramic composite coating and analyze its impact on corrosion properties in both untreated and treated conditions. The composition of the coatings is identified using energy-dispersive X-ray (EDX) spectroscopy and particle dispersion and coating thickness are investigated using scanning electron microscopy (SEM). Further, hardness is evaluated through Vickers micro hardness tests and structural analysis by X-ray diffraction (XRD). Potentiodynamic polarization provides insights into the corrosion resistance or susceptibility of the material. At the same time, electrochemical impedance spectroscopy (EIS) evaluates the electrochemical properties of a system or material over a broader frequency range (10 mHz-1 MHz). The findings indicate that the heat-treated coatings exhibit high hardness due to strengthening mechanisms associated with the crystalline structure, but it also results in a decrease in corrosion resistance. Specifically, in the case of the Ni-B alloy, the heat-treated (HT) coatings display lower corrosion resistance compared to the as-plated Ni-B coatings. Conversely, in the case of heat-treated Ni-B-YSZ coatings, the corrosion resistance exceeds that of the as-plated nano-composite coatings. These findings reveal potential applications of YSZ-reinforced Ni-B coatings for combating environments prone to corrosion and thus demonstrating enhanced strength for numerous versatile fields of application.

Keywords: *Electroless, Nickel Boron, Corrosion, EIS, Ni-B-YSZ.*

1. Introduction

The behaviour of coatings in harsh environments has a significant impact on the reliability and durability of components in industries such as automotive, aerospace, gas turbine and marine [1,2]. Electroless nanocomposite coatings offer a promising solution by providing uniform coating thickness and strong adhesion to complex shapes [3]. These coatings typically contain a high boron content of approx. 6-8%, which can contribute to increased hardness. Heat treatment can lead to further improvement in the hardness of the material [4]. This improvement is attributed to changes in its crystalline structure, which promotes the formation of nickel borides (Ni_2B and Ni_3B). This transition enhances wear resistance but may deteriorate the corrosion resistance of the coating due to its heterogeneous composition that can induce galvanic coupling [5]. In addition to that, Ni-B alloy coatings are less corrosion-resistant than Ni-P variant [6]. To address this, YSZ (Yttria-Stabilized Zirconia) ceramic nanoparticles are incorporated into the Ni-B matrix to form nanocomposites. These nanocomposites possess unique properties, such as excellent thermal insulation, high wear resistance and resistance to corrosive environments, making them suitable for various applications across different industries. However, despite their potential, the behaviour and corrosion protection of YSZ coatings within the Ni-B matrix, particularly under heat-treated conditions, have not been extensively investigated.

This research investigates the corrosion resistant properties of YSZ-reinforced Ni-B matrix in untreated and treated conditions. In order to accomplish this, the study utilized various characterization techniques to analyze the

coatings' surface morphology, structural features, microhardness, and electrochemical properties. This comprehensive evaluation provides valuable insights into their performance and resistance to corrosion, facilitating their suitability for diverse applications.

2. Materials and Methods

In this study, a coating was applied to high-strength low alloy steel (AISI 4140) using the well-known electroless coating. The steel samples were 20 x 20 x 4 mm3 in size and were first prepared by grinding and polishing with 800 and 1200 grit abrasive papers. Consequently, after acetone cleaning for 10 minutes at 55°C in an ultrasonic bath, the surface was pickled in a 50% HCl solution for one minute and rinsed with de-ionized water before being coating [7].

An electroless coating bath was prepared as per the given Table 1 [8,9]. In addition to the Ni-B alloy, the YSZ particles were plated by electroless method using an alkaline borohydride-reduced type-2 coating process in accordance with ASTM B607-91 (2003) [10], The YSZ nano-suspensions were prepared separately with sodium dodecyl sulphate (SDS) using ultrasonic agitation process [11]. The prepared nano-suspension (1 g/L) was added to the plating solution after 15 minutes of initial Ni-B coating to improve particle adherence and dispersion in the Ni-B matrix [12]. The coating process was done in a 200 mL bath with a pH of 13.5 and the temperature of 95±1 °C.

Table 1. Electrolyte bath composition

Chemical	Formula	g/L
Nickel Chloride hexahydrate	$NiCl_2$ $6H_2O$	20.0
Sodium Borohydride	$NaBH_4$	01.0
Ethylenediamine	$C_2H_8N_2$	59.0
Sodium Hydroxide	NaOH	40.0
Lead Nitrate	Pb $(NO_3)_2$	0.015
Sodium dodecyl sulfate	$CH_3(CH_2)_{11}OSO_3Na$	0.025
Yttria stabilized zirconia (30-80 nm)	3 mol % Y_2O_3-ZrO_2--	1.0

A baffle furnace was used to heat-treat the coated samples. The heating technique entailed increasing the temperature from ambient to 400 °C and soaking it for an hour. Subsequently, the samples were cooled inside the furnace until they reach room temperature. This heat treatment method is widely used and has been optimized by many researchers for such coatings [4,13]. Scanning electron microscopy (SEM, FEI) was used to analyze the surface morphology of coatings. An X-ray diffractometer (XRD) with Cu-Kα radiation was used to ascertain structural properties. Microhardness testing was conducted on the coatings using a Matsuzawa MMT-X7 model with a Vicker's diamond indenter, by ASTM standards E92-03 [14] and E384. Hardness measurements were performed at multiple locations, and the analysis considered the average of five different locations for the evaluation. The corrosion test of both, polarization tests in accordance with ASTM G5-14 [15] and electrochemical impedance tests in accordance with ASTM G106-10 [16] were carried out in a 3.5% NaCl solution at ambient temperature using an AMETEK multichannel potentiostat with a three-electrode configuration, the experiment scans between -0.25 and 0.25 V vs. open circuit potential at a rate of 1 mV/s using graphite as the counter electrode and a standard calomel electrode (SCE) as the reference electrode.

3. Results and Discussion

3.1 Microstructural characteristics

Figure 1a illustrates the surface morphology of Ni-B-YSZ coating which shows a distinctive broccoli-like structure characterized by smaller and finer nodules than Ni-B alloy coatings [17]. The inset of Fig 1a with enlarged image highlights the embedded particles which hinder the grain flow. The particles dispersion of YSZ in the Ni-B matrix is shown in Fig.1b. The plating process efficiently incorporates particles into the coating without much agglomeration. Particle dispersion in the coating plays a crucial role in enhancing its hardness, wear resistance, and corrosion resistance [18]. The particles act as barriers, impeding the movement of corrosive species and restricting their access to the substrate [11]. This dispersion is essential

for achieving improved protective properties in the coating. As a result, the corrosion process is decelerated, ensuring long-term protection against corrosion [19].

Figure 1c depicts a cross-sectional image of Ni-B-YSZ, HT coating with typical thickness of ~18 ± 1 µm, which is within the usual range of electroless coating deposition rates [17]. The coating looked uniform and was devoid of pin holes, voids, or agglomeration, emphasizing its strength. Heat treatment strengthens the coating further, potentially sealing pores. This results in higher impedance across a broad frequency spectrum indicating enhanced corrosion resistance. Further, the white layer is absorbed at the coating-substrate interface as a result of chemical reactions or phase transformations. This white layer serves as an additional barrier layer, offering supplementary protection against corrosion, wear and environmental factors.

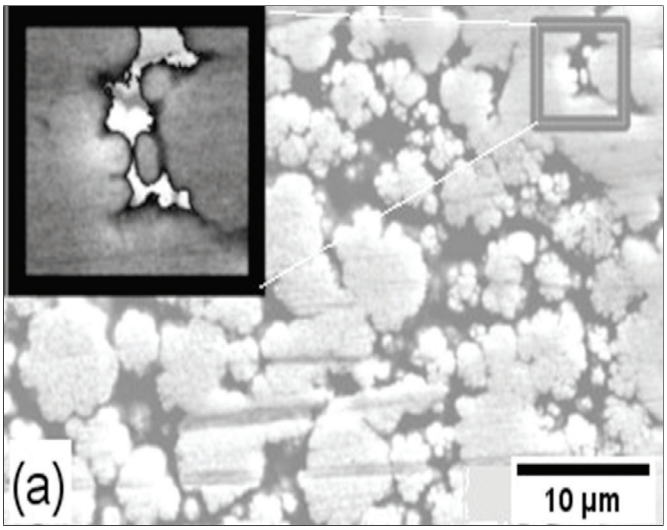

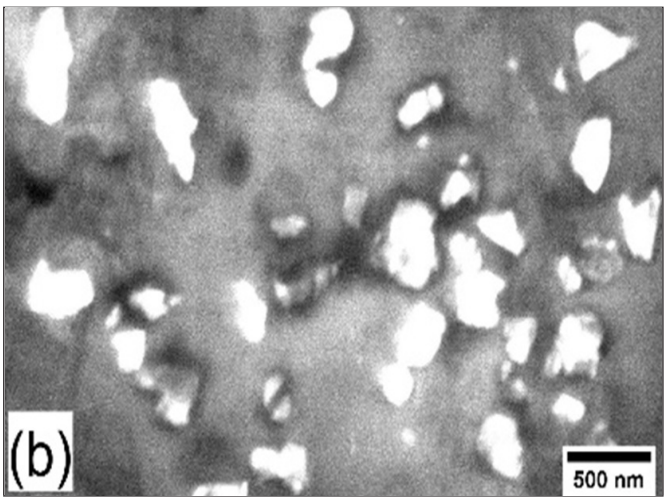

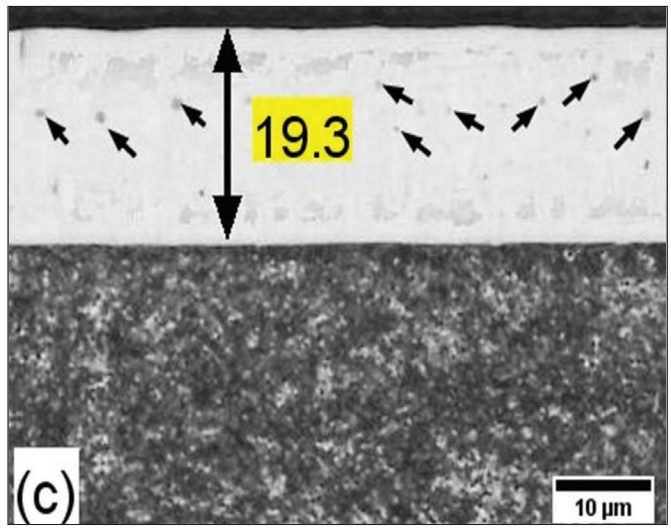

Fig 1. SEM images of (a) Ni-B-YSZ surface and its (b) dispersion and (c) cross section

The XRD analysis of the Ni-B coating, illustrated in Fig. 2a, reveals its amorphous nature in the untreated condition [20]. It exhibits a single broad peak corresponding to (111) at 2θ ≈ 43.64° plane of FCC nickel. During heat-treatment, electroless Ni-B coating undergoes a transformation and the nickel (Ni) and boron (B) atoms rearrange and react with each other to form Ni2B and Ni3B solid solutions. This transformation occurs as a result of diffusion and interatomic bonding at elevated temperatures, leading to the formation of new crystalline phases within the coating structure. The crystalline phases are identified as Ni2B (211) at 2θ ≈ 45.24° and Ni3B (201) at 2θ ≈ 46.32°. These compounds are harder than the base alloy matrix, resulting in improved wear resistance and mechanical properties [21,22].

Figure 2b illustrates the phase orientation and structural characteristics of heat treated Ni-B-YSZ coatings. The analysis reveals the presence of several peaks, with notable peaks observed at 2θ ≈ 45.78° corresponding to the NiY (131) phase and at 2θ ≈ 46.89° corresponding to the YSZ (222) phase.

These peaks provide clear identification of the YSZ material within the coating. The sharp and well-defined nature of these peaks indicates a high degree of crystallinity in the heat-treated coatings [23].

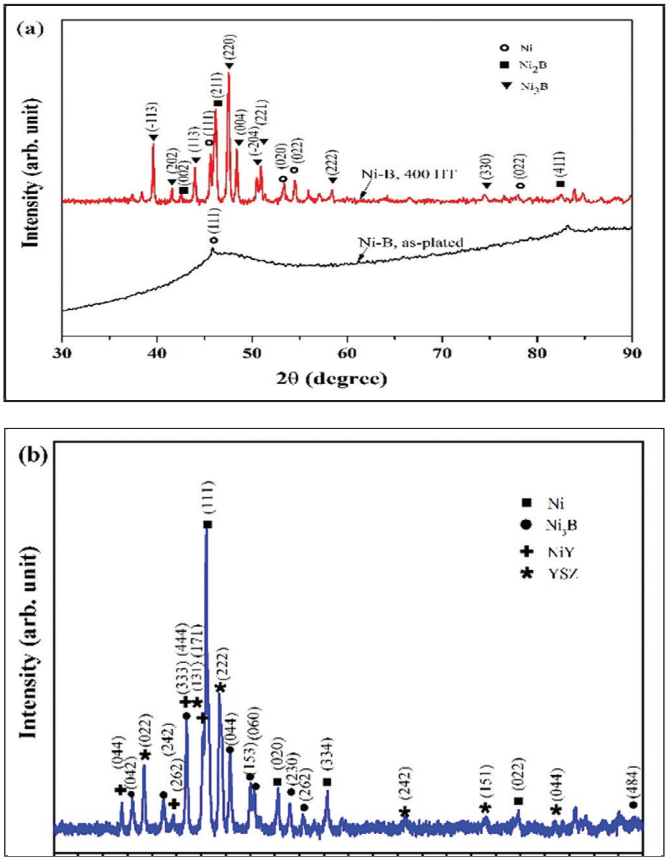

Fig. 2. XRD spectra of (a) Ni-B alloy coatings un-treated and treated condition and (b) heat treated Ni-B-YSZ.

Figure 3a shows the EDX spectra containing 6-8% of nickel and boron elements. The content of boron is an influential factor for the mechanical and corrosion properties of the coating. In the case of Ni-B-YSZ electroless coating (Fig 3b), the EDX analysis reveals the presence of Y and Zr elements, providing information about their distribution within the coating. Additionally, any potential impurities or undesired elements that could influence the coating's performance can be identified through this analysis.

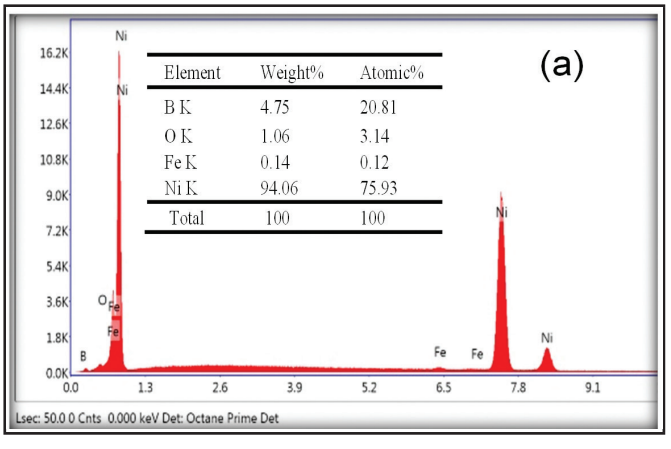

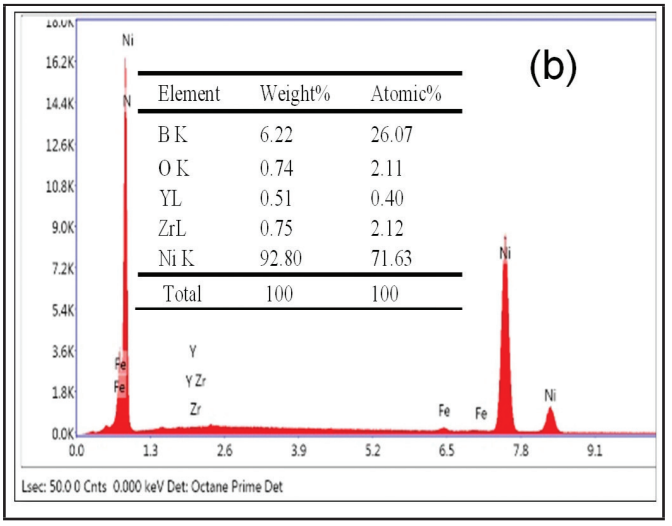

Fig. 3. The EDX elemental composition includes coatings made of (a) Ni-B alloy and (b) Ni-B-YSZ composite.

Vickers` microhardness is employed to assess hardness of the coatings. Upon heat treatment, the untreated Ni-B coating exhibits an increase in hardness from 806 ± 10 HV0.1 to 1080 ± 14 HV0.1. In comparison, the substrate exhibits a hardness of 364 ± 12 HV0.1. The transition from amorphous to crystalline phases during the annealing process is responsible for the noticeable improvement in hardness of the coating. Additionally, the structural arrangement of tetragonal boron within the coating contributes to the enhanced hardness [24-26].

The untreated Ni-B-YSZ coating exhibits a hardness value of 980 ± 12 HV0.1, which increases to 1265 ± 16 HV0.1 after undergoing heat treatment. It is primarily due to the Orowan dispersion strengthening process. In this mechanism, the dispersed particles within the coating serve as obstacles, impeding the movement of dislocations and offering additional resistance. Several factors, including the distance between dispersed particles, the ability of hard particles to prevent dislocation motion, and the influence of grain refinement, contribute to the overall strengthening effect [11].

3.2 Corrosion properties

Figure 4a demonstrates the Tafel extrapolation curve, providing insights into the mixed anodic and cathodic reaction. The corrosion potential (Ecorr)

and logarithm of current density (icorr) were obtained by extrapolating the data from the cathodic and anodic branches of the polarization curves (βc and βa, respectively). Additionally, the polarization resistance (Rp) was calculated using the Stern-Geary equation, as described in Eq. (1) [27]. The resulting values are summarized in Table 2.

$$R_p = \frac{\beta_a * \beta_c}{2.303 * i_{corr} * (\beta_a + \beta_c)} \quad \text{-------- (1)}$$

The Ni-B as-plated coating displays a lower corrosion current density (icorr) and a noble shift in corrosion potential (Ecorr) compared to the substrate, indicating improved protective ability. The cathodic overpotential reaction also shows a lower response, indicating a higher absorption of dissolved oxygen compared to the substrate. Additionally, the cathodic curve, except for the substrate, exhibits a similar reaction for coatings. The corrosion resistance of the heat-treated Ni-B coating is inferior to that of the Ni-B coating in its as-plated state. This is attributed to the presence of a non-homogeneous and amorphous structure in the as-plated coatings. The absence of a well-defined crystal structure in the as-plated state reduces the availability of sites for corrosion initiation, thereby improving the corrosion resistance of the coating [28].

In the case of heat-treated nanocomposite coatings, exhibit relatively higher corrosion resistance. It exhibited the highest Rp value of ~ 36 kΩ-cm^2 (Table 2). This improvement in passivation behaviour can be attributed to several factors. Firstly, the heat treatment promotes the formation of a more protective and stable oxide layer on the coating surface, which acts as a barrier against corrosion. Secondly, the transformation to a more crystalline structure enhances the coating's overall corrosion resistance and passivation properties. Further, particle dispersion causes grain boundary obstruction, caused improved microstructure reduces the availability of corrosion pathways, hindering the diffusion of corrosive species and slowing down the corrosion process. Also, the interactions between the matrix and nanoparticles can create interfaces and boundaries that impede corrosion propagation, further enhancing the overall corrosion resistance [29,30].

On the other hand, in the as-plated state of nanocomposites, the corrosion processes may be accelerated due to the formation of micro-galvanic couplings between the matrix and particles. These micro-galvanic cells arise from the difference in electrochemical potentials between the dissimilar materials. As a result, an electrochemical reaction takes place, involving the transfer of electrons from the more active material (anode) to the less active material (cathode) within the galvanic cell. This electron transfer leads to the corrosion of the anodic material and the dissolution process during this anodic reaction [31].

The EIS technique was employed to obtain a Nyquist plot (Fig. 4b), which was then curve-fitted using an equivalent circuit. Figure 4b' represents the inset of substrate with equivalent circuit, while Fig. 4b'' represent the other coatings circuit. Rs denotes the resistance of the electrolyte solution, while Rct represents the charge transfer resistance. To account for the non-ideal behaviour of the double layer capacitance, a constant phase element, Qf, is employed. The double layer capacitance represents the charge transfer reaction occurring at the interface of coating and substrate called Qd.

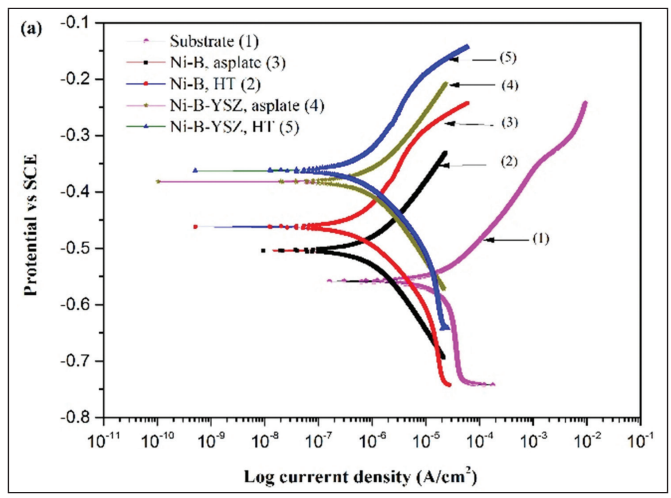

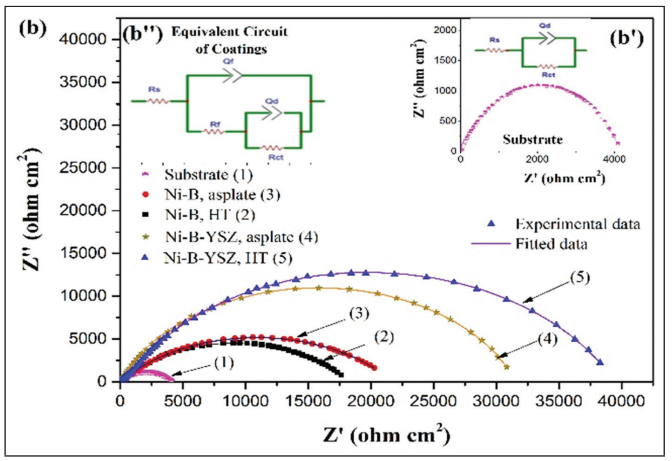

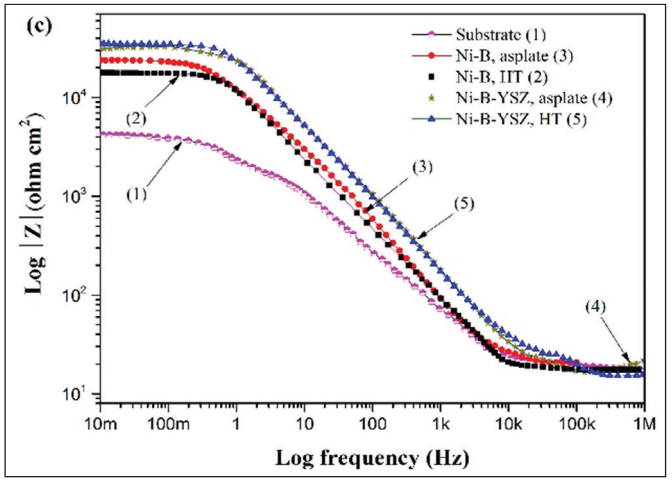

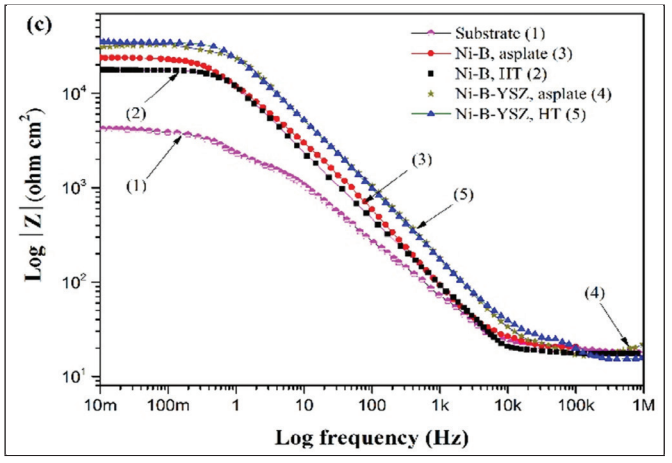

Fig. 4. Potentiodynamic polarization and EIS results for the substrate, Ni-B and Ni-B-YSZ (a) Tafel curve (b) Nyquist Curve (b') Nyquist Equivalent circuit for substrate and (b'') coatings (c) Bode impedance and (d) Bode phase angle plot.

The substrate exhibits a capacitance loop accordance to the charge transfer reaction, which can be assessed based on the diameter of the loop [26]. The enhanced resistance to corrosion of amorphous coatings can be attributed to lack of distinct crystallographic orientations or preferential pathways for corrosion propagation. Additionally, the amorphous coatings have higher chemical stability due to their disordered atomic arrangement, resulting in higher resistance than heat-treated ones [24]. Simultaneously, in other side, the charge transfer resistance (Rct) of the heat-treated Ni-B alloy coating is lower compared to that of the as-plated coating.

Table 2. The estimated corrosion parameters with use of potentiodynamic polarization curve.

Coating material	E_{corr} (V)	i_{corr} (μA/cm²)	β_a (mV/dec)	β_c (mV/dec)	R_p (kΩ-cm²)	Rct (kΩ-cm²)	CR (mm/yr)
Substrate	-0.56	22.0	134	708	2.23	4.18	0.507
Ni-B as plated	-0.46	0.92	134	100	27.06	23.88	0.019
Ni-B, HT	-0.51	1.18	134	146	25.66	17.83	0.025
Ni-B-YSZ as plated	-0.38	1.01	133	148	30.15	31.34	0.035
Ni-B-YSZ, HT	-0.36	0.65	128	95	36.47	35.19	0.022

The inclusion of nanocomposite coatings leads to an expansion of the Nyquist curve diameter, indicating an improvement in corrosion resistance. Specifically, in heat-treated conditions, the charge transfer resistance (Rct) of YSZ nano coatings is 35 kΩ.cm², which is notably higher than that of Ni-B/αZrP nano coatings (25 kΩ.cm²) [32]. Moreover, when compared to other nano coatings such as Ni-B-Al_2O_3 [21] and Ni-P-ZrO_2 [27], the value for YSZ nano coatings is approx. four and seven times higher, respectively. It should be noted that direct comparisons between these values are challenging due to variations in particle materials, matrix compositions, synthesis techniques for particle size and dispersion, and coating uniformity. Nevertheless, this demonstrates the better process control, ability of nanoparticle reinforcements to fill cracks and defects, resulting in enhanced corrosion resistance [31]. The as-plated Ni-B-YSZ shows slightly lower corrosion protection compared to the treated condition. This may be due to the porosity of the coating. These defects provide pathways for corrosive species to penetrate and attack the substrate. Additionally, the as-plated coating may have a less uniform and less dense microstructure

compared to the heat treated coating. This can result in the exposure of more active sites on the surface, increasing the likelihood of corrosion initiation and propagation.

A Bode plot is a valuable graphical tool that provides important insights into the frequency response of a system. It comprises of two plots: one illustrating the magnitude response and the other illustrating the phase response, as depicted in Fig. 4 (c and d). It is crucial to analyze the phase shift in conjunction with the corresponding magnitude response. The substrate exhibits unstable corrosion at lower frequencies, indicating lower resistance to corrosion. The as-plated coating of Ni-B alloy demonstrates a higher and stable magnitude, suggesting a significant resistance component associated with processes such as charge transfer resistance, diffusion, or ionic conduction. The heat-treated Ni-B coating shows lower impedance than as plated coating. In contrast, the heat-treated Ni-B-YSZ composite coating shows larger impedance than the as-plated coating. A higher magnitude in the impedance plot indicates a significant capacitive component, indicating the presence of a dielectric layer, oxide film, or double-layer capacitance at the electrode-electrolyte contact. The behaviour of impedance with respect to frequencies provides an indirect indication of the coating's low porosity, compact microstructure, columnar structure, chemical stability, and particle dispersion properties [33].

Further investigation of the Bode phase shift reveals similar resistance characteristics among the coatings. The existence of second-phase angle peaks found at the intersection of low frequencies in the Bode phase plot is recognised by experts as a sign of increased corrosion resistance [29]. The substrate demonstrates a bell-shaped curve indicating the continuous corrosion activity. The as-plated Ni-B coating shows a progressive shift, indicating the presence of a capacitive element at the contact area. The heat-treated Ni-B coating illustrates a shift towards higher frequencies, indicating a capacitive behaviour. The negative second phase shift observed at low frequencies in the nano-coatings indicates capacitive behavior associated with charge storage, often observed in passive or protective films on metal surfaces [34]. The similar second phase shift observed in the as-plated state of nanocomposite coatings suggests a comparatively reduced resistance to corrosion. The phase shift provides valuable insights into the favourable kinetics and reaction mechanisms involved in the corrosion process.

As a result, the as-plated Ni-B alloy coating demonstrated the lowest corrosion rate (CR) of approx. 0.019 mm/yr. (Table 2), while also having relatively low strength. Conversely, the treated Ni-B-YSZ coatings exhibited the highest strength with a comparable corrosion rate of 0.022 mm/yr.

4. Conclusions

In conclusion, an electroless nanocomposite coating was successfully applied by utilizing YSZ particles reinforced with a Ni-B matrix. This study's principal findings are summarised below:

a) Incorporating YSZ nanoparticles contributes to forming a more continuous and homogeneous Ni-B matrix, leading to a reduction in inherent defects in the coating.

b) Heat treatment enhances the mechanical characteristics of the coatings by promoting the formation of boride phases, including Ni_2B and Ni_3B, resulting in higher microhardness.

c) The corrosion resistance is deteriorated in heat treated condition than as-plated in case of Ni-B alloy coating.

d) In contrast, the corrosion resistance of Ni-B-YSZ coatings improves considerably with increased charge transfer resistance (~35 $K\Omega.cm^2$) under heat-treated conditions over as-plated states.

These findings emphasize the potential of electroless Ni-B-YSZ composite coatings for diverse applications, surpassing the performance of recent ceramic nano coatings.

References

[1] H. Li, G. Chen, K. Zhang, G. Luo, Z. Ye, Degradation failure features of chromium-plated gun barrels with a laser-discrete-quenched substrate, Surf. Coat Technol. 201 (2007) 9558–9564. https://doi.org/10.1016/j.surfcoat.2007.04.034.

[2] J.H. Underwood, G.N. Vigilante, C.P. Mulligan, Review of thermo-mechanical cracking and wear mechanisms in large caliber guns, Wear 263 (2007) 1616–1621. https://doi.org/10.1016/j.wear.2006.12.005.

[3] C.T. Dervos, J. Novakovic, P. Vassiliou, Vacuum heat treatment of electroless Ni-B coatings, Mater. Lett. 58 (2004) 619–623. https://doi.org/10.1016/S0167-577X(03)00581-0.

[4] B. Oraon, G. Majumdar, B. Ghosh, Improving hardness of electroless Ni-B coatings using optimized deposition conditions and annealing, Mater. Des. 29 (2008) 1412–1418. https://doi.org/10.1016/j.matdes.2007.09.005.

[5] S.K. Das, P. Sahoo, Study of potentiodynamic polarization behaviour of electroless ni-b coatings and optimization using Taguchi method and grey relational analysis, J. Miner. Mater. Charact. Eng. 10 (2011) 1307–1327. https://doi.org/10.4236/jmmce.2011.1014103.

[6] T.S.N.S. Narayanan, K. Krishnaveni, S.K. Seshadri, Electroless Ni-P/Ni-B duplex coatings: Preparation and evaluation of microhardness, wear and corrosion resistance, Mater. Chem. Phys. 82 (2003) 771–779. https://doi.org/10.1016/S0254-0584(03)00390-0.

[7] A. Mukhopadhyay, T.K. Barman, P. Sahoo, Tribological behavior of electroless Ni–B–W coating at room and elevated temperatures, Mater. Today Proc. 5 (2018) 3306–3315. https://doi.org/10.1016/j.matpr.2017.11.573.

[8] A. Mukhopadhyay, P. Sahoo, Effect of operating temperature on tribological behavior of as-plated Ni-B coating deposited by electroless method, Tribol. Trans. 61 (2018) 41–52.

[9] S. Duari, A. Mukhopadhyay, T.K. Barman, P. Sahoo, Optimization of wear performance of electroless Ni-B coating under lubrication, Int. J. Eng. Technol. 7 (2016) 94–103. https://doi.org/10.18052/www.scipress.com/ijet.7.94.

[10] A. standard B607-91(2003), Standard specification for autocatalytic nickel boron coatings for engineering use, ASTM Int. 02 (2009).

[11] D.E. and F. Bulbul, Preparation and characterization of electroless Ni–B/nano-SiO_2, $Al2O_3$, TiO_2 and CuO composite coatings, J. Sol-Gel Sci. Technol. 31 (2004) 83–86. https://doi.org/10.1023/B:JSST.0000047965.22232.53.

[12] S. Karthikeyan, L. Vijayaraghavan, S. Madhavan, A. Almeida, Study on the mechanical properties of heat-treated electroless NiP coatings reinforced with Al_2O_3 nano particles, Metall. Mater. Trans. A. 47 (2016) 2223–2231. https://doi.org/10.1007/s11661-016-3413-y.

[13] P. Sahoo, S.K. Das, Tribology of electroless nickel coatings - A review, Mater. Des. 32 (2011) 1760–1775. https://doi.org/10.1016/j.matdes.2010.11.013.

[14] A.E.-82(2003) Standard, Standard test method for Vickers hardness of metallic materials, ASTM Int. (n.d.).

[15] ASTM G5-14, Standard Reference test method for making potentiodynamic anodic polarization, Annu. B. ASTM Stand. (2014) 1–9. https://doi.org/10.1520/G0005-14.2.

[16] ASTM Norma G 106, Standard practice for verification of algorithm and equipment for electrochemical impedance measurements, ASTM 03 (1999) 1–11. https://doi.org/10.1520/G0106-89R10.2.

[17] K. Krishnaveni, T.S.N. Sankara Narayanan, S.K. Seshadri, Electroless Ni-B-Si_3N_4 composite coating: Deposition and evaluation of its characteristic properties, Synth. React. Inorganic, Met. Nano-Metal Chem. 42 (2012) 920–927. https://doi.org/10.1080/15533174.2011.618475.

[18] Y. Yang, W. Chen, C. Zhou, Fabrication and characterization of electroless Ni–P–ZrO_2 nano-composite coatings, Appl Nanosci. 1 (2011) 19–26. https://doi.org/10.1007/s13204-011-0003-6.

[19] M. Cecilia, C. De Sá, D. Moraes, C. Nelson, J. Duailibi, L. Guimarães, D. Oliveira, Mechanical properties of alumina-zirconia composites for ceramic abutments, Mater. Res. 7 (2004) 643–649.

[20] Z.A. Hamid, H.B. Hassan, A.M. Attyia, Influence of deposition temperature and heat treatment on the performance of electroless Ni-B films, Surf. Coat. Technol. 205 (2010) 2348–2354. https://doi.org/10.1016/j.surfcoat.2010.09.025.

[21] D. Mohanty, T.K. Barman, P. Sahoo, Characterisation and corrosion study of electroless Nickel-Boron coating reinforced with alumina nanoparticles, Mater. Today Proc. 19 (2019) 317–321. https://doi.org/10.1016/j.matpr.2019.07.216.

[22] Z.H. Huang, Y.J. Zhou, T.T. Nguyen, Study of nickel matrix composite coatings deposited from electroless plating bath loaded with TiB_2, ZrB_2 and TiC particles for improved wear and corrosion resistance, Surf. Coat. Technol. 364 (2019) 323–329. https://doi.org/10.1016/j.surfcoat.2019.01.060.

[23] Ş. Ürdem, E. Duru, H. Algül, M. Uysal, H. Akbulut, Evaluation of high temperature tribological behavior of electroless deposited NiB–Al_2O_3 coating, Wear (2021) 482–483. https://doi.org/10.1016/j.wear.2021.203960.

[24] K.N. Srinivasan, R. Meenakshi, A. Santhi, P.R. Thangavelu, S. John, Studies on development of electroless Ni-B bath for corrosion resistance and wear resistance applications, Surf. Eng. 26 (2010) 153–158. https://doi.org/10.1179/174329409X409468.

[25] V. Vitry, L. Bonin, Increase of boron content in electroless nickel-boron coating by modification of plating conditions, Surf. Coat. Technol. 311 (2017) 164–171. https://doi.org/10.1016/j.surfcoat.2017.01.009.

[26] A.F. Kanta, M. Poelman, V. Vitry, F. Delaunois, Nickel-boron electrochemical properties investigations, J. Alloys Compd. 505 (2010) 151–156. https://doi.org/10.1016/j.jallcom.2010.05.168.

[27] M.H. Sliem, K. Shahzad, V.N. Sivaprasad, R.A. Shakoor, Enhanced mechanical and corrosion protection properties of pulse electrodeposited NiP-ZrO_2 nanocomposite coatings, Surf. Coat. Technol. 403 (2020) 126340. https://doi.org/10.1016/j.surfcoat.2020.126340.

[28] A.F. Kanta, V. Vitry, F. Delaunois, Effect of thermochemical and heat treatments on electroless nickel–boron, J. Alloys Compd. 486 (2009) 21–23. https://doi.org/10.1016/j.jallcom.2009.07.038.

[29] Y.W. Song, D.Y. Shan, E.H. Han, Comparative study on corrosion protection properties of electroless Ni-P-ZrO_2 and Ni-P coatings on AZ91D magnesium alloy, Mater. Corros. (2007) 506–510. https://doi.org/10.1002/maco.200604033.

[30] M. Ghaderi, M. Rezagholizadeh, A. Heidary, S.M. Monirvaghefi, The effect of Al_2O_3 nanoparticles on tribological and corrosion behavior of electroless Ni–B–Al_2O_3 composite coating, Prot. Met. Phys. Chem. Surfaces,. 52 (2016) 854–858. https://doi.org/10.1134/S2070205116050087.

[31] Z. Wei, S. Hong, Z. Wei, N. Hu, G. Ying, Y. Wu, Comparison on long-term corrosion performance of WC-CoCr and Al_2O_3-TiO_2 ceramic coatings in sulphide-containing 3.5 wt% NaCl solution, Int. J. Refract. Met. Hard Mater. 107 (2022) 105906. https://doi.org/10.1016/j.ijrmhm.2022.105906.

[32] L. Yan, S. Yan, Y. He, Y. He, H. Li, R. Song, H. Zhou, X. Cheng, Preparation, corrosion resistance and mechanical properties of electroless Ni-B/α-ZrP composite coatings, Colloids Surf. A Physicochem. Eng. Asp. 654 (2022) 130132. https://doi.org/10.1016/j.colsurfa.2022.130132.

[33] T.S.N. Sankara Narayanan, S.K. Seshadri, Electro and electroless deposited composite coatings: Preparation, characteristics, and applications, Wiley Encycl. Compos. (2012) 1–17. https://doi.org/10.1002/9781118097298.weoc072.

[34] V. Niksefat, M. Ghorbani, Mechanical and electrochemical properties of ultrasonic-assisted electroless deposition of Ni-B-TiO_2 composite coatings, J. Alloys Compd. 633 (2015) 127–136. https://doi.org/10.1016/j.jallcom.2015.01.250.

Technical Note

The electrocrystallization process in its footings of the new phase

P. B. Rotti

KLE JT College, Gadag-582201

Email: jagdishrotti@yahoo.co.in

The modern advances in technology has enabled all the branches of science to provide new insights into the origin of the universe and "Big Bang theory [1]" is a typical example. The researchers involved in the field of chemical Kinetics and the electrochemists [2-4] too are involved in new approaches, for unravelling the isomorphism between chemical kinetics and electrode kinetics. The reaction constant 'k' of the chemical reaction is often perceived as a scalar quantity by the chemical kinetics researchers whereas the electrochemists have accepted it as a vector quantity which builds up the new product from the reactants. The concentration goes as the parameter in the Kinetics whereas the electrochemists refer to the "current density" as vector parameter along with concentrations. The electrolysis process mimics the nature in almost all the oxidation and reduction reactions [5-7].

Thus, the general form of the Chemical equation

$$[\text{Reactants}] \rightleftharpoons [\text{Products}] \pm \text{energy} - ①$$

can now be expressed as

$$\left[\begin{array}{c}\textit{Mass of the concentration of the reacting material} \\ (\textbf{\textit{Scalar quantity}})\end{array}\right] + \left[\begin{array}{c}\textit{Concentration of the charge in terms of current denisty} \\ (\textbf{\textit{Vector quantity}})\end{array}\right] \rightleftharpoons \left[\begin{array}{c}\textit{Chemical substance formed within from or on the surface of the substrate cathode compex of scalar and vector quantity}\end{array}\right] \pm \text{energy} - ②$$

The product formed from the reversible reaction is ascertained by the forward directional growth of the reaction. The concepts of the reactant and the product can be clarified using derivative and antiderivative notions. The derivative term goes to the product side, leaving behind the antiderivative concept for the reactant.

Introductions of the new concepts of scalar and the electrolytes in terms of the vectors quantities leads to:

$$\left[\begin{array}{c}\textit{Mass of the concentration of the reacting material} \\ (\textbf{\textit{Scalar quantity}})\end{array}\right] \text{x} \left[\begin{array}{c}\textit{Concentration of the charge in terms of current denisty} \\ (\textbf{\textit{Vector quantity}})\end{array}\right] \rightleftharpoons \left[\begin{array}{c}\textit{Chemical substance formed within from or on to the surface of the substrate cathode}\end{array}\right] \pm \text{energy} - \{2\}$$

A B C

i.e [A][**B**]⇌**C**

in ionic forms

$$[(M^{+++})_{aq}] + \begin{bmatrix}\bar{e}\\ \bar{e}\\ E\end{bmatrix}^{\bar{e}} \rightleftharpoons {}^{\bar{e}}[(M^{++})_{aq}] + \begin{bmatrix}\bar{e}\\ E\end{bmatrix} \rightleftharpoons [(M^{+})_{aq}] + \begin{bmatrix}\bar{e}\\ E\end{bmatrix} \rightleftharpoons [M_{\text{solid atom in crystal lattice}}] \Delta = nFE - \{3\}$$

The ultimate antiderivative of $[M^{+3}]$ is the **M** itself

The ultimate antiderivative of $[M^{+3}]$ is the **M** itself

The antiderivative [$\bar{e}$] is the part of the energy. The antiderivative of the universe and of the vacuum encompasses the space chemistry and the antiderivatives of space chemistry goes to **the galaxy** and so on. The above reactions can be expressed in empirical form as shown below {4}

$$[\text{Mass}]_{\text{uni}} \cdot [\text{ Vacuum}]_{\text{uni}} \rightleftharpoons \rightleftharpoons [(M^{+++})_{aq}] + [\text{Anion}_{aq}] \pm \text{energy} - \{4\}$$

The reactions of the mass and of the vacuum of {4} the universe goes on to that space of the universe which in turn goes to as that of the galaxies. These subtle concepts seem to be implied by Bragg and Bragg and Sommerfeld while studying the spectra.

Such situation has the occasion to generate chemisorbed product of the mass and vacuum which in turn generates the Electron and other ingredients of the nucleons and form ionosphere of the chain reactions of the Electron massive surfaces.

J J Thomson was successful in his endeavour to break the ATOM into two ions of oppositely charged particles (cation and electron). Willard Gibbs enunciated the Phase rule to study the heterogeneous equilibrium.

$$(P + F) = C + 2 \text{ ---------- (5)}$$

where

P = number of phases

F = number of the degrees of the freedom

C = number of components

2 = The number of natural forces required to generate 'C' from (P + F) phases

Substituting C =2,

(P+F) = 4 ----------(6)

Let this number be also an algebraic term 'z' Hence

(P + F) = z ----------(7)

Thus, one can study the influence of variables in the heterogeneous equilibrium system up to 4 phases of the universe.

The phase diagram of sulphur may be considered as a typical example, consisting of 4 phases with negative parameter

(F = -1) ---------- (8)

This negative parameter implies the presence of the vacuum within the mass. Thus, the vacuum present on both the sides of the mass plays the dual role as the potential energy and the kinetic energy respectively.

The method of electrolysis process of (0.25M $CuSO_4$ +0.M H_2SO_4) of aqueous solution using highly purified copper, electropolished single crystal substrate follows the equation (4). The coated surface of such crystals near its vacuum is the deposition process. So, the second step now involves the polarised form of faces of copper ions. Hence the process repeats in a cyclic manner, yielding multiple layers. There is thus the synergy between massive phase of vacuum plane on the single crystal cathodes of (100) and (111) planes respectively. The adsorption deposition process of the successive layers helps in this process. But the crystal deposits on to the surfaces (110) planes separates into two parts on either side of its central planes at (π distance apart) giving the shape of the propeller of the planes addressed as RIDGE crystals.

The intercepts obtained in the graph of logei ->η (Over Potentials) at 10 mA/cm^2 current density of 10 Coulomb/ cm^2 are of the magnitudes of 2,2 and 4 of (100) (110) and (111) planes and yield i_0 of polycrystalline substrates as

$i_0 = \sum_{100}^{111} (i_0)^2 = \sqrt{24} = 5$ No of forces imparting the surface of the crystal ----(10)

The magnitude of 'C' of the phase rule (5) goes to '2' while studying the reactions of mass and vacuum of the reversible reaction of the universe, which is confirmed by the value of 'C' of J. J.Thomson's experiments of an atom splitting into two oppositely charged particles. So if the process is on account of both the processes then the total value of C becomes 4.

The substitution of this value in the phase rule one gets

(P + F) = 6 ---------- (9).

Let 'z' represent 6 in equation (10) then we can reach dynamic form of phase rule as

(P + F) = z --------- (10)

The differential study of equation (7) from rectangular to the hexagonal... The study of the copper crystals up to the hexagonal form, and the study of sulphur system is in the lines of equation form (5), up to the 3 phases of equilibrium and indicates a negative value for the phase of Sulphur. This may be attributed to the presence of vacuum in the interior surfaces of sulphur. And the differential study of equation (5) goes as the galvanostatic and potentiostatic crystals of electrolysis.

$(dp/de)_f = 1$ ------- (11) and $(df/dc)_p = 1$ ----------(12)

The above considerations point out to the need for the vector concepts in the electrolysis processes. The current density plays a role similar to the concentration in the chemical kinetics.

Conclusions

The importance of the derivative and antiderivative concepts is indicated. The application of the phase rule to interpret the possible shapes of the electro crystalized products of electrolysis is emphasized in a novel manner.

Acknowledgement: The author wishes to express his gratitude to the late Prof Dr B.S Sheshadri.

References:

1. Jean Pierre Lemaitre, Big Bang Theory, Frontiers of Fundamental Physics FFP 14 15-18 July 2014, Aix marseill. Paris
2. S.Glasstone, Text book of Physical Chemistry, MaC Millan and Co, Limited, 2006, Van Nostrand Company, New York.
3. Gordon, Roy, G.William Klemperer, and I. Jeffrey Steinfeld. "Vibrational and rotational relaxation." Annual Review of Physical Chemistry 19.1 (1968): 215-250. https://doi.org/10.1146/annurev.pc.19.100168.0012435. A. Damjanovic, Th HV Setty, and JO'M. Bockris. Effect of crystal plane on the mechanism and the kinetics of copper electrocrystallization, Journal of the Electrochemical Society 113 (1966): 429. DOI 10.1149/1.2423989
4. B.S.Sheshadri, Ph.D Thesis, Bangalore University (1970).
5. N.C. Subramanyam, B. S. Sheshadri, and S. M. Mayanna. Acridine and Quinolines as Acid Corrosion Inhibitors for Copper. Key Engineering Materials 20 (1988): 3023-3037. https://doi.org/10.4028/www.scientific.net/KEM.20-28.3023
6. M. D. Wear, J. Hass, Frank R Giordano, Thomas Calculus, 2nd Edn., Pearson Education India, New Delhi, 2012
7. M.D.Tomashow, L.P.Vershinina Kinetics of some electrodes processes continuously renewed surface of solid metals, Electrochimica Acta Vol 15 No 4 April(1970) 501-508 https://doi.org/10.1016/0013-4686(70)80001-9.
8. P.B.Rotti and B.S.Sheshadri, Residual Potential of Standard and Hydrogen Electrode (SHE), Journal of Electrochemical Society of India (JECSI) vol 61-4 (2012) 40-46.
9. P.B.Rotti,The use of dynamic resistance, resistance, and capacitance concept during electrocrystallization of copper, Journal of Electrochemical Society of India (JECS) Vol 60 [1,2](2011)65-68.
10. P.B.Rotti, Concept and Functions of an Electron with Schrodinger wave form of the electron, Journal of Electrochemical Society of India (JECSI)Vol 68 No 1 Jan 2019
11. L.Marchnao and A.I. Arvia, Theoretical steady current/voltage characteristic for simple electrode process under laminar isothermal and non-isothermal free convection, Electrochimica Acta, 15 (2) (1970) 395-338, https://doi.org/10.1016/0013-4686(70)80025-1

Development of electrochemical sensor for dopamine using PEDOT-rGO-CuNPs modified electrode

Venkatesan Sethuraman[1], Thirumal Balaraman[2], Raman Sasikumar[2*]

[1] Research and Development, New Energy Storage Technology, Lithium-ion Battery Division, Amara Raja Battery Ltd, Karakambadi - 517520, Tirupati, Andhra Pradesh, India.

[2]Department of Physical Chemistry, University of Madras, Chennai - 600025, India.

Corresponding author E-mail: skumaratr@gmail.com

Abstracta

Designing of electrode materials for sensing of biological compounds has been attracting researchers for many decades. In this work, the nanocomposite electrode material, Copper nanoparticles (CuNPs) decorated Poly(3,4-ethylenedioxythiophene)-reduced Graphene Oxide (PEDOT-rGO), was developed to modify the Glassy carbon electrode (GCE) for the determination of the electrochemical characteristics of dopamine on a). The composite was characterised by common analytical techniques. The TEM image of the composite showed the deposition of CuNPs on PEDOT-rGO. Cyclic voltammetric studies were carried out on PEDOT-rGO-CuNPs at pH 6.0. Differential Pulse Voltammetry (DPV) was used to study the relationship between response current and dopamine concentration. The linear range of dopamine concentration was obtained as 3×10^{-8} to 6.4×10^{-5} M and lower limit of detection 5×10^{-9} M. The composite, PEDOT-rGO-CuNPs, was verified excellent for the detection of dopamine.

Keywords: *Dopamine; CuNPs; Electrochemical sensors; PEDOT; rGO; composite*

1. Introduction

Dopamine plays a critical role in the way our brain controls our movements and is thought to be a crucial part of the basal ganglia motor loop [1, 2]. Thus, shortage of dopamine, particularly the death of dopamine neurons in the nigrostriatal pathway, is the cause of Parkinson's disease, in which a person loses the ability to execute smooth and controlled movements [3]. So, its quantitative determination in a living body is crucial, therefore, dopamine sensor is a device of importance in the analytical task. Poly(3,4-ethylenedioxythiophene) (PEDOT) is one of the most commonly employed conducting polymer in many fields because of its excellent electrochemical and optical properties [4, 5]. This polymer can be simply obtained by anodic oxidation of the relevant monomer, even in aqueous solutions, in the presence of various anionic counter-ions [6]. Graphene oxide (GO) is of great interest due to its low cost, easy access and widespread ability to convert back to graphene. GO is viewed as the precursor to produce graphene (reduced GO) by chemical and thermal reduction. Furthermore, in recent years, many GO derivatives, such as GO-based composites, GO-based coating and thin films, as well as GO-based nanoparticles, emerged as functional materials for various applications [7-8]. The aim of this work is to study the electrochemical behaviour and the direct electrochemical determination of dopamine by developing a composite composed of CuNPs decorated on PEDOT-rGO. Advantages of the modified glassy carbon electrode and electrochemical techniques led to a development of a sensor for dopamine with features of low cost, sensitivity selectivity and reproducibility of the method.

2. Experimental

Dopamine was purchased from Alfa Aesar 3,4-ethylenedioxythiophene (EDOT) from Sigma Aldrich (India). Copper sulphate, sodium sulphate, di-potassium hydrogen phosphate and potassium dihydrogen phosphate from Merck (India) were used as received.

2.1. Fabrication of PEDOT-rGO-CuNPs

PEDOT-GO was deposited on the GCE. GO doped PEDOT film was deposited by electro-polymerisation method on the GC electrode by potential cycling from -0.2 to 1.2V vs Ag/AgCl at a scan rate of 50mV/s. Solution containing 10 mM of EDOT and 1 $mgml^{-1}$ of GO was used. The electrochemical reduction of PEDOT-GO was carried by amperometric method by applying -0.9V for 600s in the presence of pH 7.4. For the further deposition of Cu nanoparticles, the PEDOT-rGO nanocomposite modified electrode was deposited solution containing 10 mM of $CuSO_4$ and 100 mM of Na_2SO_4 and electrodeposition was carried out at a potential of -1.0V (vs. Ag/AgCl) for 200 s [9].

3. Results and Discussions

3.1. Surface Study

The scanning electron microscopy (SEM) image of PEDOT-GO and PEDOT-rGO modified electrode was discussed earlier [10]. Cu nanoparticles on the PEDOT-rGO surface was studied by SEM and AFM. The SEM image of Cu NPS -PEDOT-rGO showed random distribution CuNPs on the surface (Fig. 1a). The surface roughness parameters, indicated as mean roughness (Ra), root mean square of Z data (Rq) and mean difference (Rz) in the five highest peaks and five lowest valleys were 3.2, 28 and 34. The surface roughness of PEDOT-rGO- CuNPS is shown in Fig. 1b. The GO was electrochemically reduced and its surface exhibited higher roughness as shown in AFM. Porous morphology was observed for PEDOT-rGO-CuNPs electrode which confirms incorporation of CuNPs in the modified electrode.

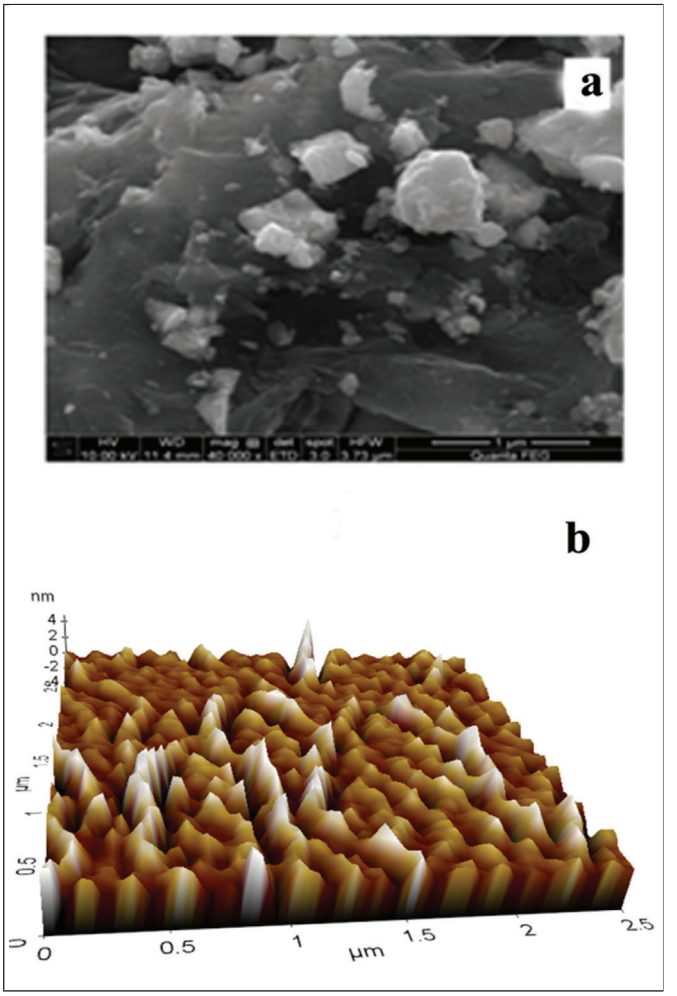

Fig.1. SEM images of a) PEDOT-rGO-CuNPs and AFM images of b) PEDOT-rGO-CuNPs.

3.2. Fourier Transform Infrared (FT-IR)

The following FT-IR peaks indicate the presence of characteristic functional group in PEDOT-GO (Fig.2a). The peak at 3401 cm^{-1} is due to –O-H stretching vibration. The peak at 1645cm^{-1} corresponds the –C=O stretching vibration, 1084 cm-1 corresponding to the –C-O- stretching vibration, peaks at 988 and 863 cm^{-1} attribute due to –C-S bending vibration in the PEDOT-GO presented in (curve a). Similar peaks at 3435 cm^{-1} for –O-H stretching vibration, peaks at 1035 and 1394 cm^{-1} are corresponding to –C-O, -C-H bending vibrations, respectively. The absence of peak at 1645 cm^{-1} suggests that GO is reduced to rGO (Fig. 2b). The presence CuNPs are absorption band at 624 and 689 cm^{-1}suggests CuNPs asymmetric stretching bond was observed (Fig. 2c).

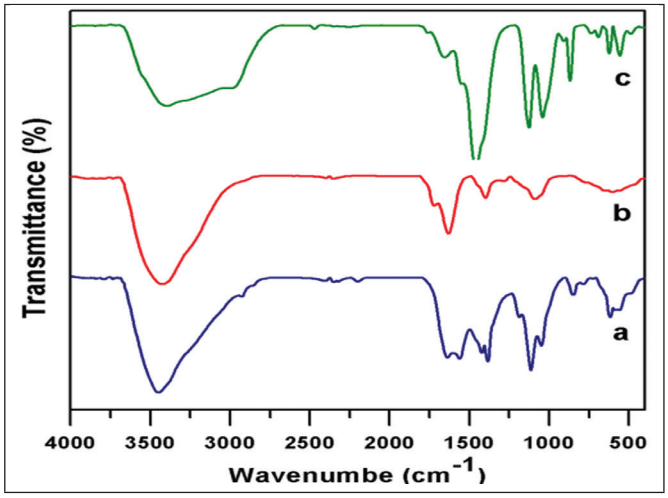

Fig. 2. FT-IR spectrum of a) PEDOT-GO, b) PEDOT-rGO and c) PEDOT-rGO-CuNPs. SEM images of a) PEDOT-GO, b) PEDOT-rGO and c) PEDOT-rGO-CuNPs.

3.3. Electrochemical studies of PEDOT-rGO-CuNPs

The cyclic voltammograms (CV) of 1mM $[Fe(CN)_6]^{3-/4-}$ on the bare GC electrode (curve a), PEDOT-GO (curve b), PEDOT-rGO (curve c) and PEDOT-rGO- CuNPs (curve d) modified electrodes were recorded in 0.1M of KCl at a scan rate of 50 mVs^{-1} (Fig. 3A). Modification of the PEDOT-GO (curve b), PEDOT-rGO (curve c) GC electrode led to an increase in the peak current when compared to the bare GC electrode. This could be attributed to high surface coverage and electrocatalysis. Now, the modification of PEDOT-rGO-CuNPs onto the GC electrode significantly increased the redox peak current compared to the other modified electrodes. This is due to the conducting surface on the electrode.

Performance of the modified electrode was further studied by Electrochemical Impedance Spectroscopy (EIS), which provides useful information on the modification of the electrode surface. The charge transfer resistance is indicated by semicircle portion. The charge transfer process of the CuNP-PEDOT-rGO modified GC electrode was recorded by monitoring charge transfer resistance (R_{ct}) at the electrode/electrolyte interface. Therefore, the modified electrode agreed with the Randles equivalent circuit of $R_s(Q_{dl}(R_{ct}W))$. In this circuit, R_s is the solution resistance, Q_{dl} is the capacitance, R_{ct} is the charge transfer resistance of the modified electrode PEDOT–GO–PPO and W is the Warburg element. Fig. 3B displays the EIS of bare GC (curve a), PEDOT-GO (curve b), PEDOT-rGO (curve c) and CuNP-PEDOT-rGO (curve d) modified electrodes at the polarization potential 25 mV and frequency of 1-1,00,000 Hz. The Nyquist diagrams for bare, PEDOT-GO, PEDOT-rGO and PEDOT-rGO-CuNPs arrived at the R_{ct} values of 359, 143, 105 and 65 Ω, respectively. Comparatively, the R_{ct} value of PEDOT-rGO-CuNPs (curve d) is the lowest one. These results demonstrate that the large conducting surface is present in PEDOT-rGO-CuNPs, which can lead to good conducting reaction pathways between the electrode/electrolyte interactions and provides a good platform for sensing application.

The major parameter to set for response of the sensor is pH. To set this, 0.1mM of dopamine was mixed with the buffer solution. The pH is a highly affecting parameter for the sensor. There is a close relationship between the response current and pH. Fig.3C shows effect of pH on the response current of the PEDOT-rGO-CuNPs sensor. Response current for the sensor at the pH 4 - 8 was studied for 0.1mM of dopamine. The activity of the sensor decreased below and above pH 7.0. However, the change of response current with increase of pH with decrease of conductivity of the sensor was observed. The sensor PEDOT-rGO-CuNPs got good response current. The optimum pH of the sensor was 7.0 to detect dopamine using this nanocompsite. Fig. 3D shows the cyclic voltammograms of 0.1mM dopamine on plain bare GC (curve a), PEDOT-GO (curve b), PEDOT-rGO (curve c) and PEDOT-rGO-CuNPs (curve d) at pH 7.0. There was a characteristic reversible redox peak observed in the curve a. When the modified electrode employed, the redox peaks became quasi reversible and increase in the oxidation and reduction peak currents were observed. This indicates that the modified GCE catalyzes the oxidation and reduction of dopamine. In all the cases, dopamine and *o*-dopaquinone redox reaction was observed. Comparatively, the highest

redox currents for dopamine were observed only at PEDOT-rGO-CuNPs-GCE electrode. Dopamine showed 2e-process. This confirms the effective incorporation of CuNPs onto the PEDOT-rGO matrix and better sensing capability of the modified electrode.

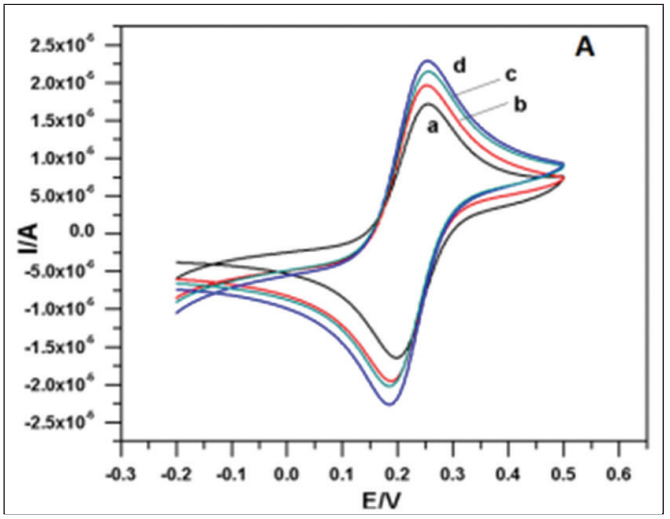

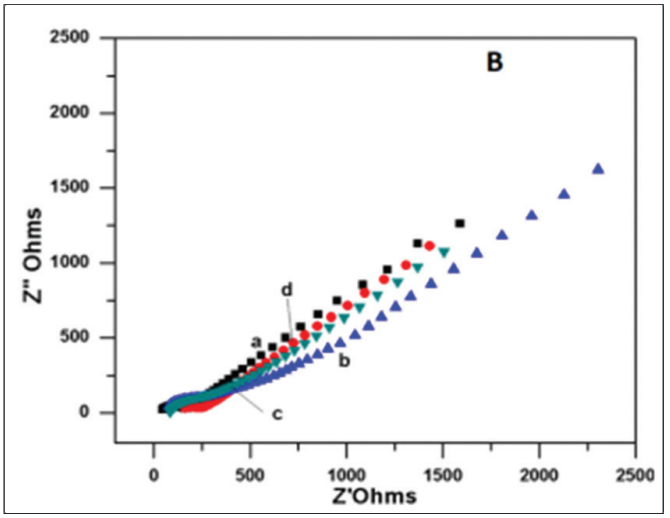

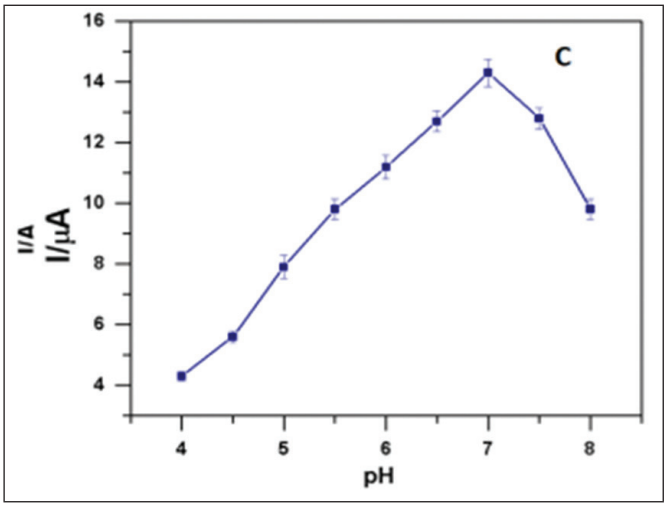

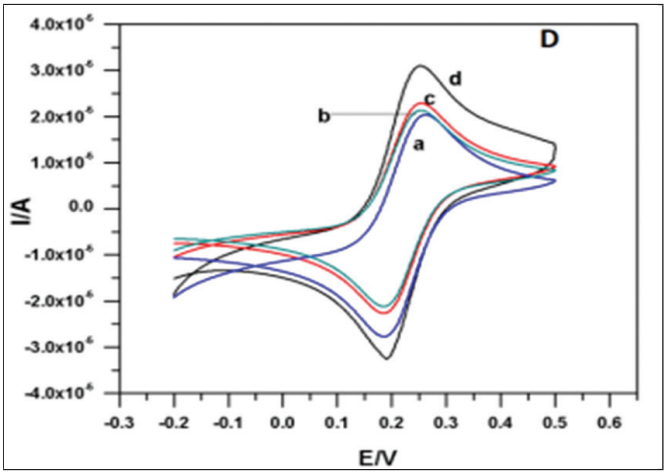

Fig. 3A. Cyclic Voltammetric studies in the presence of 1 mM $[Fe(CN)_6]^{3-/4-}$ in 0.1 M KCl. B) EIS of (a) GCE (b) PEDOT-GO,(c) PEDOT-rGO and (d) PEDOT-rGO-CuNPsv measured in presence of 1 mM $[Fe(CN)_6]^{3-/4-}$ in 0.1 M KCl. C) Effect of pH by response current study for the PEDOT-rGO-CuNPs. D) CVs obtained for dopamine of 0.01mM at the (a) bare GC, (b) PEDOT-GO (c) PEDOT-rGO and (d) PEDOT-rGO-CuNPs in PB solution (pH 7.0) at a scan rate of 50 mVs^{-1}.

3.4. Effect of concentration

Differential pulse voltammetry was employed to determine the concentration of dopamine by using the PEDOT-rGO-CuNPs/GCE. The DPVs (Fig. 4A) were recorded for dopamine with different known concentrations under identical experimental conditions and in each voltammogram the oxidation peak current was measured. The peak currents were correlated with the dopamine concentration. The concentration of dopamine was directly proportional to the response current at pH 7.0 in a particular range and then it reached a steady state. The catalytic reaction was a first-order reaction, in the linear range and attained steady state and then it followed zero-order kinetics. The linear range of dopamine concentrations (Fig. 4B) showed a detection range 3×10^{-8} to 6.4×10^{-5} M and the lower limit of detection determined was equal to 5×10^{-9}M. The experimental results showed that the methods were simple and rapid with high accuracy. A plot of inverse of current verses substrate concentration was constructed to find out maximum current response

(I_{max}). The (I_{max}) was 1.24x10^{-4}µA which showed the possibility of detection of dopamine at both low and high concentrations. The modified electrode was compared with already existing sensors, and the results are shown in table.1.

Table 1. Comparison of existing electrode for neurotransmitters with PEDOT-rGO-CuNPs

Sl. No.	Modified Electrode	Linear Range (µM)	Lower Limit of Detection (µM)	Reference
1.	Au@PSi-P3HT/GCE	1 to 460 x 10^{-6}	0.63 x 10^{-6}	11
2.	AuNPs/ PM/CPE electrodes	0.2 to 11 x 10^{-6}	0.067 x 10^{-6}	12
3.	PT/Au/CNT	1.0 to 10 x 10^{-6}	0.69 x 10^{-6}	13
4.	OPEDOT–AuNPs–ERGO	4.0 to 100 x 10^{-6}	1.0 x 10^{-6}	14
5.	Ti_3C_2/G-MWCNTs/ ZnO	0.01 to 30 x 10^{-6}	3.2 x 10^{-9}	15
6.	Ag/PPy/ Cu_2O/GCE	0.01 to 250 x 10^{-6}	0.0124 x 10^{-6}	16
7.	PEDOT-rGO-CuNPs	0.03 to 64 x 10^{-6}	5 x 10^{-9}	This Work

The results of amperometric response of dopamine in presence of potential interferences such as ascorbic acid, D-glucose and L-glutamic acid with phosphate buffer at pH 7.0 are illustrated in Fig. 4C. The interfering substances were added serially to the same solution and the DPV measurements were carried out. As there was no change in the current response, the selectivity of the sensing is verified excellent.

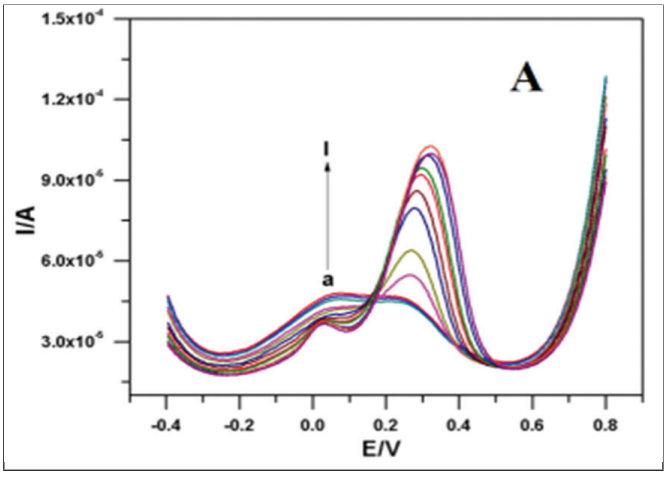

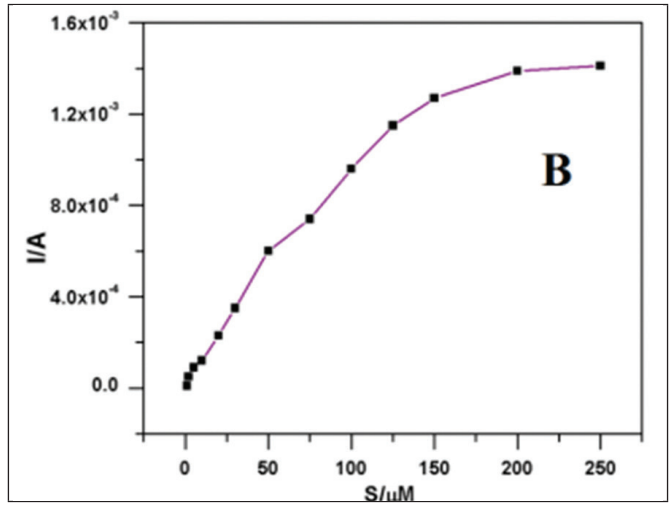

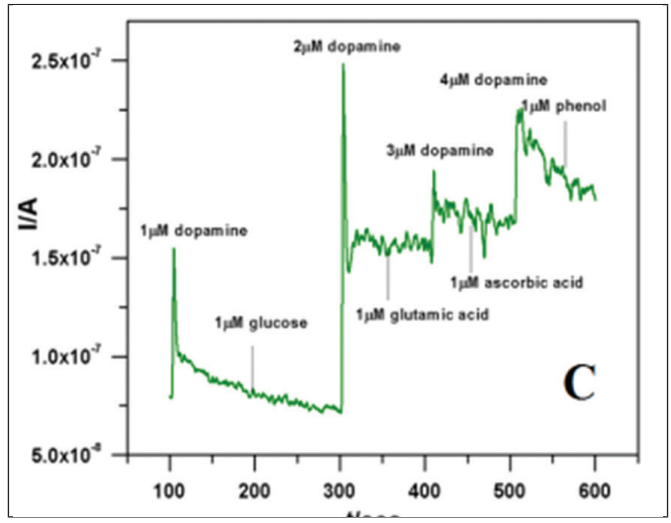

Fig. 4A. DPVs of PEDOT-rGO-CuNPs film dopamine concentrations buffer (a-l). (B) Correlation between response current and dopamine concentration at pH 7.0 and 25.0◦C. (C) Effect of interference on the response of the dopamine biosensor.

3.5. Recovery, Stability and Reproducibility

The performance of the fabricated electrochemical biosensor using PEDOT-rGO-CuNPs was compared with the results of High-Performance Liquid Chromatography (HPLC) for dopamine detection. The quantification and percentage of recovery were determined for live samples.

The recovery was determined by spiking a human urine extract sample with three different additions of dopamine. The standard of dopamine and one human urine extract sample. The results obtained from the present method and HPLC are compared in the following table.

Table.2 Determination of dopamine in human urine.

Sl. No.	Sample	Dopamine Spiked*[M]*	Dopamine Found*[M]*	Recovery *(%)*	Dopamine found by HPLC*[M]*	Recovery *(%)*
1	Human urine	1.00×10^{-6} 1.00×10^{-7}	0.99×10^{-6} 1.03×10^{-7}	99 103	0.98×10^{-6} 1.02×10^{-7}	98 102
2	Human urine	1.00×10^{-6} 1.00×10^{-7}	0.99×10^{-6} 1.01×10^{-7}	99 101	1.01×10^{-6} 1.03×10^{-7}	101 103
3	Human urine	1.00×10^{-6} 1.00×10^{-7}	1.01×10^{-6} 1.04×10^{-7}	101 104	1.02×10^{-6} 1.05×10^{-7}	102 105

4. Conclusion

PEDOT-rGO-CuNPs modified GCE electrode fabricated for sensing of dopamine. The electrode was very sensitive at pH 7.0. DPV was used to study the relationship between response current and dopamine concentration. The linear range of dopamine obtained for the concentration of dopamine was 3×10^{-8} to 6.4×10^{-5} M and the lower limit of detection 5×10^{-9} M. So, the present electrode material may be a convenient one for the fabrication of electrochemical sensor towards dopamine sensing.

Acknowledgement

The authors gratefully acknowledge RUSA 2.0 (Theme 2) Research Innovation & Quality Improvement, University of Madras, Chennai (Grant Ref no. C3/RI & QI /RUSA 2.0/Theme-2/ Award/2021/033) for providing funding.

Conflict of Interest

There is no conflict of interest

Reference

[1] Ronan Baron, Maya Zayats, Itamar Willner, Ronan Baron, Maya Zayats, Itamar Willner, Dopamine-, L-DOPA-, Adrenaline-, and Noradrenaline-Induced Growth of Au Nanoparticles: Assays for the Detection of Neurotransmitters and of Tyrosinase Activity, Analytical Chemistry, 77 (6), 1566-1571 (2005). Analytical Chemistry, 77 (6), (2005) 1566-1571, https://doi.org/10.1021/ac048691v.

[2] T.K.Aparna, R.Sivasubramanian, Mushtaq, One-pot synthesis of Au-Cu2O/rGO nanocomposite based electrochemical sensor for selective and simultaneous detection of dopamine and uric acid Journal of Alloys and Compounds, (2012), 741, 1130-1141, https://doi.org/10.1016/j.jallcom.2018.01.205.

[3] Sarah X. Luo and Eric J. Huang, Dopaminergic Neurons and Brain Reward Pathways: From Neurogenesis to Circuit Assembly, The American Journal of Pathology, 186(3), (2016)478-488 https://doi.org/10.1016/j.ajpath.2015.09.023

[4] Noemi Rozlosnik, New directions in medical biosensors employing poly(3,4-ethylenedioxy thiophene) derivative-based electrodes Analytical and Bioanalytical Chemistry, (2009)395(3), 637–645, DOI 10.1007/s00216-009-2981-8.

[5] H.Yoon, M.Chang, J.Jang, Formation of 1D Poly(3,4-ethylenedioxythiophene) Nanomaterials in Reverse Microemulsions and Their Application to Chemical Sensors Advanced Functional Materials,(2007)17(3),431436,https://doi.org/10.1002/adfm.200600106

[6] Stelain Lupu et al., Development of Amperometric Biosensors Based on Nanostructured Tyrosinase-Conducting Polymer Composite Electrodes Sensors, (2013)13(5) 6759-6774, https://doi.org/10.3390/s130506759

[7] Kyungwha Chung et al., Enhancing the Performance of Surface Plasmon Resonance Biosensor via Modulation of Electron Density at the Graphene–Gold Interface Advanced Materials Interfaces, (2018) 5(19), 1800433, https://doi.org/10.1002/admi.201800433.

[8] Uling Yang, Gang Li, Meifang Hu, Lingbo Qu, Preparation of electrochemically reduced graphene oxide/multi-wall carbon nanotubes hybrid film modified electrode, and its application to amperometric sensing of rutin, Journal of Chemical Science, 126(4) (2014) 1021-1029, https://www.ias.ac.in/article/fulltext/jcsc/126/04/1021-1029

[9] Siqiu Ye, Xinhao Shi, Wei Gu, Yixuan Zhang,Yuezhong Xian, A colorimetric sensor based on catechol-terminated mixed self-assembled monolayers modified gold nanoparticles for ultrasensitive detections of copper ions, Analyst, (2012)137, 3365-3371, https://doi.org/10.1039/C2AN35311C.

[10] V. Sethuraman, P. Muthuraja, J. Anandha Raj, P. Manisankar, A highly sensitive electrochemical biosensor for catechol using conducting polymer reduced graphene oxide–metal oxide enzyme modified electrode Biosensor and Bioelectronics, (2016)84, 112-119, https://doi.org/10.1016/j.bios.2015.12.074.

[11] J.Ahmed, M.Faisal, S.A.Alsareii, M.Jalalah, F.A.Harraz, A novel gold-decorated porous silicon-poly(3-hexylthiophene) ternary nanocomposite as a highly sensitive and selective non-enzymatic dopamine electrochemical sensor Journal of Alloys and Compounds, (2022) 931, 167403, https://doi.org/10.1016/j.jallcom.2022.167403.

[12] M.Harsini, et.al., Electrochemical synthesis of polymelamine/gold nanoparticle modified carbon paste electrode as voltammetric sensor of dopamine Chinese Journal Analytical Chemistry, 50, 100052 (2022), https://doi.org/10.1016/j.cjac.2022.100052

[13] C.S.Inagaki, et.al., Facile synthesis and dopamine sensing application of three component nanocomposite thin films based on polythiophene, gold nanoparticles and carbon nanotubes, Journal of Electroanalytical Chemistry, 840 (2019) 208-217 https://doi.org/10.1016/j.jelechem.2019.03.066.

[14] J.Pan, M.Liu, D.Li, H.Zheng, D. Zhang, Overoxidized poly(3,4-ethylenedioxythiophene)–gold nanoparticles–graphene-modified electrode for the simultaneous detection of dopamine and uric acid in the presence of ascorbic acid Journal of Pharmaceutical Analysis, 11 (2021) 699-708, https://doi.org/10.1016/j.jpha.2021.09.005.

[15] Meijun Ni, Jia Chen, Chenxi Wang, Yilin Wang, Linzi Huang, Weicheng Xiong, Pengcheng Zhao, Yixi Xie, Junjie Fei, A high-sensitive dopamine electrochemical sensor based on multilayer Ti_3C_2 MXene, graphitized multi-walled carbon nanotubes and ZnO nanospheres Microchemical Journal, (2022) 178, 107410, https://doi.org/10.1016/j.microc.2022.107410.

[16] S.Selvarajan, A.Suganthi, M. Rajarajan, A novel highly selective and sensitive detection of serotonin based on Ag/polypyrrole/Cu_2O nanocomposite modified glassy carbon electrode Ultrasonics Sonochemistry, (2018).44, 319-330

Electrochemical chemical performance of green synthesis of NiO-Syzygium cumini complex as corrosion inhibitor on mild steel in low pH environment

Sivakumar Sivalingam [a*], Jayagopi Gayathri [b], S.Suja [c] and S.Mohandoss[d]

[a,b] *Department of Chemistry, Vel Tech Rangarajan Dr. Sagunthala R & D Institute of Science and Technology, Avadi, Chennai-600 062.*

[c] *Department of Chemistry, S.A Engineering College, Chennai - 600 077.*

[d] *Department of Chemistry, Rajalakshmi Engineering College, Thandalam, Chennai - 602 105.*

[*] *Corresponding author E-mail: drsivakumars@veltech.edu.in*

Abstract

The efficiency of novel synthesized NiO-Syzygium cumini complex as a corrosion inhibitor was evaluated on mild steel in 0.5 molar sulphuric acid by potentiodynamic polarization (PDP) and electrochemical impedance spectroscopy (EIS) measurements. It was noticeably confirmed that the inhibition efficiency increased with increasing concentration of inhibitor, due to a decrease in the corrosion currents and impeding of the active sites. Due to presence of organic molecules from the NiO on the carbon steel surface was confirmed by FT-IR spectroscopy. The adsorption of species on the alloy surface was modelled using the Langmuir isotherm. A decrease in the carbon steel acid corrosion in the presence of NiO-Syzygium cumini was also confirmed through contact angle measurements and scanning electron microscopy (SEM)

Keywords: *Corrosion Inhibitor; Mild steel; PDP:, EIS, SEM*

1. Introduction

Green synthesis methods in the field of chemistry are going to be superior alternatives over conservative synthesis methods. These recent methodologies are more effective, modest, low cost, eco-friendly and can be suitable for large scale manufacturing processes [1]. In environmental science, metal oxide nanoparticles play vital role for the adsorption based on removal of metals from the wastewater [2]. Nanomaterials are potential materials that are cost-effective, can be reused, and possess high stability [3, 4]. Employing corrosion inhibitors is one of the best practical methods for protection from corrosion environment, specifically in acidic medium to inhibit unexpected metal dissolution and acid ingestion [5, 6]. Acidic solutions are widely used for cleaning machinery parts that get affected by corrosion. Corrosion inhibitors are used to minimize material losses during the cleaning process [7]. In general, aromatic organic compounds that are commonly used are harmful to the human health and environment. Hence, eco-friendly materials like plant extracts containing particular organic molecules have been used as substitute to traditional corrosion inhibitors. In general, organic molecules are used as corrosion inhibitors and the activity is attributed to their adsorption on the metal surface. Due to the presence of heteroatoms like N, O, S, P and C=C bonds contain π electrons that interact with vacant metal d-orbitals [8-12]. Vegetal extracts usually act as mixed inhibitors [13]. Natural extracts show outstanding efficacy as environment-friendly corrosion inhibitors which offer simple and practical formulations and applied in low pH environment [14]. The naturally occurring corrosion inhibitor on mild steel such as caffeic acid [15], tannic acid and gallic acid [16]. Some other organic molecules are also examined as corrosion inhibitors that contain alkaloids [17], flavonoids [18] and phenolic acids [16]. Different nanoparticles and superficial modified nanoparticles were used to increase the protective

barrier properties of epoxy coating [19–27]. Nickel oxide (NiO) is a transition metal oxide with cubic structure and is drawing increasing attention due to its potential use for a variety of applications such as: catalysis [28], electrochromic films [29], battery cathodes [30, 31], gas sensors [32], and magnetic materials [33]. It exhibits anodic electrochromism, excellent durability and electrochemical stability, large spin optical density and various manufacturing possibilities. It can also be widely used in dye sensitized photocathodes [34]. The inhibitor is used mostly for protection against corrosion in acid environment. In most of the industries inhibitors are used to control metal dissolution, particularly in acidic, basic and neutral environments. In most of the industries, efficient corrosion inhibitors used are organic compounds that contains at least one functional group (Hetero atoms) which act as active centre for the adsorption on the surface metal and blocking the active sites on the metal [35]. Most of the industrial machine parts are made of mild steel and machinery parts are cleaned using descaling and acid pickling. To overcome the drawbacks, it has been envisaged to use nickel oxide to form a complex, due to less toxicity compared with other metal oxides and are also eco-friendly to our environment. Hence, in the present study, the novel NiO-syzygium cumini complex has been prepared by a novel green synthesis method and its corrosion inhibition, its characterization techniques followed by the electrochemical performance of the corrosion inhibitor complex in low pH environment

2. Materials and Methods

2.1 Instrumentation

Pellets made from NiO-Syzygium cumini complex and KBr were subjected to FTIR investigation on a Perkin-Elmer 337 spectrometer in the frequency range between 4000-500 cm^{-1}. XRD spectrum was record using Rigaku Maniflex diffractometer (Japan) and JSM-6390 Scanning Electron Microscope was used to determine the structural morphology of the synthesized NiO-Syzygium cumini complex materials. EIS and Potentiodynamic polarization studies were registered in ECLAB 10.37 model instrument. Weight loss method (gravimetric) was used for the study of corrosion inhibition efficiency.

2.2 Preparation of aqueous leaf extract of syzygium cumini (java plum)

Syzygium cumini (Java plum) leaves were collected from Veltech University, Chennai, Tamil Nadu, India. The freshly prepared leaf extract was slightly modified as reported in literature [36]. The collected Syzygium cumini leaves were washed with double-distilled water repeatedly to remove the impurities. Then, 10 g of sample leaf was powdered and boiled in 200 ml of double distilled water for 30 min until the colour changes to dark solution. The leaf extract was filtered by Whatman filter paper grade No. 1 filter paper. The filtrate solution was used for further analysis.

2.3 Green synthesis of nickel oxide nanoparticles (NiO NPs)

20 ml of aqueous Syzygium cumini leaf extract was added into 200 ml of 0.1 M nickel nitrate aqueous solution at normal room temperature. The mixed solution was further heated to 60 °C with constant magnetic stirring for 1 h. The reaction mixture was adjusted at a pH of 10 using sodium hydroxide until acquiring greyish green powder [37]. The resultant product was allowed to cool and centrifuged for 15 min. The precipitate collected was dried at around 400 °C in hot air oven for 2 h. The dried powder samples were used for further characterization. The steps involved in the formation of nickel oxide nanoparticles using green synthesis approach are shown in scheme.1

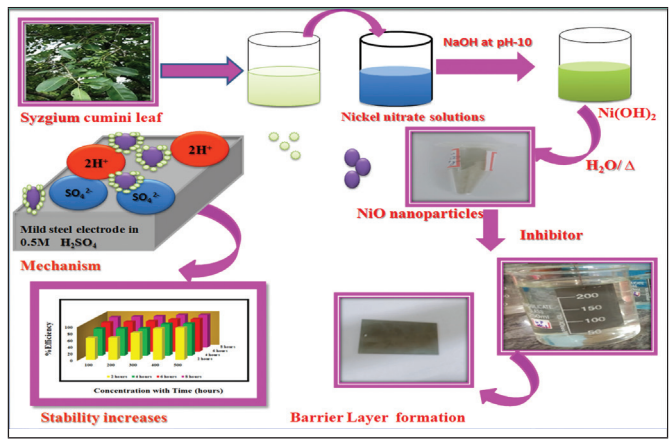

Scheme.1. The mechanism of formation of green synthesized nickel oxide nanoparticles

3. Results and discussion

3.1 FTIR analysis NiO-Syzygium cumini complex

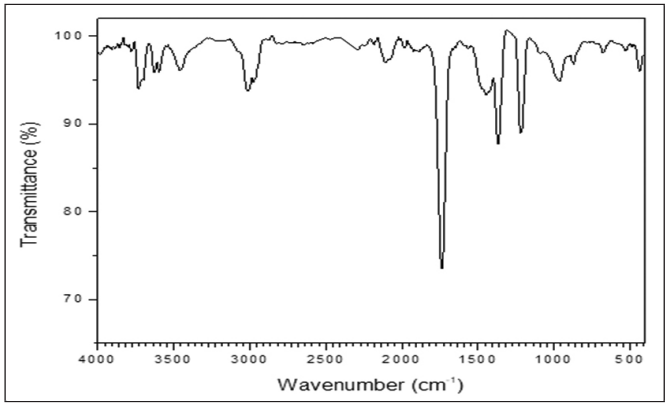

Fig. 1. FT-IR spectrum of NiO-Syzygium cumini complex

The FTIR spectrum of NiO-Syzygium cumini complex synthesized from the leaf extract in the range of 4000-500 cm^{-1} is shown in Fig.1. The FT-IR spectrum shows stretching vibrations at 3403 cm^{-1} due to hydroxyl ions presence, 3300 cm^{-1} due to stretching frequency of -NH, 1631 cm^{-1} due to carbonyl group, 1446 cm^{-1} and 1072 cm^{-1} due to stretching frequency of aromatic saturated and unsaturated carbon atom (Fig.1). These strong peaks indicate the presence of -OH, -NH, -C=O, C=C and C-C groups on the surface of nickel oxide nanoparticles. The IR band at 800 cm^{-1} is due to stretching band of nickel oxide [37, 38].

3.2 XRD analysis of NiO-Syzygium cumini complex

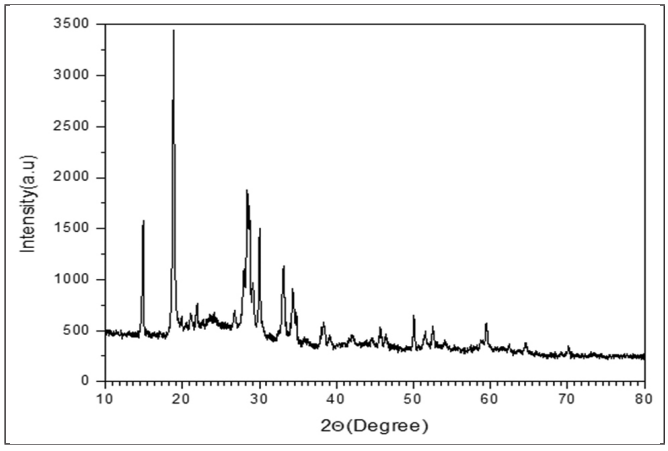

Fig. 2. XRD pattern of NiO-Syzygium cumini complex

The broader peaks (Fig.2) in the XRD pattern of nickel oxide- Syzygium cumini complex confirmed that the formation of NiO nano particles [24]. The characteristic peaks of NiO nanoparticles were observed at 23.8º (012), 36.02º (110), 38.73º (320) 49.80º (024), 62.70º (214) and 61.17º (300) in the XRD pattern [37, 38].

3.3 SEM/EDX analysis of NiO-Syzygium cumini complex

The scanning electron microscope (SEM) image of NiO-Syzygium cumini complex is shown in Fig.3. **Fig. 3(A)** shows that the granular like structure having diameter 61.69 nm to 84.70 nm. Some slight modification in synthesis process results in the modification of spherical shape to irregular shape [22,36,37]. The EDX analysis (**Fig. 3(B)**), showed the presence of Ni, O, C and N in the NiO-Syzygium complex that acts as protective layer in aggressive environment [39].

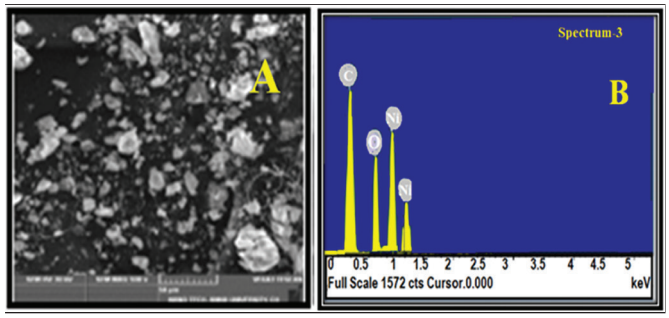

Fig. 3 SEM image and EDX of NiO-Syzygium cumini complex

3.4 Preparation of electrode materials

Plates of mild steel, having dimension of 4 cm x 2 cm x 0.2 cm with the composition corresponding to C: 0.21%, Si: 0.035%, Mn: 0.25%, P: 0.082% and Fe: 99.28% were abraded with various grades of emery papers. The abraded specimens were cleaned by distilled water, ethanol, acetone and desiccated. Gravimetric studies were accomplished with freshly polished coupons [26].

3.5 Preparation of hostile solutions

0.5 M aggressive solution used for dwindling of metal pieces were obtained by diluting the AR. grade sulphuric acid. Solutions employed for inhibition measurements were prepared by adding different amounts of NiO-Syzygium cumini complex (100-500 ppm) to hostile solutions.

3.6. Exploration of inhibition property

3.6.1 Deterioration measurements

NiO-Syzygium cumini complex was synthesized using various proportions of NiO and plant leaf extract. Among them, the composition containing 10 g leaf extract and 0.1M of nickel nitrate gave good inhibition properties on mild steel in aggressive environments. Effect of aggressive environment on mild steel surfaces was estimated by evaluating the loss in weight on keeping the pre weighed mild steel in 250 ml of blank and test solutions. The corroded mild steel coupons were removed from the low pH environment at regular two hour time intervals up to 8 h and cleaned with bristle brush in distilled water repeatedly, absolute ethanol and acetone. They were reweighed to determine inhibition efficacy (IE %) and surface coverage (θ) after drying. The formulae reported earlier [35] were adopted to calculate the above said parameters and are presented in Table 1

$$\%Efficiency = \frac{Wo-Wi}{Wo} X100\ g \text{ ----------(1)}$$

Where W_i and W_0 are weight loss values (g) on mild steel in 0.5 M H_2SO_4 with and without NiO-Syzygium cumini complex, respectively.

Table 1: Values of IE and θ deliberated from the weight loss measurements in 0.5 M blank and test solutions.

Conc. Of Composite (ppm)	2 hrs			4hrs			6hrs			8hrs		
	Weight	I.E (%)	ϴ	Weight	I.E (%)	ϴ	Weight	I.E (%)	ϴ	Weight	I.E (%)	ϴ
Blank	0.3495	-		0.3727	-		0.5836	-		0.8190	-	
100	0.1217	65	0.6517	0.0737	80	0.8022	0.0803	86	0.8624	0.0808	90	0.9013
200	0.1183	66	0.6615	0.0701	81	0.81	0.0649	88	0.887	0.0627	92	0.9234
300	0.0666	80	0.8094	0.0671	81	0.8199	0.0555	90	0.9049	0.0555	93	0.9322
400	0.0231	93	0.9339	0.0221	94	0.9407	0.0287	95	0.9508	0.0171	97	0.97912
500	0.0169	95	0.9516	0.0161	95	0.9546	0.0224	96	0.9616	0.0235	97	0.9724

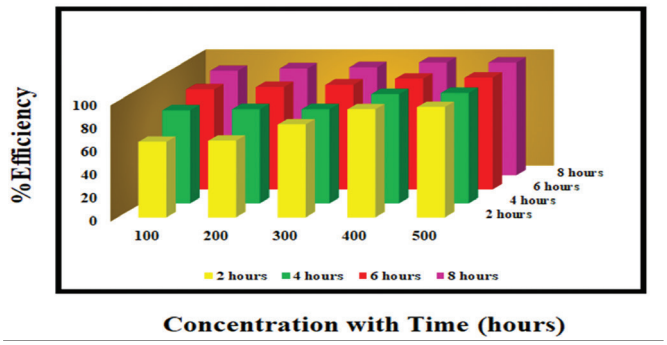

Fig. 4. Inhibition efficiency portrayal by bar chart for 0.5 M test solution

Data provided in the above table reveals that the NiO-Syzygium cumini complex is competent of giving protection against 0.5 M acidic solution with 97% efficacy for 500 ppm concentration of inhibitor solution at 8 h. Above results indicate that NiO-Syzygium cumini complex can be added with cleaning agents having acidic concentration less than or equal to 0.5 M [40].

3.6.2 Potentiodynamic polarization studies

The potentiodynamic polarization was conducted as per ASTM 415 to study the mild steel specimen response in 0.5 M sulphuric acid with the addition of different concentrations of NiO-Syzygium cumini complex. Fig. 5 shows the Tafel polarization curves of the working electrode submerged in the NiO-Syzygium cumini complex inhibitor at concentrations of 100, 200, 300, 400, and 500 ppm, including the blank solution measured at normal room temperature. The electrochemical parameters such as corrosion current density (I_{corr}), corrosion potential (E_{corr}), anodic (βa) and cathodic (βc) Tafel slopes, and inhibition efficiency (η). Fig. 5 shows that the anodic and cathodic Tafel curves shift to a lower current density (I_{corr}) after the addition of NiO-Syzygium cumini complex inhibitors. In the

repressed working electrode, the corrosion potential (E_{corr}), shifted towards the negative region. On the other hand, the corrosion current density (I_{corr}) shows desperation when the inhibitor is mixed to the test solution. The results of calculated E_{corr} and I_{corr} similarly indicate the corrosion protection of the inhibitor. **Table. 2** shows the recorded data of some electrochemical parameters E_{corr}, I_{corr}, βa, βc and η efficiency to obtain from the corrosion process, including the calculation of inhibition efficiency, η, using as shown below equation (2):

$$\%\,\eta\, Efficiency = \frac{I^0\text{corr} - Icorr}{I^0\text{corr}} X100 \quad \text{---------- (2)}$$

In the above equation, I^0_{corr} and I_{corr} are corrosion current densities in the absence and presence of inhibitors [41]. From the potentiodynamic polarization curve, we observed, that when increasing the inhibitor concentration 100 ppm to 500 ppm, the corrosion current density (I_{corr}) value decreases from (750 µA cm^{-2} to 201µA cm^{-2}) the inhibition efficiency observed was 62% for 100 ppm and 90% for 500 ppm. Since at lower concentration itself higher efficiency was noticed and with further addition there were no major changes.

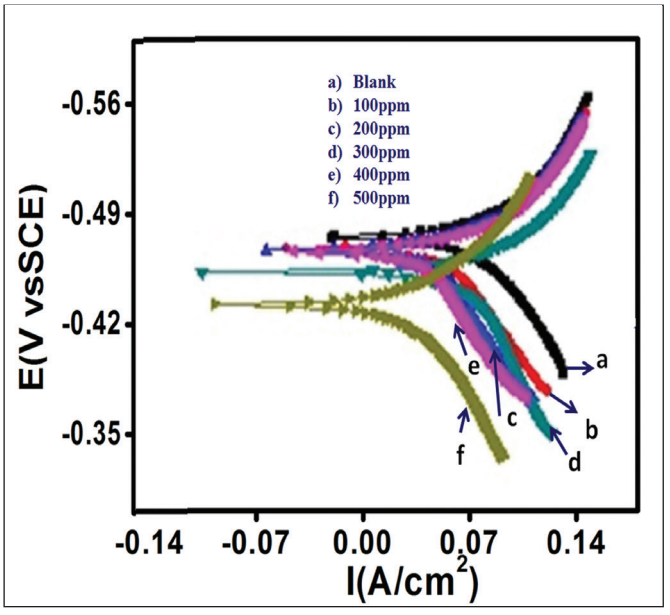

Fig 5: Potentiodynamic polarization curve of mild steel in 0.5 M blank and test solutions

Table 2: Corrosion resistive parameters in 0.5 M H_2SO_4 and test solution

Conc. of Inhibitor (ppm)	E_{Corr} (mV vs. SCE)	βa (mV dec^{-1})	β_c (mV dec^{-1})	I_{corr} (µA cm^{-2})	Inhibition Efficiency (η %)	Surface coverage (θ)
Blank	-452	63	66	1972	--	--
100	-497	29	38	750	62	0.6196
200	-479	37	39	680	65	0.6551
300	-497	25	20	501	75	0.7456
400	-474	26	40	350	82	0.8225
500	-487	22	23	201	90	0.8980

3.6.3. Electrochemical Impedance Spectroscopy (EIS) Measurements

The Impedance spectral data of mild steel in 0.5 M H_2SO_4 in the absence of inhibitor and presence of various concentration of NiO-Syzygium cumini complex are shown in the impedance plot **Fig. 6**. It clearly indicates that inhibition property on the mild steel has drastically changed after the addition of inhibitor to aggressive solution. By careful observation of the plot, the diameter of the semicircles increases in the inhibitor solution compared to without the inhibitor. The increase in size of capacitive loop with increase in inhibitor concentration indicates that, the NiO-Syzygium cumini complex inhibitor gets adsorbed over the metal surface and inhibits the flow of corrosion current and thereby act as a very efficient inhibitor in very low pH environment. According to the impedance results in **Table 3**, the charge transfer resistance (R_{ct}) value rises as the NiO-Syzygium cumini complex inhibitor concentration increases and the value of the double-layer capacitance (C_{dl}) decreases. The results of EIS parameters such as charge transfer resistance (R_{ct}) and double layer capactiance (C_{dl}) were determined and the electrical equivalent circuit diagram as depicted in **Fig. 7.** [22,41] was evolved. The percentage efficiency (η) was calculated using the below equation (3).

$$\%\,\eta\, Efficiency = \frac{Rct - R^0ct}{Rct} X100 \quad \text{----------(3)}$$

In the above equation, R^0_{ct} and R_{ct} are the charge transfer resistance of the blank and the inhibitor solution.

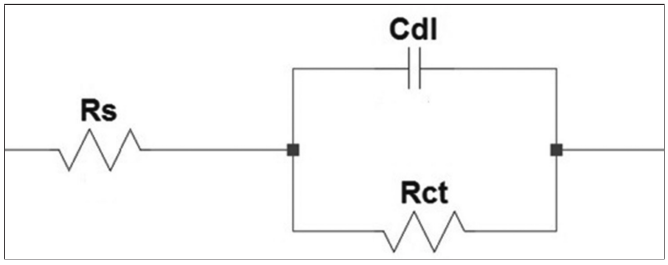

Fig. 7: Electrical equivalent circuit diagram

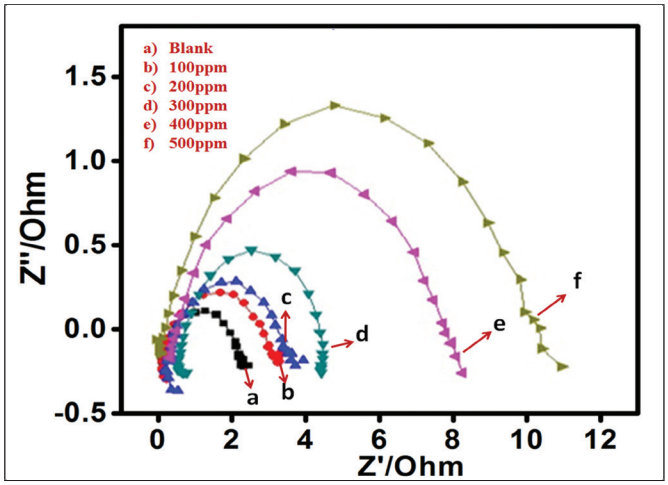

Fig 6: Impedance plot for mild steel in 0.5 M blank and test solution.

Table 3: Impedance parameters derived for 0.5 M blank and test solution

Conc. of Inhibitor (ppm)	R_s (Ω)	C_{dl} (μ F cm^{-2})	R_{ct} (Ω cm^2)	Inhibition efficiency (%)	Surface Coverage (θ)
Blank	0.9997	542	0.7685	--	--
100	1.0490	552	2.164	64	0.6455
200	1.0940	501	2.525	69	0.6956
300	1.1540	552	2.901	73	0.7351
400	1.0450	383	3.846	80	0.8001
500	0.9898	320	6.821	88	0.8874

4. Conclusions

The anti-corrosive electrochemical performance of NiO-Syzygium cumini complex synthesized from green synthesis was evaluated as a corrosion inhibitor on mild steel in low pH environment. IE of 97% was observed even with an immersion time up to eight hours by weight loss method. IE was also found to increase with surface coverage area. Potentiodynamic polarization study presented 90% efficacy and the NiO-Syzygium cumini complex system functioned mostly as a mixed type of inhibitor. The electrochemical impedance indicates that, owing to enlarged thickness of the surface layer on the mild steel surface an increase in Rct value and decrease in Cdl and Icorr values due to charge transfer. Therefore the result revealed that the inhibitor substance forms a protective barrier film on the mild steel surface. The increasing trend of protection efficiency with respect to increase in the concentration of inhibitor observed in weight loss, PDP and EIS studies implies that the water soluble substance can act as good safeguarding agent during the industrial cleaning process.

Acknowledgement

The authors are thankful to the Dean R & D and University Management Committee Members of Vel Tech Rangarajan, Dr. Sagunthala R & D Institute of Science and Technology, Avadi, Chennai for providing necessary instrumental facilities to carry out research work.

References

[1] Mukherjee, Debarati, Sourja Ghosh, Swachchha Majumdar, and K. Annapurna, Green synthesis of α-Fe_2O_3 nanoparticles for arsenic (V) remediation with a novel aspect for sludge management, Journal of Environmental Chemical Engineering 4, no. 1 (2016) 639-65 https://doi.org/10.1016/j.jece.2015.12.010

[2] Fu, Fenglian, and Qi Wang. Removal of heavy metal ions from wastewaters: a review Journal of Environmental Management 92, no. 3 (2011) 407-418. https://doi.org/10.1016/j.jenvman.2010.11.011

[3] Mwafy, A.Eman, S. Mohamed , Hasanin, and M.Ayman, Mostafa, Cadmium oxide/ TEMPO-oxidized cellulose nanocomposites produced by pulsed laser ablation in liquid environment: synthesis, characterization, and antimicrobial activity, Optics & Laser Technology 120(2019) 105744 https://doi.org/10.1016/j.optlastec.2019.105744

[4] Darwish, M. Ayman , H. Wael Eisa, Ali , A. Shakta, and H. Mohamed Talaat, Investigation of factors affecting the synthesis of nano-cadmium sulfide by pulsed laser ablation in liquid environment, Spectrochimica Acta Part A*:* Molecular and Biomolecular Spectroscopy 153 (2016) 315-320. https://doi.org/10.1016/j.saa.2015.08.007

[5] H. Ashassi-Sorkhabi, D. Seifzadeh, and M. G. Hosseini, EN, EIS and polarization studies to evaluate the inhibition effect of 3H-phenothiazin-3-one, 7-dimethylamin on mild steel corrosion in 1 M HCl solution, Corrosion Science 50, no. 12 (2008) 3363-3370. https://doi.org/10.1016/j.corsci.2008.09.022

[6] A.K. Satapathy, G. Gunasekaran, S. C. Sahoo, Kumar Amit, and P. V. Rodrigues, Corrosion inhibition by Justicia gendarussa plant extract in hydrochloric acid solution, Corrosion science 51, no. 12 (2009) 2848-2856. https://doi.org/10.1016/j.corsci.2009.08.016

[7] Zaferani, Sadeq Hooshmand, Majid Sharifi, Davood Zaarei, and Mohammad Reza Shishesaz, Application of eco-friendly products as corrosion inhibitors for metals in acid pickling processes–A review, Journal of Environmental Chemical Engineering 1, no. 4 (2013) 652-657. https://doi.org/10.1016/j.jece.2013.09.019

[8] Fernandes, Caio Machado, X.Leonardo, Alvarez, Nazir Escarpini dos Santos, Adriana, C. Maldonado Barrios, and Eduardo Ariel Ponzio, Green synthesis of 1-benzyl-4-phenyl-1H-1, 2, 3-triazole, its application as corrosion inhibitor for mild steel in acidic medium and new approach of classical electrochemical analyses, Corrosion Science 149 (2019) 185-194. https://doi.org/10.1016/j.corsci.2019.01.019

[9] Fernandes, Caio Machado, Thayssa da S. Ferreira Fagundes, Nazir Escarpini dos Santos, Talita Shewry de M. Rocha, Rafael Garrett, Ricardo Moreira Borges, Guilherme Muricy, Alessandra Leda Valverde, and Eduardo Ariel Ponzio, Ircinia strobilina crude extract as corrosion inhibitor for mild steel in acid medium. Electrochimica Acta 312 (2019) 137-148. https://doi.org/10.1016/j.electacta.2019.04.148

[10] Michael, Nwaugbo Chinenye, and James Abosede Olubunmi, The corrosion inhibition of mild steel in sulphuric acid solution by flavonoid (catechin) separated from Nypa fruticans Wurmb leaves extract." Science Journal of Chemistry 2, no. 4 (2014) 27-32. doi: 10.11648/j.sjc.20140204.11

[11] Tan, Bochuan, Shengtao Zhang, Yujie Qiang, Wenpo Li, Hao Li, Li Feng, Lei Guo, Chunliu Xu, Shijin Chen, and Guangyi Zhang, Experimental and theoretical studies on the inhibition properties of three diphenyl disulfide derivatives on copper corrosion in acid medium. Journal of Molecular Liquids 298 (2020)111975. https://doi.org/10.1016/j.molliq.2019.111975

[12] Tan, Bochuan, Shengtao Zhang, Hongyan Liu, Yuwan Guo, Yujie Qiang, Wenpo Li, Lei Guo, Chunliu Xu, and Shijin Chen, Corrosion inhibition of X65 steel in sulfuric acid by two food flavorants 2-isobutylthiazole and 1-(1, 3-Thiazol-2-yl) ethanone as the green environmental corrosion inhibitors: Combination of experimental and theoretical researches, Journal of colloid and interface science 538 (2019) 519-529. https://doi.org/10.1016/j.jcis.2018.12.020

[13] Chung, Ill-Min, Ramalingam Malathy, Rameshkumar Priyadharshini, Venkatesan Hemapriya, Seung-Hyun Kim, and Mayakrishnan Prabakaran, Inhibition of mild steel corrosion using Magnolia kobus extract in sulphuric acid medium, Materials Today Communications 25 (2020) 101687. https://doi.org/10.1016/j.mtcomm.2020.101687

[14] Raja, Pandian Bothi, and Mathur Gopalakrishnan Sethuraman. Natural products as corrosion inhibitor for metals in corrosive media-a review. Materials letters 62 (2008) 113-116. https://doi.org/10.1016/j.matlet.2007.04.079

[15] de Souza, Fernando Sılvio, and Almir Spinelli. Caffeic acid as a green corrosion inhibitor for mild steel. Corrosion science 51 (2009) 642-649. https://doi.org/10.1016/j.corsci.2008.12.013

[16] I.B. Obot, and A. Madhankumar, Enhanced corrosion inhibition effect of tannic acid in the presence of gallic acid at mild steel/HCl acid solution interface. Journal of Industrial and Engineering Chemistry 25 (2015) 105-111. https://doi.org/10.1016/j.jiec.2014.10.019

[17] Li, Hui-Jing, Weiwei Zhang, and Yan-Chao Wu. Anti-corrosive properties of alkaloids on metals. In *Alkaloids-Their Importance in Nature and Human Life*. Intech Open, 2018.

[18] I. Ikeuba, B. I. Ita, P. C. Okafor, B. U. Ugi, and E. B. Kporokpo. Green corrosion inhibitors for mild steel in H_2SO_4 solution: Comparative study of flavonoids extracted from gongronema latifoliunm with crude the extract. Protection of Metals and Physical Chemistry of Surfaces 51 (2015): 1043-1049 https://doi.org/10.1134/S2070205115060118

[19] M. Schem, T. Schmidt, J. Gerwann, M. Wittmar, M. Veith, G. E. Thompson, I. S. Molchan et al. CeO_2-filled sol–gel coatings for corrosion protection of AA2024-T3 aluminium alloy. Corrosion Science 51, no. 10 (2009): 2304-2315. https://doi.org/10.1016/j.corsci.2009.06.007.

[20] Bierwagen, Gordon, Dennis Tallman, Junping Li, Lingyun He, and Carol Jeffcoate, EIS studies of coated metals in accelerated exposure, Progress in organic coatings 46 (2003) 149-158. https://doi.org/10.1016/S0300-9440(02)00222-9

[21] Liu, Jie, Lunwu Zhang, Xianliang Mu, and Peiqing Zhang, Studies of electrochemical corrosion of low alloy steel under epoxy coating exposed to natural seawater using the WBE and EIS techniques, Progress in Organic Coatings 111 (2017) 315-321. https://doi.org/10.1016/j.porgcoat.2017.06.012

[22] P. Kamatchi Selvaraj, S. Sivakumar, and S. Selvaraj, NiO-PANI composite as potential inhibitor for mild steel in acidic corrosion environment. Int J Chem Sci 16 (2018) 268. DOI: 10.21767/0972-768X.1000268

[23] Zhang, Wei, Jia Wang, Yu-Nan Li, and Wei Wang, Evaluation of metal corrosion under defective coatings by WBE and EIS technique, Acta Physico-Chimica Sinica 26 (2010) 2941-2950.

[24] Hosseini, Mir Ghasem, and Pariya Yardani Sefidi. Electrochemical impedance spectroscopy evaluation on the protective properties of epoxy/DBSAdoped polyaniline-TiO_2 nanocomposite coated mild steel under cathodic polarization. Surface and Coatings Technology 331 (2017) 66-76. https://doi.org/10.1016/j.surfcoat.2017.10.043

[25] Shunmugaperumal, Selvaraj, P. Kamatchi Selvaraj and Sivakumar Sivalingam. "Water soluble CdO-PANI composite as corrosion resistive delegate in acidic abode for mild steel, Egyptian Journal of Chemistry 65 (2022)117-133. DOI: 10.21608/ejchem.2022.118204.5336

[26] Selvaraj, P. Kamatchi, S. Sivakumar, and S. Selvaraj, Impervious Nature of Al_2O_3-PANI composite against corrosion on mild steel in strong acidic environment. Oriental Journal of Chemistry 34 (2018) :1832-1841, DOI:10.13005/ojc/3404017

[27] Dooley, M. Kerr, Shang-Yang Chen, and Julian RH Ross, Stable nickel-containing catalysts for the oxidative coupling of methane. Journal of catalysis 145 (1994) 402-408. https://doi.org/10.1006/jcat.1994.1050

[28] Wang, Gongming, Xihong Lu, Teng Zhai, Yichuan Ling, Hanyu Wang, Yexiang Tong, and Yat Li. Free-standing nickel oxide nanoflake arrays: synthesis and application for highly sensitive non-enzymatic glucose sensors. Nanoscale 4 (2012) 3123-3127. https://doi.org/10.1039/C2NR30302G

[29] H.X. Yang, Q. F. Dong, X. H. Hu, X. P. Ai, and S. X. Li, Preparation and characterization of $LiNiO_2$ synthesized from $Ni(OH)_2$ and $LiOH{\cdot}H_2O$, Journal of power sources 79 (1999) 256-261.https://doi.org/10.1016/S0378-7753(99)00158-5

[30] Hotový, I. J. Huran, Li Spiess, R. Čapkovic, and Š. Haščík, Preparation and characterization of NiO thin films for gas sensor applications, Vacuum 58 (2000) 300-307. https://doi.org/10.1016/S0042-207X(00)00182-2

[31] Miller, L. Eric and Richard E. Rocheleau, Electrochemical behavior of reactively sputtered iron-doped nickel oxide. Journal of the Electrochemical Society 144 (1997) 3072. DOI 10.1149/1.1837961

[32] Ichiyanagi, Yuko, Naoto Wakabayashi, Junichiro Yamazaki, Saori Yamada, Yoshihide Kimishima, Eriko Komatsu, and Hiroyuki Tajima. Magnetic properties of NiO nanoparticles. Physica B: Condensed Matter 329 (2003) 862-863. https://doi.org/10.1016/S0921-4526(02)02578-4

[33] El-Kemary, M., N. Nagy, and I. El-Mehasseb. Nickel oxide nanoparticles: Synthesis and spectral studies of interactions with glucose. Materials Science in Semiconductor Processing 16 (2013) 1747-1752. https://doi.org/10.1016/j.mssp.2013.05.018

[34] Deng, XiangYi, and Zhong Chen, Preparation of nano-NiO by ammonia precipitation and reaction in solution and competitive balance, Materials letters 58 (2004) 276-280. https://doi.org/10.1016/S0167-577X(03)00469-5

[35] Raja, T., SS Syed Abuthahir, and K. Vijaya, Anticorrosion Performance of Syzygium Cumini Leaves Extract for Carbon Steel Immersed in a Hydrochloric Acid Medium. Portugaliae Electrochimica Acta 42 (2024) 173-189. https://doi.org/10.4152/pea.2024420302

[36] Arumugam, Manikandan, Dinesh Babu Manikandan, Elayaraja Dhandapani, Arun Sridhar, Karthiyayini Balakrishnan, Manickavasagam Markandan, and Thirumurugan Ramasamy. Green synthesis of zinc oxide nanoparticles (ZnO NPs) using Syzygium cumini: Potential multifaceted applications on antioxidants, cytotoxic and as nanonutrient for the growth of Sesamum indicum. Environmental Technology & Innovation 23 (2021) 101653. https://doi.org/10.1016/j.eti.2021.101653

[37] El-Kemary, M., N. Nagy, and I. El-Mehasseb. Nickel oxide nanoparticles: Synthesis and spectral studies of interactions with glucose. Materials Science in Semiconductor Processing 16 (2013)1747-1752. https://doi.org/10.1016/j.mssp.2013.05.018

[38] Riastuti, Rini, Giannisa Mashanafie, Vika Rizkia, Ahmad Maksum, Siska Prifiharni, Kaban Agus Paul Setiawan, Gadang Priyotomo, and Johny Wahyuadi Soedarsono, Effect of syzygium cumini leaf extract as a green corrosion inhibitor on API 5l carbon steel in 1M HCL." Eastern-European Journal of Enterprise Technologies 6 (2022)120. doi.10.15587/1729-4061.2022.267232

[39] Xavier, Joseph Raj, Electrochemical, mechanical and adhesive properties of surface modified NiO-epoxy nanocomposite coatings on mild steel, Materials Science and Engineering: B 260 (2020) 114639 https://doi.org/10.1016/j.mseb.2020.114639

[40] Yaro, S. Aprael, Rafal, K. Wael, and Anees A. Khadom, Reaction kinetics of corrosion of mild steel in phosphoric acid, Journal of the University of Chemical Technology and Metallurgy 45, no. 4 (2010) 443-448.

[41] Singh, Ambrish, and M. A. Quraishi, The extract of Jamun (Syzygium cumini) seed as green corrosion inhibitor for acid media, Research on Chemical Intermediates 41 (2015) 2901-2914. https://doi.org/10.1007/s11164-013-1398-3.

Compositionally modulated Ni-W multilayers to alleviate the residual stresses in coatings for superior wear resistance

Nitin P. Wasekar

Centre for Engineered Coatings

International Advanced Research Centre for Powder Metallurgy and New Materials, Hyderabad - 500005, India

Email: nitin@arci.res.in

Abstract

The presence of tensile residual stresses in the Ni-W alloy coatings generated during the electrodeposition has restricted their industrial deployment. In the present study, the multilayering strategy is employed in developing the Ni-W coatings with the best combination of hardness and residual stresses. Ni-W multilayer coatings composed of alternate soft (~ 2.6 GPa) and hard (~ 8.5 GPa) Ni-W layers with individual layer thickness (λ) ranging from 2.5 μm to 0.05 μm were deposited by using the pulse reverse current electrodeposition. These multilayer coatings have demonstrated a significant reduction in the residual stresses while retaining the high hardness. Ni-W multilayer coating with λ ~0.1 μm has exhibited superior resistance to wear damage compared to its homogeneous counterparts. The improved wear degradation resistance of the multilayer coating was rationalized through assessment of residual stresses and thermal properties.

Keywords: *Pulse reverse electrodeposition; Ni-W alloy; Multilayer coatings; Microstructure; Wear.*

1. Introduction

For the past three decades, multilayers have been studied for wide variety of applications [1]–[4] after the pioneering theoretical framework proposed by Koehler [5] that paved the way for studying the mechanical aspects of multilayers. Techniques such as sputtering, vapor deposition and electrodeposition are extensively utilized to synthesize a wide range of multilayers. Early stages of metallic multilayer developments had majorly utilized the dual bath electrodeposition [6]–[10]. Later, with the advancement of microelectronics, sophisticated pulse power rectifiers were developed and enabled to control the pulses with narrow widths (as low as few microseconds) [11], [12]. This has revolutionized the electroplating industry and the fundamental research on metallic multilayers. The pulse electrodeposition process has facilitated the deposition of discrete layers with varying modulus, composition, grain size, microstructure etc., [13], [14].

The potential of the electrodeposited nanocrystalline Ni-W coatings to replace the hard chrome coatings has been widely recognized [15]–[18]. However, these nanocrystalline Ni-W coatings suffer from two major setbacks: (i) presence of tensile residual stresses [19] and (ii) inherent low toughness associated with the nanocrystalline microstructure [20]–[22], which limited their wide industrial applications. The tribological performance of coatings is heavily influenced by both the properties mentioned above. Hence, for superior tribological performance, ensuring improved toughness along with high hardness/strength is vital. In pursuit of establishing the strength-ductility synergy in nanocrystalline materials, recent studies have elaborated the paradigm of microstructural engineering [23]–[25]. In brief, it is noticed that the deliberate inclusion of spatial gradients in microstructure and/or mechanical properties at various length scales has enabled the nanocrystalline metals to regain an appreciable amount of balance between the strength and ductility. A similar microstructural engineering strategy can also facilitate in reducing the tensile residual stresses often encountered in electrodeposited alloy coatings [26], [27].

Recent studies involving the electrodeposition of metallic multilayers for tribological applications have tried to address some of the above-mentioned issues and succeeded to an extent. Extensive studies conducted by Ruff and Lashmore [28] have concluded that the Cu/Ni multilayers (layer thickness, λ ~4 to 100 nm) have superior wear resistance compared to their homogeneous counterparts. The high wear resistance of multilayers is attributed to the interfacial barrier effects and the increase in the flow strength. Ghosh et al. [29] have investigated the effect of Ni layer thickness while keeping that of Cu layer constant, on the wear resistance of Cu/Ni alloys. They observed that layering has reduced the residual stresses with a concurrent increase in the hardness leading to improved wear properties. Similar observation was found in Ni-P [30]. Karimazadeh et al. [31] have used the pulse reverse current method to deposit the compositional modulated Ni-Co-P multilayers (λ ~90 to 3000 nm). The hardness of multilayers has shown a Hall-Petch type of relationship with layer thickness. The high wear resistance of multilayers is attributed to the enhanced hardness. Papachristos et al. [32] have reported that the brittle failure of Ni-P-W multilayer coatings under sliding is inhibited as the layer thickness is reduced, and it was attributed to the increased number of interfaces which may deflect the growing crack. However, explicit evidences for the crack deflection at the layer interfaces are not available. A similar wear behavior is also observed in the other multilayer systems [33]–[36].

The perusal of the literature suggests two important design guidelines: (a) sandwiching the hard layers between the soft layers to alleviate the residual stresses in addition to improve the toughness, and (b) layer thickness of few nanometers for increasing hardness. Despite the efforts, the multilayer systems mentioned above are still inferior to the existing hard chrome coatings in terms of their hardness and wear resistance. There is limited work carried out in this direction to develop wear resistant Ni-W multilayer coatings [16], [35-37]. Furthermore, there is lack of understanding on the effect of layering on the improved tribological properties especially in case of the multilayers which do not satisfy the Koehler's criteria i.e., the multilayers constituting of layers with marginal difference in the modulus. Therefore, the focus of the current study is to develop a method for depositing Ni-W multilayers consisting of alternate hard and soft Ni-W layers from single bath and subsequently, to understand the origin of the improved mechanical, tribological performance. The effect of thermal diffusion during wear has been emphasized.

2. Experimental

2.1 Controlling the W-content and microstructure

The advantage with the electrodeposited Ni-W system is that the W is a "weak grain boundary segregating" element unlike phosphorus in Ni-P system and widens the window of accessible grain size range [38-40]. Therefore, in the present study, pulse reverse current electrodeposition technique has been utilized to access the extreme grain size regimes and deposit soft and hard Ni-W layers from single bath consisting of citrate based electrolyte. The pulse parameters (such as anodic/cathodic current density and duty cycle) were optimized to obtain the homogeneous Ni-W coatings with extreme W-contents and grain sizes. The details on pulse parameters and deposition conditions are given in Table 1. Exploiting the recipe feature of the DPR 20-60-200 module, the Ni-W multilayers with equal layer thickness (λ) were deposited by alternating the deposition parameters. The individual layer thickness was controlled by passing equal amount of charge during each recipe. AISI 1045 steel plate (60 × 60 × 5 mm^3) is used as the substrate (cathode) material while the platinized titanium is employed as anode. The substrates were polished, cleaned in acetone and activated in a 50% HCl solution before introducing into the deposition bath. A fresh electrolytic bath of 2 L volume is used for every coating. After the deposition, the coated samples were cleaned in fresh water and dried. The deposition duration was tuned such that all the coatings have at least 30-40 μm thickness.

2.2 Coating characterization

Residual stresses were computed using the $Sin^2\Psi$ method by XRD technique (PANalytical X'Pert pro, 40 kV, 45 mA). The (2 2 0) plane (at 2θ = 75˚) was selected for the residual stress analysis.

The diffraction profile of this peak was collected at different Ψ-angles (± 71.57˚ with a step size of ~8˚) by tilting the sample stage. The obtained XRD profile data was corrected for the instrument-specific effects. Then, the peak position of each profile was determined and was used for the *d*-spacing calculations using the Bragg's law. The computed *d*-spacing values were plotted as a function of $Sin^2\Psi$. The procedure outlined in [41], [42] has been used to calculate the residual stress values. The elastic modulus values of the Ni-W alloys required for the calculations were taken from [43]. The thermal conductivity of coatings was estimated using electrical resistivity measurements. To measure the electrical resistivity of the coatings, free standing foils with ~30 μm thickness were prepared by depositing on copper substrate and later dissolving the substrate in a chromic acid solution (250 g/l chromium oxide and 15 ml/l sulfuric acid). The free-standing foils were carefully sectioned into 15×15 mm^2 samples for resistivity measurements. Four-probe instrument was used and at least three readings were taken at different regions of the film to arrive at an average resistivity value.

Table 1. Pulse parameters utilized for the deposition of compositionally modulated Ni-W layers

Parameter	Ni-1W layer	Ni-15W layer
Cathodic current density, A/cm^2	0.1	0.1
Anodic current density, A/cm^2	0.3	0
Duty cycle, %	87	97.5
Frequency, Hz	43	48.7
Temperature, °C	60 ± 3	

2.3 Sliding wear performance

Wear resistance of the coatings was evaluated using the ball-on-disc configuration with a universal tribometer (MFT-5000, Rtec instruments, USA) in accordance with the ASTM-G99 standard. The coated substrates were cut into 10×10×5 mm^3 specimens for wear tests. All the specimens were polished to a roughness (R_a) value <0.05 μm and cleaned in acetone before carrying out the test. Tungsten carbide (WC) ball having 6 mm diameter was used as the counter body. A fresh ball was employed for each test in order to avoid the debris transfer from one specimen to another. A constant normal load of 5 N at a sliding speed of 0.15 m/s was applied and the track diameter was set to 6 mm. The total sliding distance for each test was fixed to 200 m. Friction coefficient was continuously recorded. The specimens were ultrasonically cleaned to remove any loose particles on the wear track. Using an integrated profilometer, three-dimensional wear track profiles were recorded at different locations to estimate the wear volume loss as suggested in [15]. At least three tests were carried out and the average wear rate is reported. The SEM analysis of the wear tracks was carried out to understand wear mechanism.

3. Results and discussion

3.1 Microstructure

The cross-sectional SEM images in backscattered electron (BSE) mode for the Ni-W multilayers with varying layer thickness are shown in Fig. 1. The gray layers are Ni-1W while the bright layers are Ni-15W. The sharp interfaces between the individual layers as can be observed are intact and devoid of any cracks or pores. The waviness of the individual layers is attributed to the application of high anodic pulses during the deposition of Ni-1W layers. In fact, presence of such wavy interlayer interfaces could be advantageous, and the exact reasons will be discussed later while dealing with the residual stresses in the following sections. The elemental mapping reveals the compositional modulation of W-content between the layers.

3.2 Effect of multilayered architecture on the residual stresses

Fig. 2 shows the residual stresses computed using the $Sin^2\Psi$ method. All the coatings have shown tensile residual stresses. The homogeneous Ni-1W coating has shown the lowest stress of ~200 MPa which is much smaller than the earlier reports [19] while the Ni-15W coating has exhibited stress of ~1300 MPa, almost 7-fold higher than the former. In case of the multilayer coatings, irrespective of the layer thickness, residual stresses have significantly decreased compared to the homogeneous hard Ni-15W coating. The soft Ni-1W layers sandwiched between the hard Ni-15W layers could have

alleviated the residual stresses in the multilayer coatings. Furthermore, the presence of concave and convex type of topographic features on the Ni-1W layers can locally allow effective stress reduction and redistribution [44].

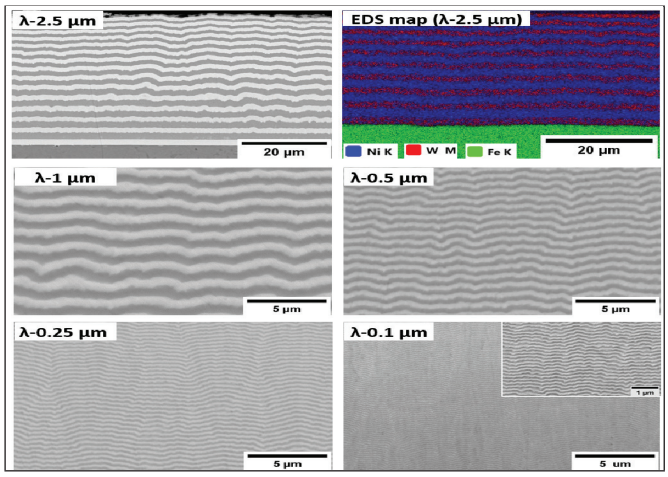

Fig.1 Cross-sectional images of Ni-W multilayer coatings with layer thickness (λ) ranging from 2.5 μm to 0.1 μm. EDS elemental mapping is shown for the Ni-W multilayer coating having λ ~2.5 μm to elaborate the compositional modulation between the layers.

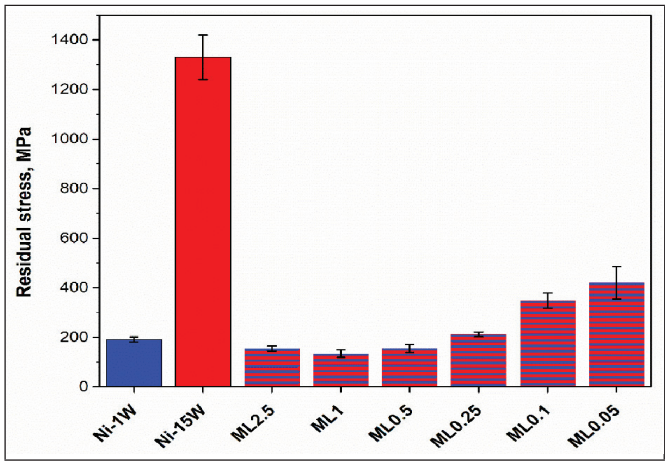

Fig.2. Residual stresses of the Ni-W homogeneous coatings (Ni-1W and Ni-15W) and multilayer coatings. ML represents multilayer while the number after ML indicates the layer thickness in micrometers.

3.3 Hardness and tribological behavior of multilayer coatings

The hardness of multilayer coatings is plotted against the layer thickness as shown in Fig. 3. Hardness increased with decrease in the layer thickness demonstrating the Hall-Petch type of behavior. An important observation from Fig. 3 is that the peak hardness of the multilayer coatings (which is obtained at λ ~0.1 μm) is only marginally higher than the hardness of homogeneous Ni-15W coating. This can be rationalized based on the Koehler's theory. Koehler proposed that the extent of multilayer strengthening is directly proportional to the difference in the elastic modulus of individual layers [5]. Since both the constituent layers (Ni-1W and Ni-15W) in the present study are solid solutions of W in Ni, the modulus difference is not large enough to produce extra strengthening.

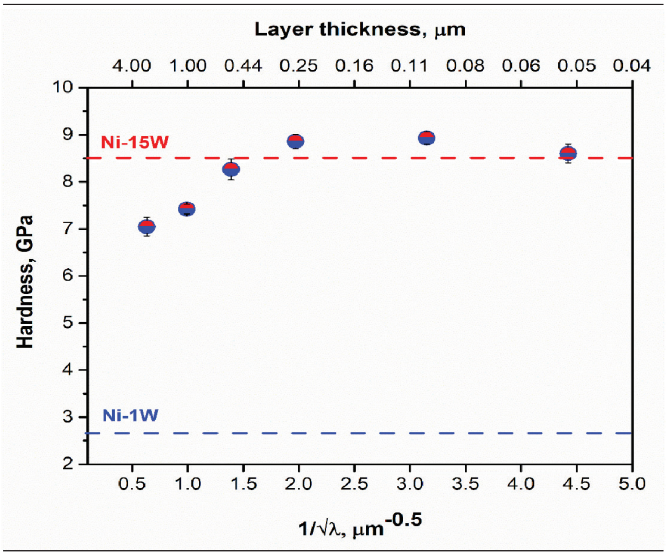

Fig.3. Hall-Petch type plot of Ni-W multilayer coatings

Tribological performance of the multilayer coatings were evaluated using the ball-on-disc configuration. Fig. 4 (a,b) shows the wear rate and friction coefficient of homogeneous and multilayer coatings. The Ni-W multilayer coating with λ ~0.1 μm (indicated as ML0.1) has shown superior wear resistance and lower friction coefficient compared to the homogeneous counterparts. Presence of tensile residual stresses exaggerates the severity of contact stresses during the sliding and leads to sub-surface cracking and delamination [26], [45], [46]. Higher hardness and lower residual stresses of the multilayer coating have led to its superior wear performance. It is well known that the toughness along with the strength play an important role in improving the wear resistance of the coatings [47], [48].

A mere improvement in the hardness renders the brittleness and consequent failure of the coatings at higher loads. Since, the multilayers are composed of alternate hard and soft Ni-W layers, we expect the toughness of these multilayers to be higher than the homogeneous hard Ni-W coating [49] which might have assisted in the improvement of tribological properties.

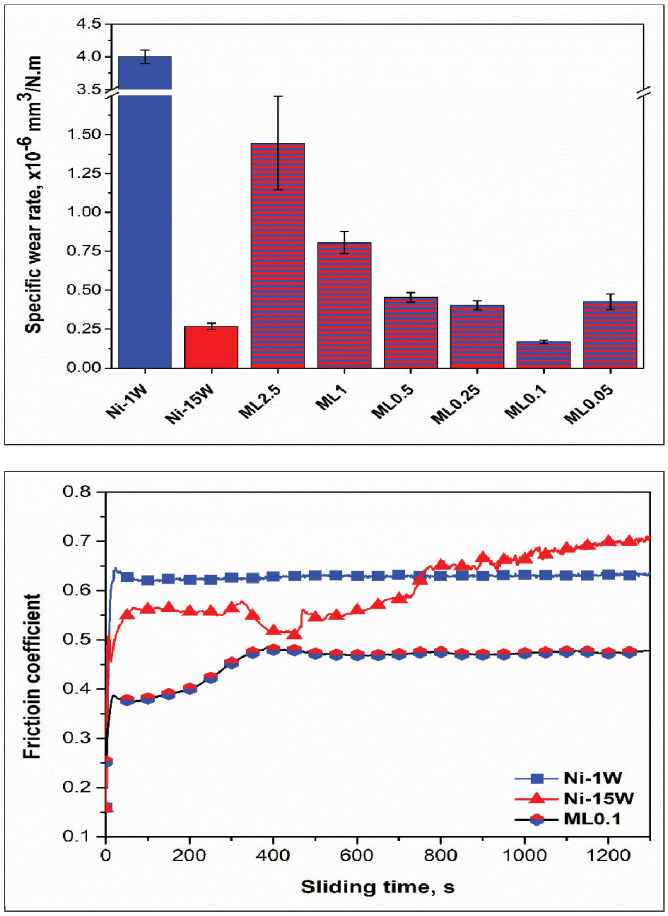

Fig. 4 (a) Specific wear rate and (b) friction coefficient values of homogenous coatings and multilayer coatings determined using the ball-on-disc configuration.

3.4 Influence of layering on thermal properties and wear behavior

During the sliding contact, almost all the frictional energy is converted into heat [50]. This heat, except at very low speeds, leads to an appreciable temperature raise. The highest temperature during the sliding is expected to be located at the true contact regions i.e., the asperities. The raise in the temperature at the contact interface affects the frictional properties of various materials due to the formation of various types of oxides, local phase transformations and sometimes even interface melting. Thus, thermal properties play a crucial role in controlling the wear resistance of materials. For better performance, it is important for the materials to effectively dissipate this heat energy during the sliding contacts. The electrical resistivity of the coatings was measured using the four-probe technique. Later, by applying the Wiedemann-Franz law, the electrical resistivity is converted to the thermal conductivity and thermal diffusivity as per the formulae below [51], [52]:

$$\kappa = \frac{L\,T}{\rho} \qquad \text{--------- Eq. (1)}$$

$$\alpha = \frac{\kappa}{d\,C_p} \qquad \text{--------- Eq. (2)}$$

Where; κ = Thermal conductivity, L = Lorentz number, T = absolute temperature and ρ = electrical resistivity, α = thermal diffusivity, C_p = specific heat capacity and d = density. At room temperature, L $T = 7.5\times10^{-6}$ W.Ω/°K. Since, specific heat capacity and density are structure-insensitive properties, they were calculated using the rule of mixtures. Table 2 provides the calculated electrical and thermal properties of homogeneous and multilayer coatings. Evidently, the multilayer coatings have exhibited higher thermal diffusivity compared to the hard Ni-15W coating.

The kinetics of effective heat dissipation to establish the quasi-steady-state condition is often represented by a dimensionless parameter called Peclet number (P), given as [50]:

$$P = \frac{\upsilon\, r}{2\alpha} \qquad \text{--------- Eq. (3)}$$

Where, υ = velocity of the heat source i.e., sliding speed, r = contact radius which can be calculated using the Hertzian contact model [61], [67]. Essentially, Peclet number (P) is the ratio of true velocity to speed of heat flow. The contact radius calculated for the present experimental conditions is ~40 μm. The computed Peclet numbers for homogeneous and multilayers coatings are given in Table 2. P<0.1 is considered as a regime of very slow sliding speeds where the frictional heat has sufficient amount of time to be dissipated effectively to the surroundings and the system attains quasi-

stationary regime [53]. While, $P>5$ is considered as a regime of high sliding speeds, and the system is not allowed to dissipate the heat effectively resulting in adiabatic heating. From Table 2, it can be observed that the homogeneous Ni-15W has the highest Peclet number and therefore is expected to experience relatively higher interfacial heating and oxidation. It is the rate of generation of oxide and its subsequent detachment from the interface, which determines wear rate. When oxide film is formed steadily and is intact (which is the case of ML0.1), the friction coefficient and wear rate are low. On the other hand, higher rate of oxidation due to extreme heat generation (which is the case of Ni-15W), it is unlikely that oxide film is intact resulting in higher wear rates. In fact, the wear track analysis of the homogeneous Ni-15W indicated the higher amount of oxidation compared to the multilayer coating (ML0.1) providing direct evidence on the effect of the thermal properties. Besides the thermal diffusivity, hardness of the material also affects the extent of raise in the interfacial temperature [50].

Table. 2. Electrical and thermal properties of homogeneous and multilayer Ni-W coatings

The Peclet numbers and therefore, the maximum raise in the interface

Nomenclature	Electrical resistivity x10^{-7} (Ω.m)	Thermal conductivity (W/m.K)	Thermal diffusivity ×10^{-2} (cm^2/s)	Peclet number (*P*)
Ni-1W	2.5 ± 0.9	29.6 ± 1.0	7.28	0.412
Ni-15W	10.9 ± 1.0	6.9 ± 0.7	1.38	2.164
ML2.5	2.6 ± 0.2	29.0 ± 2.0	6.34	0.473
ML0.1	2.8 ± 0.2	26.7 ± 1.5	5.84	0.514

temperature can be compared directly only if their hardness values are in the same range, which is true for homogeneous Ni-15W and multilayer coating. Thus, for similar hardness values and sliding velocity, the value of P is determined by thermal diffusivity. The lower P in case of multilayer coatings is due to higher thermal diffusivity. It has been observed by Lim and Ashby [54] that friction coefficient decreases with decrease in P. Thus, lower wear rate and friction coefficient in case of multilayered coatings compared to Ni-15W is due to their higher thermal diffusivity and lower residual stresses.

4. Conclusions

Exploiting the advantage of reverse/anodic pulsed current, Ni-W multilayer coatings comprised of alternate soft and hard Ni-W layers with layer thickness (λ) ranging from ~2.5 μm to 0.05 μm have been deposited from a single electrodeposition bath. The multilayer coatings have shown a substantial reduction in the residual stresses. The multilayering architecture has allowed to deposit hard coatings with lower residual stresses. Despite the similar hardness, Ni-W multilayer coating (λ ~0.1 μm) has demonstrated superior wear resistance compared to the homogeneous Ni-W coating. The enhanced wear resistance of multilayer coating is attributed to lower residual stresses and relatively higher thermal diffusivity. The multilayer coating has shown lower friction coefficient due to the presence of thin and adherent oxide film.

References

[1] C. A. Ross, 'Electrodeposited Multilayer Thin Films', *Annual Review of Materials Science*, 2003, 24(1), 159–188.

[2] I. Bakonyi and W. E. G. Hansal, 'Development of pulse-plating technology for the preparation of coatings with varying composition along their thickness: a historical overview', *Transactions of the Institute of Metal Finishing*, 2018, 96(5), 237–243.

[3] M. Aliofkhazraei *et al.*, 'Development of electrodeposited multilayer coatings: A review of fabrication, microstructure, properties and applications', *Applied Surface Science Advances*, vol. 6. Elsevier B.V., Dec. 01, 2021. doi: 10.1016/j.apsadv.2021.100141.

[4] A. Sáenz-Trevizo and A. M. Hodge, 'Nanomaterials by design: A review of nanoscale metallic multilayers', *Nanotechnology*, vol. 31, no. 29, May 2020, doi: 10.1088/1361-6528/ab803f.

[5] J. S. Koehler, 'Attempt to design a strong solid', *Phys Rev B*, vol. 2, no. 2, pp. 547–551, 1970, doi: 10.1103/PhysRevB.2.547.

[6] A. S. M. A. Haseeb, 'Dual-Bath Electrodeposition of Cu/Ni Compositionally Modulated Multilayers', *J Electrochem Soc*, vol. 141, no. 1, p. 230, 1994, doi: 10.1149/1.2054689.

[7] K. Matsuoka, M. Okuhata, and M. Takashiri, 'Dual-bath electrodeposition of n-type Bi-Te/Bi-Se multilayer thin films', *J Alloys Compd*, vol. 649, pp. 721–725, 2015, doi: 10.1016/j.jallcom.2015.07.166.

[8] N. V. Myung, K. H. Ryu, J. H. Kim, M. Schwartz, and K. Nobel, 'Electrodeposition of NiFe thin films and NiFe/Cu multilayers with a recirculating electrochemical flow reactor', *Mat. Res. Soc. Symp. Proc.*, vol. 562, pp. 1–4, 1999.

[9] S. Esmaili, M. E. Bahrololoom, and K. L. Kavanagh, 'Electrodeposition, characterization and morphological investigations of NiFe/Cu multilayers prepared by pulsed galvanostatic, dual bath technique', *Mater Charact*, vol. 62, no. 2, pp. 204–210, 2011, doi: 10.1016/j.matchar.2010.11.017.

[10] W. Blum, 'Deposition of Ni/Cu multilayers by dual-bath technique', *Trans. of American Electrochemical society*, vol. 40, pp. 307–320, 1921.

[11] N. IBL, 'Some theoretical aspects of pulse electrolysis', *Surface Technology*, vol. 10, pp. 81–104, 1980.

[12] M. S. Chandrasekar and M. Pushpavanam, 'Pulse and pulse reverse plating-Conceptual, advantages and applications', *Electrochim Acta*, vol. 53, no. 8, pp. 3313–3322, 2008, doi: 10.1016/j.electacta.2007.11.054.

[13] K. S. R. Krishnan, K. Srinivasan, and S. Mohan, 'Electrodeposition of compositionally modulated alloys - An overview', *Transactions of the Institute of Metal Finishing*, vol. 80, no. 2, pp. 46–48, 2002, doi: 10.1080/00202967.2002.11871430.

[14] F. C. Walsh, 'The continued development of multilayered and compositionally modulated electrodeposits', *Transactions of the IMF*, vol. 100, no. 5, pp. 1–12, Jul. 2022, doi: 10.1080/00202967.2022.2094078.

[15] T. J. Rupert and C. A. Schuh, 'Sliding wear of nanocrystalline Ni–W: Structural evolution and the apparent breakdown of Archard scaling', *Acta Mater*, vol. 58, no. 12, pp. 4137–4148, 2010, doi: 10.1016/j.actamat.2010.04.005.

[16] A. J. Detor and C. A. Schuh, 'Tailoring and patterning the grain size of nanocrystalline alloys', *Acta Mater*, vol. 55, pp. 371–379, 2007, doi: 10.1016/j.actamat.2006.08.032.

[17] N. P. Wasekar and G. Sundararajan, 'Sliding wear behavior of electrodeposited Ni-W alloy and hard chrome coatings', *Wear*, vol. 342–343, pp. 340–348, 2015, doi: 10.1016/j.wear.2015.10.003.

[18] M. H. Allahyarzadeh, M. Aliofkhazraei, A. R. Rezvanian, V. Torabinejad, and A. R. S. Rouhaghdam, 'Ni-W electrodeposited coatings: Characterization, properties and applications', *Surf Coat Technol*, vol. 307, pp. 978–1010, 2016, doi: 10.1016/j.surfcoat.2016.09.052.

[19] T. D. Ziebell and C. A. Schuh, 'Residual stress in electrodeposited nanocrystalline nickel-tungsten coatings', *J Mater Res*, vol. 27, no. 9, pp. 1271–1284, 2012, doi: 10.1557/jmr.2012.51.

[20] M. A. Meyers, A. Mishra, and D. J. Benson, 'Mechanical properties of nanocrystalline materials', *Prog Mater Sci*, vol. 51, no. 4, pp. 427–556, 2006, doi: 10.1016/j.pmatsci.2005.08.003.

[21] T. Yamasaki, 'High-strength nanocrystalline ni-w alloys produced by electrodeposition and their embrittlement behaviors during grain growth', *Scr Mater*, vol. 44, pp. 1497–1502, 2001, doi: https://doi.org/10.1016/S1359-6462(01)00720-5.

[22] T. Yamasaki, N. Oda, H. Matsuoka, and T. Fukami, 'Tensile strength of electrodeposited nanocrystalline Ni-W alloys with finely dispersed micrometer-sized array through-holes', *Materials Science and Engineering A*, vol. 449–451, pp. 833–835, Mar. 2007, doi: 10.1016/j.msea.2006.02.410.

[23] J. Li, Q. Zhang, R. Huang, X. Li, and H. Gao, 'Towards understanding the structure–property relationships of heterogeneous-structured materials', *Scr Mater*, vol. 186, pp. 304–311, 2020, doi: 10.1016/j.scriptamat.2020.05.013.

[24] E. Ma and T. Zhu, 'Towards strength–ductility synergy through the design of heterogeneous nanostructures in metals', *Materials today*, vol. 20, no. 6, pp. 323–331, 2017.

[25] D. Vijay Kumar and M. J. N. V. Prasad, 'Pulsed electrodeposition and hardness of microstructurally graded iron', *Surf Coat Technol*, vol. 342, pp. 121–128, May 2018, doi: 10.1016/j.surfcoat.2018.03.001.

[26] L. Bathini, M. J. N. V. Prasad, and N. P. Wasekar, 'Development of continuous compositional gradient Ni-W coatings utilizing electrodeposition for superior wear resistance under sliding contact', *Surf Coat Technol*, vol. 445, p. 128728, Sep. 2022, doi: 10.1016/j.surfcoat.2022.128728.

[27] S. Lee, M. Choi, S. Park, H. Jung, and B. Yoo, 'Mechanical properties of electrodeposited Ni-W thin films with alternate W-rich and W-poor multilayers', *Electrochim Acta*, vol. 153, pp. 225–231, 2015, doi: 10.1016/j.electacta.2014.11.190.

[28] A. W. Ruff and D. S. Lashmore, 'Effect of layer spacing on wear of Ni/Cu multilayer alloys', *Wear*, vol. 151, no. 2, pp. 245–253, 1991, doi: 10.1016/0043-1648(91)90252-P.

[29] S. K. Ghosh, P. K. Limaye, S. Bhattacharya, N. L. Soni, and A. K. Grover, 'Effect of Ni sublayer thickness on sliding wear characteristics of electrodeposited Ni/Cu multilayer coatings', *Surf Coat Technol*, vol. 201, no. 16–17, pp. 7441–7448, May 2007, doi: 10.1016/j.surfcoat.2007.02.014.

[30] C. A. Vlaic *et al.*, 'Improved wear resistance of alternating amorphous and crystalline layers in electrodeposited Ni-P multilayers', *Surf Coat Technol*, vol. 386, Mar. 2020, doi: 10.1016/j.surfcoat.2020.125470.

[31] A. Karimzadeh, A. S. Rouhaghdam, M. Aliofkhazraei, and R. Miresmaeili, 'Sliding wear behavior of Ni–Co–P multilayer coatings electrodeposited by pulse reverse method', *Tribol Int*, vol. 141, Jan. 2020, doi: 10.1016/j.triboint.2019.105914.

[32] V. D. Papachristos, C. N. Panagopoulos, P. Leisner, M. B. Olsen, and U. Wahlstrom, 'Sliding wear behaviour of Ni-P-W composition-modulated coatings', *Surf Coat Technol*, vol. 105, pp. 224–231, 1998, doi: https://doi.org/10.1016/S0257-8972(98)00459-9.

[33] V. Torabinejad, M. Aliofkhazraei, A. Sabour Rouhaghdam, and M. H. Allahyarzadeh, 'Tribological Behavior of Electrodeposited Ni-Fe Multilayer Coating', *Tribology Transactions*, vol. 60, no. 5, pp. 923–931, Sep. 2017, doi: 10.1080/10402004.2016.1230687.

[34] V. Torabinejad, M. Aliofkhazraei, A. S. Rouhaghdam, and M. H. Allahyarzadeh, 'Tribological properties of Ni-Fe-Co multilayer coatings fabricated by pulse electrodeposition', *Tribol Int*, vol. 106, pp. 34–40, Feb. 2017, doi: 10.1016/j.triboint.2016.10.025.

[35] M. H. Allahyarzadeh, M. Aliofkhazraei, A. S. Rouhaghdam, H. Alimadadi, and V. Torabinejad, 'Mechanical properties and load bearing capability of nanocrystalline nickel- tungsten multilayered coatings', *Surf Coat Technol*, vol. 386, p. 125472, 2020, doi: 10.1016/j.surfcoat.2020.125472.

[36] N. Udompanit, P. Wangyao, S. Henpraserttae, and Y. Boonyongmaneerat, 'Wear response of composition-modulated multilayer Ni-W coatings', in *Advanced Materials Research*, 2014, vol. 1025–1026, pp. 302–309. doi: 10.4028/www.scientific.net/AMR.1025-1026.302.

[37] M. V. N. Vamsi, N. P. Wasekar, and G. Sundararajan, 'Influence of heat treatment on microstructure and mechanical properties of pulse electrodeposited Ni-W alloy coatings', *Surf Coat Technol*, vol. 319, pp. 403–414, 2017, doi: 10.1016/j.surfcoat.2017.03.074.

[38] A. J. Detor and C. A. Schuh, 'Grain boundary segregation, chemical ordering and stability of nanocrystalline alloys: Atomistic computer simulations in the Ni-W system', *Acta Mater*, vol. 55, no. 12, pp. 4221–4232, Jul. 2007, doi: 10.1016/j.actamat.2007.03.024.

[39] N. P. Wasekar, A. P. O'Mullane, and G. Sundararajan, 'A new model for predicting the grain size of electrodeposited nanocrystalline nickel coatings containing sulphur, phosphorus or boron based on typical systems', *Journal of Electroanalytical Chemistry*, vol. 833, no. May 2019, pp. 198–204, 2019, doi: 10.1016/j.jelechem.2018.11.057.

[40] N. P. Wasekar, P. Haridoss, S. K. Seshadri, and G. Sundararajan, 'Influence of mode of electrodeposition, current density and saccharin on the microstructure and hardness of electrodeposited nanocrystalline nickel coatings', *Surf Coat Technol*, vol. 291, pp. 130–140, 2016, doi: 10.1016/j.surfcoat.2016.02.024.

[41] A. M. El-Sherik, J. Shirokoff, and U. Erb, 'Stress measurements in nanocrystalline Ni electrodeposits', *J Alloys Compd*, vol. 389, no. 1–2, pp. 140–143, Mar. 2005, doi: 10.1016/j.jallcom.2004.08.010.

[42] P. S. Prevey, 'X-Ray Diffraction Residual Stress Techniques', in *Materials Characterization*, vol. 10, ASM International, 1986, doi: 10.31399/asm.hb.v10.a0001761.

[43] M. V. N. Vamsi, N. P. Wasekar, and G. Sundararajan, 'Influence of heat treatment on microstructure and mechanical properties of pulse electrodeposited Ni-W alloy coatings', *Surf Coat Technol*, vol. 319, pp. 403–414, 2017, doi: 10.1016/j.surfcoat.2017.03.074.

[44] J. H. Lee, J. T. Oh, Y. C. Kim, and J. H. Lee, 'Stress reduction and enhanced extraction efficiency of GaN-based LED grown on cone-shape-patterned sapphire', *IEEE Photonics Technology Letters*, vol. 20, no. 18, pp. 1563–1565, Sep. 2008, doi: 10.1109/LPT.2008.928844.

[45] G. M. Hamilton, 'Explicit Equations for the Stresses beneath a Sliding Spherical Contact', *Proc Inst Mech Eng C J Mech Eng Sci*, vol. 197, no. 1, pp. 53–59, Jan. 1983, doi: 10.1243/PIME_PROC_1983_197_076_02.

[46] Y. C. Huang, S. Y. Chang, and C. H. Chang, 'Effect of residual stresses on mechanical properties and interface adhesion strength of SiN thin films', *Thin Solid Films*, vol. 517, no. 17, pp. 4857–4861, 2009, doi: 10.1016/j.tsf.2009.03.043.

[47] N. A. A. R. Aly and M. R. El-Koussy, 'Relationship between Ductility and Wear Resistance of High Mn-Steels', in *Surface Engineering*, Dordrecht: Springer Netherlands, 1990, pp. 640–651. doi: 10.1007/978-94-009-0773-7_63.

[48] E. Hornbogen, 'Role of fracture toughness in wear of metals', *Wear*, vol. 33, no. 2, pp. 251–259, 1975, doi: https://doi.org/10.1016/0043-1648(75)90280-X.

[49] F. Liang, Z. X. Wang, Y. W. Luo, B. Zhang, X. M. Luo, and G. P. Zhang, 'Enhancing co-deformation ability of nanograined Ni-W layers in the Ni/Ni-W laminated composites', *Acta Mater*, vol. 216, Sep. 2021, doi: 10.1016/j.actamat.2021.117138.

[50] J. F. Archard, 'The temperature of rubbing surfaces', *Wear*, vol. 2, no. 6, pp. 438–455, 1959, doi: https://doi.org/10.1016/0043-1648(59)90159-0.

[51] S. Wang, I. Brooks, J. McCrea, G. Palumbo, G. Cingara, and U. Erb, 'Thermal conductivity and electrical resistivity in polycrystalline and nanocrystalline nickel', in *Advanced Materials Research*, 2012, vol. 409, pp. 561–565. doi: 10.4028/www.scientific.net/AMR.409.561.

[52] H. J. Cho, S. Wang, Y. Zhou, G. Palumbo, and U. Erb, 'Thermal conductivity of bulk electrodeposited nanocrystalline nickel', *Int J Heat Mass Transf*, vol. 100, pp. 490–496, Sep. 2016, doi: 10.1016/j.ijheatmasstransfer.2016.04.068.

[53] Y. X. Ye, C. Z. Liu, H. Wang, and T. G. Nieh, 'Friction and wear behavior of a single-phase equiatomic TiZrHfNb high-entropy alloy studied using a nanoscratch technique', *Acta Mater*, vol. 147, pp. 78–89, Apr. 2018, doi: 10.1016/j.actamat.2018.01.014.

[54] S. C. Lim, M. F. Ashby, and J. H. Brunton', 'Wear-rate transitions and their relationship to wear mechanisms', *Acta metallurgica*, vol. 35, no. 6, pp. 1343–1348, 1987, doi: https://doi.org/10.1016/0001-6160(87)90016-2.

PROFORMA OF SUBSCRIPTION FORM

I /We wish to subscribe **The Journal of Electrochemical Society of India (JECSI)** for ..... year(s) for which (i) a Demand Draft vide …….....……. dated …….....…… issued from (Name of the bank…….....)favouring **ELECTROCHEMICAL SOCIETY OF INDIA JOURNAL, payable at Bengaluru or (ii) NEFT/IMPS vide UTR no……..dated for Rs/US $…….is enclosed.**

NAME…….

DESIGNATION…….

POSTAL ADDRESS…….

……PIN…….....

E-MAIL…….Phone no.……

Subscriber ID (for renewal only)……

Signature…….

Bank account details	**Subscription details:**
Name: Electrochemical Society of India Journal Account No. 110045333254 Bank Name: Canara Bank Customer ID: 309740255 IFSC Code: CNRB0000683 MICR Code: 560015023 Indian Institute of Science Canara Bank IISc, Bangalore - 560012	**Print only**: For institutions & Individuals: Annual 6 issues: Rs 2000/- (India), Annual 6 issues: USD 250.00 incl. postages (abroad), For students: Annual 6 issues: Rs 1000/- **Print & Online (customer type: institution):** USD 100.00 & INR 5000.00 Please note that institutional prices are available only for libraries of higher education institutions and research organizations.

Journal of the Electrochemical Society of India

Vol. No. 72 (3 & 4), July-December 2023

CODEN - JESIA 72 [3&4] 2023 ISSN:0013-466X

Email : ecsiiisc@gmail.com

FROM IV

See Rule VIII

1.	Place of publication	:	Bengaluru
2.	Periodicity of its publication	:	Quarterly
3.	Printer name	:	Poornima Printers
	Whether the Citizen of india	:	YES
	Address of the printer	:	No. 3&4, Sy. No. 51/14, Chowdeshwarinagar, Pipeline Road, Laggere, Bengaluru - 560058
4.	Publishers Name	:	**The Electrochemical Society of India**
5.	Editor's Name	:	Dr. U. Kamachi Mudali
	Whether Citizen of India	:	Yes
	Address	:	**The Electrochemical Society of India** Indian Institute of Science Campus, Bangalore - 560 012
6.	Name and Address of Individuals who own the newspaper/holders and partners and shareholders	:	**The Electrochemical Society of India** Indian Institute of Science Campus, Bangalore - 560 012. holding more than 1% of the total capital.

I, Dr. U. Kamachi Mudali hereby declare that the particulars given above are true to the best of my knowledge and belief.

Sd/-

Dr. U. Kamachi Mudali

Chief Editor, JECSI

(Publisher)

THE ELECTROCHEMICAL SOCIETY OF INDIA

Indian Institute of Science Campus, Bengaluru - 560 012, India
Phone : +91-80-22932613
E-mail : ecsiiisc@gmial.com | www.ecsi.in

CALL FOR NOMINATIONS FOR ECSI AWARDS- 2024

Shri S.K. Seshadri Memorial Mascot National Award
(Instituted in the year 1980)

With a view to stimulate interest among Scientists and Technologists in the field of corrosion, the Electrochemical Society of India has instituted the prestigious "**Shri S. K. Seshadri Memorial Mascot National Award"** for notable and outstanding contributions in the field of Industrial Corrosion. The award is sponsored by Director, M/s. Biosafe Solutions.

1. The research work considered for this award should be in the field of Corrosion Science and Technology, Corrosion Prevention and Allied aspects. Industrial Significance to be highlighted and Industrial applicability is desired.
2. The work should have been carried out to bring it to the point of application. The process of development and test schedules may have been carried out during the preceding couple of years, but should have culminated in a fruitful result. The work need not necessarily have been published.

THE N. M. SAMPAT AWARD - 2024
(Instituted in the year 1986)

With a view to recognize outstanding services rendered to the Electroplating industry andTechnology, the Governing Council of the ECSI has with great pleasure has instituted "**The N. M. Sampat Award".** This award is sponsored by M/S Canning Mitra Phoenix Limited, Mumbai. Research work considered for this award should be in the field of Metal Finishing, Electroplating, Surface Coating and Modification, and allied fields. Work carried out in these areas with possible industrial applicability or academic excellence would be considered. The work need not have been published but industrial applications should have been established.

ECSI- METROHM National Award - 2023
(Instituted in the year 2021)

With a view to recognize the contributions made by individuals in the field of basic electrochemistry, electrochemical instrumentation and devices, theoretical and; experimental electrochemistry, the Electrochemical Society of India has instituted this prestigious award **"ECSI- METROHM National Award for Electrochemical Science".** The award is sponsored by M/s Metrohm India Ltd. Chennai. Meritorious work in any field of Electrochemical Science would qualify for this award.

ECSI- AMARA RAJA National Award- 2023
(Instituted in the year 2021)

With a view to stimulate interest among Scientists and Technologists in the field of Batteries, Fuel Cells and Sensors, the Electrochemical Society of India has instituted the prestigious award **"ECSI- AMARA RAJA National Award for Advanced Electrochemical Technology".** The award is sponsored by M/s. Amara Raja Batteries Ltd. Tirupathi. Meritorious work in the field of Batteries, Fuel Cells and Sensors would qualify for this award.

ECSI-Dr. K. Elayaperumal National Award- 2023
(Instituted in the year 2022)

With a view to recognize the outstanding contributions of individuals made in the area of Corrosion Mitigation in Industries, The Electrochemical Society of India has instituted the prestigious award "ECSI- Dr. K. Elayaperumal National Award for Excellence in Industrial **Electrochemical Science and Technology"** from this year. The award is sponsored by Dr. K. Elayaperumal and his family. Meritorious work in the area of corrosion mitigation in industries would qualify for this award.

GUIDELINES FOR NOMINATION

1. Nominations may be made by Research Organizations/Institution/ Industries/Individuals.
2. The nomination should be accompanied by the complete bio-data and important contributions for which the nomination is being made.
3. The work should have been carried out to bring it to the point of application. The process of development and test schedules may have been carried out during the preceding couple of years, but should have culminated into a fruitful result at least during the year of application.

Each of the above awards carries a Scroll of Honor and cash prize.

Awardees are required to present their work in the form of an **Award Lecture** and also submit a written manuscript for publication in the Journal of Electrochemical Society of India. Complete Nominations in all respects for the above awards should reach The Secretary, The Electrochemical Society of India, Indian Institute of Science Campus, Bengaluru - 560 012.

Nominations complete in all respects for the above awards should reach
Hon President or General Secretary,
The Electrochemical Society of India, Indian Institute of Science Campus,
Bengaluru - 560 012,
E-Mail: ecsiiisc@gmail.com

on or before 31st of July 2024
The Awards will be presented during the annual
ICONEST-2024 Conference

Dr. S. T. Aruna
Hon. President, ECSI

Dr. Ajay Krishnan
Hon. Gen. Secretary, ECSI

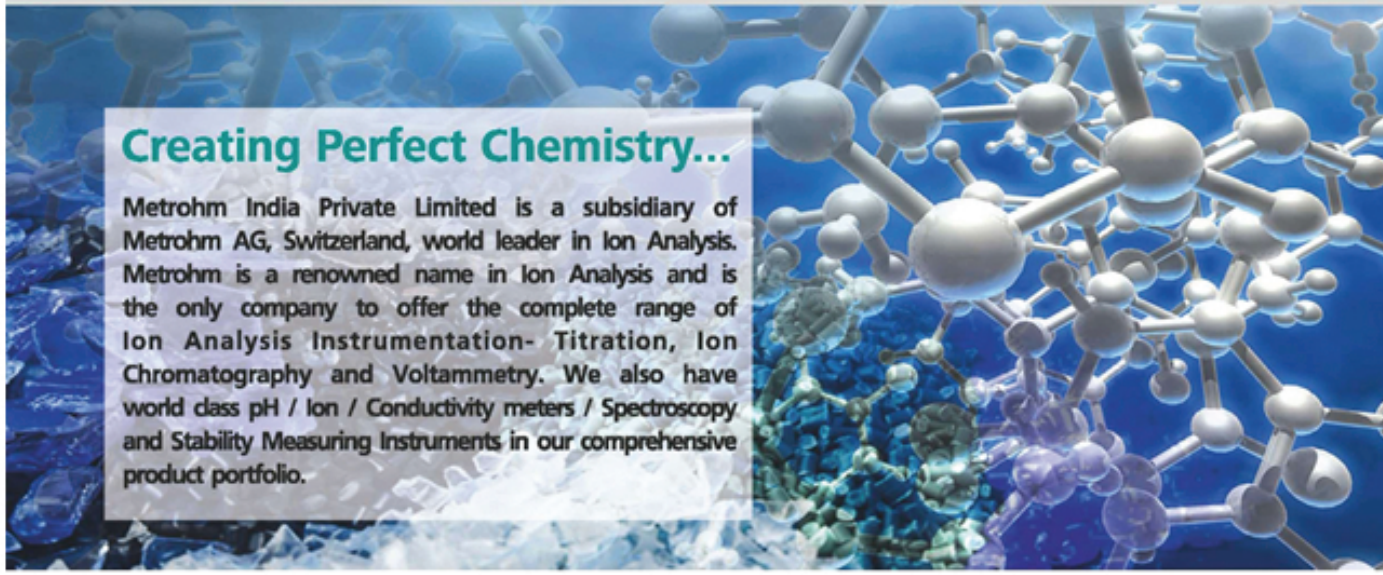

Creating Perfect Chemistry...

Metrohm India Private Limited is a subsidiary of Metrohm AG, Switzerland, world leader in Ion Analysis. Metrohm is a renowned name in Ion Analysis and is the only company to offer the complete range of Ion Analysis Instrumentation- Titration, Ion Chromatography and Voltammetry. We also have world class pH / Ion / Conductivity meters / Spectroscopy and Stability Measuring Instruments in our comprehensive product portfolio.

Titrator

Ion Chromatography

Voltammetry

Electrochemical station

NIRS Analyzer

Raman Spectroscopy

Labwater Purification

Surface Area Analyzer

We also have:

- Electrochemical research instrumentation from Metrohm Autolab
- On-line and at-line process analyzers for process monitoring from Metrohm Process Analytics
- NIR and Raman Spectroscopy solutions from Metrohm and B&W Tek
- Innovative technology for electrochemistry research from Dropsens
- BET surface area, pore size distribution from MicrotracBEL Corp., Japan
- Testing instrumentation for the energy storage device and energy conversion device markets from Arbin instruments
- Lab water solutions from Elga
- Pipetting and dispensing solutions from Socorex

PARTICIPATE IN WATER SURVEY

SCAN ME

GET YOUR FREE GIFT!

Metrohm India Private Limited
Metrohm-SIRI Towers, 3&4, Fourrts Avenue, Annai Indira Nagar
Okkiyam, Thoraipakkam, Chennai - 600097, India.
Ph: +91 44 40440440 | Customer support: +91 44 40440444

For details, e-mail us at **info@metrohm.in** or visit us at **www.metrohm.in**

Metrohm
India Private Ltd.